LUND UNIVERSITY

Exploration of Supraventricular Conduction with respect to Atrial Fibrillation. Methodological Aspects on Selected Techniques

Carlson, Jonas

2005

Link to publication

Citation for published version (APA):
Carlson, J. (2005). *Exploration of Supraventricular Conduction with respect to Atrial Fibrillation. Methodological Aspects on Selected Techniques*. [Doctoral Thesis (compilation), Cardiology]. Department of Clinical Sciences, Lund University.

Total number of authors:
1

General rights
Unless other specific re-use rights are stated the following general rights apply:
Copyright and moral rights for the publications made accessible in the public portal are retained by the authors and/or other copyright owners and it is a condition of accessing publications that users recognise and abide by the legal requirements associated with these rights.
• Users may download and print one copy of any publication from the public portal for the purpose of private study or research.
• You may not further distribute the material or use it for any profit-making activity or commercial gain
• You may freely distribute the URL identifying the publication in the public portal

Read more about Creative commons licenses: https://creativecommons.org/licenses/

Take down policy
If you believe that this document breaches copyright please contact us providing details, and we will remove access to the work immediately and investigate your claim.

LUND UNIVERSITY

PO Box 117
221 00 Lund
+46 46-222 00 00

Download date: 06. May. 2026

Exploration of Supraventricular Conduction with respect to Atrial Fibrillation

Methodological Aspects on Selected Techniques

Jonas Carlson

LUND UNIVERSITY
2005

Exploration of Supraventricular Conduction with respect to Atrial Fibrillation

Methodological Aspects on Selected Techniques

© 2005
Jonas Carlson
Department of Clinical Sciences, Lund
Division II – Cardiology
Faculty of Medicine
Lund University
Sweden

ISBN 10: 91-85481-07-6
ISBN 13: 978-91-85481-07-1
ISSN: 1652-8220

Lund University, Faculty of Medicine Doctoral Dissertation Series 2005:106

Printed by KFS i Lund AB, Lund, Sweden

Typeset using LaTeX 2ε

Contents

Papers

This dissertation is based on the following papers:

Paper I

Max P. Ingemansson, Jonas Carlson, and S. Bertil Olsson.

Modification of intrinsic AV-nodal properties by magnesium in combination with glucose, insulin, and potassium (GIK) during chronic atrial fibrillation.

Journal of Electrocardiology, 31(4):281–292, October 1998.

Paper II

Jonas Carlson, Rolf Johansson, and S. Bertil Olsson.

Classification of electrocardiographic P-wave morphology.

IEEE Transactions on Biomedical Engineering, 48(4):401–405, April 2001.

Paper III

Jonas Carlson, Rasmus Havmöller, Alberto Herreros, Pyotr Platonov, Rolf Johansson, and Bertil Olsson.

Can orthogonal lead indicators of propensity to atrial fibrillation be accurately assessed from the 12-lead ECG?

Europace, 7(Supplement 2):39–48, September 2005.

Paper IV

Jonas Carlson, Susana Santos, Pyotr G. Platonov, Ole Kongstad Rasmussen, Rolf Johansson, and S. Bertil Olsson.

Left atrial conduction along the coronary sinus during ectopic atrial tachycardia and atrial fibrillation: A study using correlation function analysis.

Journal of Cardiovascular Electrophysiology, 14(10 Supplement):s148–s153, October 2003.

Chapter 1

Introduction

I do not imagine that electrocardiography is likely to find any very extensive use in the hospital. It can at most be of rare and occasional use to afford a record of some rare anomaly of cardiac action.

Augustus Desiré Waller, 1911

Throughout this study, the objective has been described as 'computer-based analysis of signals from the heart'. Admittedly ambitious, the description indicates that the focus of the study has been on the technical and methodological aspects of using computers to analyze cardiac signals, rather than the medical conclusions and interpretations of the results.

Working with output signals from a system, the understanding of the properties of those signals is linked to the level of approximation of that system, in this case the heart. In this study, a low level of complexity was chosen in the approximation, with a system analytic view of the heart. The very complex biological and mechanical functionality of the heart is reduced to a set of pumps, commanded by an electrical control system responsible for timing and organization of the pumping.

The most common electrical cardiac arrhythmia that demands medical attention is atrial fibrillation. As numerous scientific articles state; "its underlying mechanisms are not fully understood", and atrial fibrillation research is an active, and complex field with many aspects, involving many different scientific disciplines. Since atrial fibrillation is an electrical disorder, one key component in the research is analysis of cardiac electric signals both from healthy volunteers to understand the normal state, and from patients with a history of, or ongoing, atrial fibrillation.

In this study, signals obtained from healthy individuals and from patients suffering from atrial fibrillation have been analyzed and evaluated using a few selected techniques. This dissertation will present those methods along with some results obtained with them, and certain methodological aspects.

1.1 The heart from a system analytic point of view

The purpose of the cardiovascular system is to provide all parts of the body with blood. The system is divided into two circuits: the pulmonary circuit where blood flows from the heart to the lungs and back, and the systemic circuit where blood flows to all other organs of the body, including the heart itself. The heart, which is a muscle, acts as the pump providing the flow of blood through the circuits. The pumping action is the result of a large heart volume at rest being reduced by rapid muscular contraction.

The cardiovascular system is schematically illustrated in Figure 1.1, with two containers (the lungs and the body), four pumps, and four valves. The two ventri-

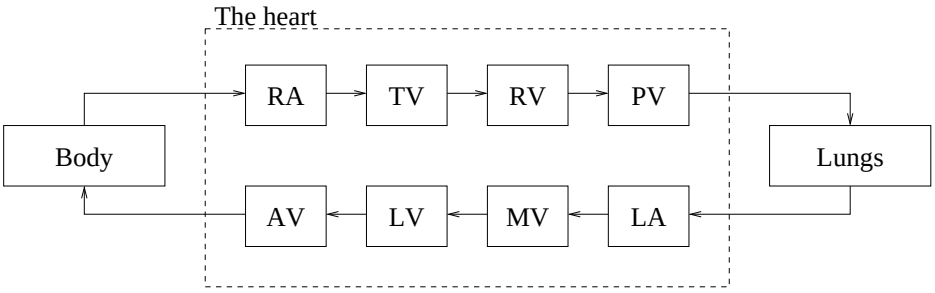

Figure 1.1: Schematic illustration of the hydraulic function of the heart, arrows indicate direction of blood flow. From the body, blood passes through the right atrium (RA), tricuspid valve (TV), right ventricle (RV), and pulmonary valve (PV) to the lungs. From the lungs, the blood passes through the left atrium (LA), mitral valve (MV), left ventricle (LV), and aortic valve (AV) to the body. The atria and the ventricles serve as pumps and all valves are unidirectional to ensure correct direction of blood flow.

cles are powerful pumps where the right ventricle pumps blood into the pulmonary circuit and the left into the systemic circuit. The two atria serve as auxiliary units, increasing the efficiency of the ventricles. To provide blood flow in the correct direction, four unidirectional valves are incorporated in the heart; the tricuspid valve between the right atrium and ventricle, the pulmonary valve at the output of the right ventricle, the mitral valve between the left atrium and ventricle, and the aortic valve at the output of the left ventricle.

In order to ensure maximum efficiency of the four-pump system that is the heart, there is a need for a control system that provides the correct timing of the muscular contraction, the electrical conduction system of the heart (Figure 1.2). The timing impulse is, in the normal case, initiated in the sinus node, a structure in the right atrium with built-in automaticity providing impulses with a frequency of about 60 bpm (beats per minute) at rest and faster when the body's need for blood increases.

From the sinus node, the impulse spreads through the right atrium and continues into the left, resulting in the pumping action of the atria. Also in the right

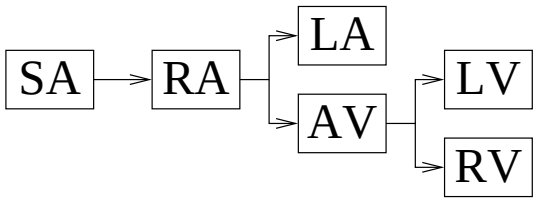

Figure 1.2: Schematic illustration of the timing of the conduction system of the heart. Conduction starts at the sinus node (sino-atrial node, SA) and propagates into the right atrium (RA). From there it continues into the left atrium (LA) and the AV node (atrioventricular node, AV) where it is slowed down before continuing to the left and right ventricles (LV and RV).

atrium, the impulse reaches the input of the AV node, where it is slowed down, or in effect delayed, before continuing into the ventricles. This delay is necessary to ensure that the atria have finished their contraction before the ventricles are activated.

Should the sinus node fail, other structures provide replacement for the missing impulses, with gradually decreasing rates. One such structure is the AV node, which has an automaticity of 40–60 bpm, providing a pumping action which, due to the lack of atrial pumping, is less effective than a normal beat but may still be adequate in producing a blood flow. Other structures that may provide impulses are the ventricles themselves which have a built-in automaticity of 20–40 bpm to provide a 'safety-level' of pumping action and blood flow.

To complete the illustration in Figure 1.2, the connections between the AV node and the ventricles should be extended with additional structures known as the bundle of His, the left and right bundle branches and the Purkinje network. These have been traded for the simplicity of the illustration.

During a lifetime, the heart will perform more than 2.5 billion beats[1]. Unfortunately, the electrical conduction system is not failsafe and in some people the normal, stable rhythm turns into an arrhythmia, some more dangerous than others. The most common cardiac arrhythmia that needs medical attention is atrial fibrillation.

1.2 Electrocardiography

1.2.1 Historical review

Augustus Desiré Waller (1856–1922)

The first non-invasive recording of the electrical activity in the human heart was made in 1887, by Augustus Desiré Waller [1]. Previous work had only been done using electrodes attached directly to the heart and even then, using the most sensitive instrument of the time, the mercury capillary electrometer, the observed deflections were very small.

[1] Based on a rhythm of 60 beats per minute and a lifetime of 80 years

Waller made two important methodological improvements. First, he improved the electrometer by aiming a light beam at the mercury and doing observations on the projected shadow of the mercury instead of on the mercury itself. This, in effect, became an amplification of the very small movements of the mercury in the capillary tube. Waller's second improvement was that he realized that the body itself may be seen as a conductor and therefore it must be possible to record the signals from the heart using skin electrodes. By putting the hands or feet in metal bowls of saline water and attaching these bowls to the electrometer, deflections could be observed. Although Waller was only able to identify two deflections, this was a major step forward in electrophysiology research.

To show his observations, Waller traveled with his bulldog Jimmy, who, on the displays, stood with his paws in jars with saline water, attached to the electrometer.

Willem Einthoven (1860–1927)

One person with interest in Waller's work was Willem Einthoven. By further improving the mercury capillary electrometer, he was able to record a signal showing four clear deflections which he named logically: A, B, C, and D. Einthoven realized that due to the inertia and friction of the electrometer, the recorded signal was not a true reproduction of the electrical signal. The solution was to find a mathematical correction algorithm that would compensate for the distortion and enable conversion from the electrometer-recorded signal to the actual signal (Figure 1.3).

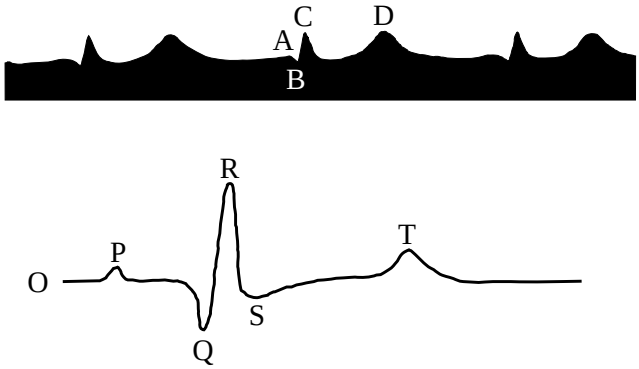

Figure 1.3: Illustration of the signals acquired using mercury capillary electrometer (Top) and after mathematical compensation (Bottom). (Redrawn from [2])

In 1895, Einthoven published his results of the mathematical conversion, showing the underlying form of the electrometer-recorded signal [3]. Five deflections were now clearly distinguishable. To avoid confusion, these could not be named A–E, instead Einthoven chose PQRST, the reason of which is not fully known. The most popular suggestion is that Einthoven, trained in mathematics and familiar

with the works of Descartes, was using the mathematical naming convention where the converted signals get names from the second half of the alphabet. They would then be N, O,... but N, and O, by tradition, has other meanings as 'number' and 'origin of coordinates'. Einthoven therefore put O at the start, or origin, of the isoelectric line and the first deflection from this would then be P, followed by Q, R, S, and T [4, 5, 6].

However, Einthoven was not satisfied with the combination of the electrometer and the mathematical conversion formula and looked for other kinds of instruments. He turned to the newly invented string galvanometer and, after increasing its sensitivity, in 1902 Einthoven was able to record the electrical activity of the heart directly, without the need for mathematical correction [2, 7].

Extensive work was then initialized, by Einthoven and others, to record and classify different heart rhythms and differences in the signals due to different medical conditions. In 1906, Einthoven had organized his work and published his observations of normal and abnormal heart rhythms, including the discovery of the U wave [8].

Einthoven's theoretical model of the conduction of the electrical signals was based on the assumption of the heart as an electrical dipole inside a homogeneous volume. In his experiments, Einthoven's study subjects were sitting with both hands and the left foot in jars filled with saline water. However, according to the model, the arms and the leg would only be conductors of the electrical signal, they would not affect its shape. Since all measurements were bipolar, their directions may be defined and standardized, something Einthoven accomplished in 1912 where he defined lead I as 'right arm to left arm', lead II as 'right arm to left leg' and lead III as 'left arm to left leg' [9]. If these leads are drawn on a human, not between the hands and the left foot but, according to the model, between the upper arms and the upper thigh, they form an equilateral triangle with the heart in the center [9] (Figure 1.4). This triangle is referred to as 'Einthoven's triangle'.

The term 'electrocardiogram' was introduced by Einthoven in 1893 [10]. He claimed that Waller was the first to use the term although Waller himself called the recorded signals 'electrograms'.

Willem Einthoven was awarded the Nobel Prize in Physiology or Medicine 1924, "for his discovery of the mechanism of the electrocardiogram" [11].

1.2.2 Adding more leads

The leads introduced by Einthoven, the limb leads, are all bipolar. By definition these are

$$\begin{cases} I &= E_R - E_L \\ II &= E_R - E_F \\ III &= E_L - E_F \end{cases} \tag{1.1}$$

where E_R, E_L, and E_F are the unipolar, electrical signals measured at the right arm, left arm, and left foot respectively. From these equations follows the important Einthoven's law:

$$I + III = II \tag{1.2}$$

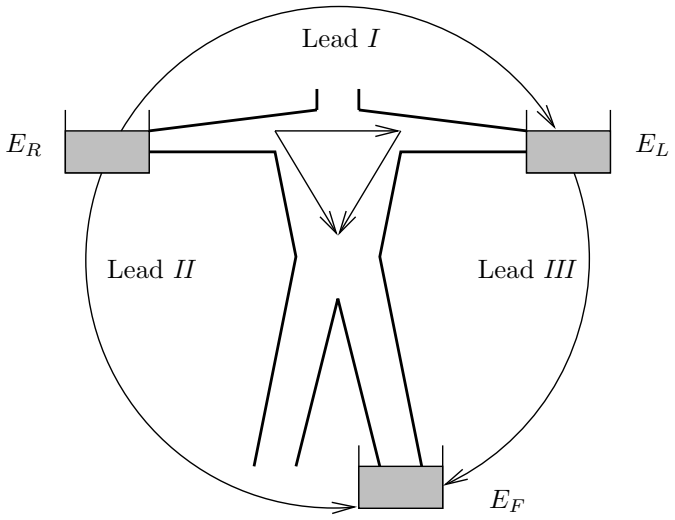

Figure 1.4: Einthoven's triangle. With right and left hand, and left foot in jars of saline water, the three leads I, II, and III can be recorded. Following Einthoven's theory, the arms and left leg only serve as 'conductors' of the signals, and the direction of the leads may then be drawn on the torso, forming an equilateral triangle.

To record the signals E_R, E_L, and E_F, the need for a reference, a 'zero potential' arises since these are unipolar. Such a reference was introduced in 1934 by Wilson [12]. By connecting the limb electrodes he produced the signal

$$E_Z = \frac{1}{3}\left(E_R + E_L + E_F\right) \tag{1.3}$$

which is not a true 'zero' [13, 14] but, nevertheless, has been recognized as the standard reference when recording unipolar signals [15]. The 'zero', or 'central terminal' was first used to record the unipolar signals E_R, E_L, and E_F, which were named V_R, V_L, and V_F (with 'V' for Voltage) [12].

Using the central terminal, it was possible to record unipolar electrocardiograms from any point on the body. For some time, there was confusion as to where these electrodes should be positioned which was settled in 1938 when the American Heart Association and the Cardiac Society of Great Britain agreed on the positions of six chest electrodes [16]. These were named V_1, V_2,... V_6.

The unipolar limb leads V_R, V_L, and V_F introduced by Wilson had lower amplitude than the bipolar leads I, II, and III. In 1942, Goldberger showed an alternative way of measuring these, which would increase their amplitude by 50% [17]. These unipolar limb leads were named 'augmented' leads and were measured as the difference between the electrode on one limb and the average of the other two:

$$\left\{\begin{array}{lcl} aVL &=& E_L - \frac{1}{2}\left(E_R + E_F\right) \\ aVR &=& E_R - \frac{1}{2}\left(E_F + E_L\right) \\ aVF &=& E_F - \frac{1}{2}\left(E_L + E_R\right) \end{array}\right. \tag{1.4}$$

So, in 1942, all the components of what is called the '12-lead ECG' were present. Following this, an enormous amount of work has been made in describing and classifying different ECG findings and connecting these with different medical conditions. Also, the advent and extremely rapid development of computers have enabled increased resolution of recording, and refined and even automated analysis. But still, the shape of the electrocardiogram interpreted by physicians today, is the same as that recorded on a string galvanometer by Einthoven in 1902.

1.2.3 12-lead ECG

The 12-lead ECG can actually be considered as the combination of two different analyses, one based on the bipolar and unipolar vectors recorded using the three limb electrodes and one based on the unipolar recordings from the six chest electrodes.

As shown in Figure 1.5, the directions of the limb electrode vectors are separated 30°, assuming that the lead aVR is rotated 180° to create $-aVR$. The leads are oriented in the up-down, right-left plane, no information is given about conduction directed front-back. Instead, the chest electrodes are positioned in such a way that they cover the heart in a horizontal plane [15], giving additional information. It should be noted that the signals recorded are intended to display the electrical activity of the heart in certain directions, however, there is an effect of locality which for example makes it difficult to observe the conduction at the back side of the heart.

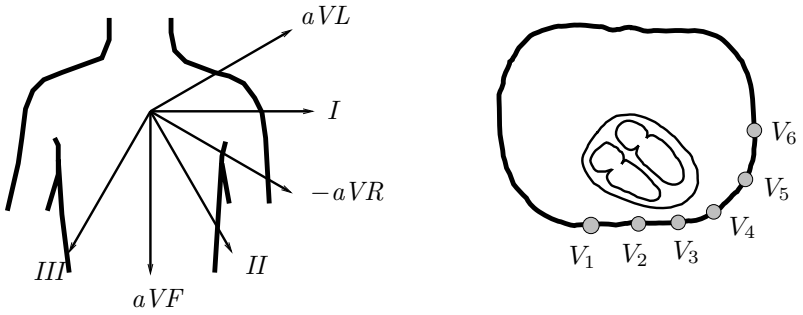

Figure 1.5: The direction of the vectors formed by the three limb lead electrodes (left) and the positioning of the chest electrodes (right) in the 12-lead ECG. The right image shows a cross-section of the torso at the height of the heart.

The interpretation of the ECG is a subject too large to be described here. The reader is referred to for example course textbooks for information.

1.2.4 Vectorcardiogram

The lead configuration of the 12-lead ECG is not based on medical considerations, instead it is the result of the practical considerations of the need for the test subject having both hands and one foot in jars of water. With modern technology,

such considerations no longer apply, and other lead systems may be used, aimed at optimizing analysis possibilities rather than technical issues.

An orthogonal 3-lead system allows interpretation of electrical conduction in the heart in three dimensions, and any possible angle from linear combinations of the three vectors. Such a lead system is named VCG (Vectorcardiogram), and the one most commonly used is that introduced by Frank [18], which is a right-hand orthogonal system with leads oriented and named as (Figure 1.6) [15]:

- right-left, Lead X;
- up-down, Lead Y;
- front-back, Lead Z.

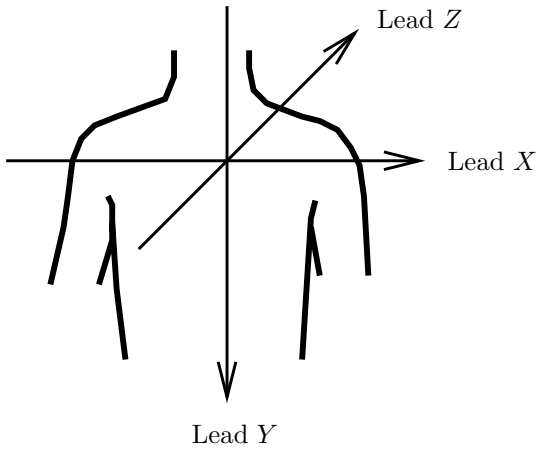

Figure 1.6: Orientation of orthogonal leads as recommended in [15]. Lead X is directed from right to left, Lead Y is directed downwards, and lead Z from front to back. An electrical impulse moving in the direction of the arrows would produce a positive deflection on the VCG. Observation of positive and negative deflections provides a way of geometrical interpretation of the direction of impulse conduction.

Although three leads are less than twelve, the information content available in each of the two systems is equal. Obviously, the knowledge of interpreting ECG may not be immediately transferred to the VCG but, if the leads of the ECG are derived from the VCG, they will present the same clinical information [19].

It should be remembered that the orthogonal axes of the VCG are oriented along the body, and not the heart. When interpreting the signals, the position and angle of the heart inside the body need consideration.

1.3 Sinus rhythm

1.3.1 Electrocardiographic evidence

In a healthy heart, the electrical impulse of the cardiac cycle is initiated at the sinus node, located in the right atrium. The impulse then propagates along the right atrium and further into the left atrium. Before the impulse leaves the right atrium, it also reaches the AV node (atrioventricular node). The impulse is there delayed before it continues towards the ventricles. This impulse conduction results in a stable heart rhythm, 'sinus rhythm', with a distinct P wave being the electrocardiographic sign of normal conduction conditions in the atria (Figure 1.7).

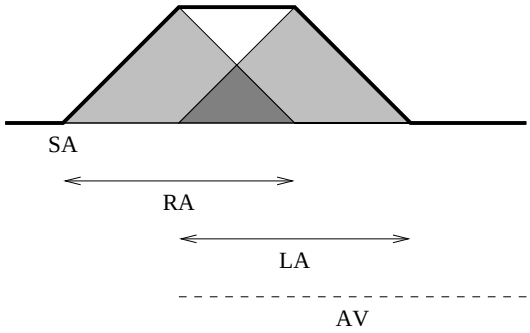

Figure 1.7: Schematic illustration of the origin of a P wave. The impulse is initiated in the sinus node (SA) and from there spreads to the right atrium (RA), left atrium (LA) and AV node. The thick line indicates the resulting electrocardiographic P wave. The AV-nodal activity is drawn with dashed lines indicating that the impulse is being slowed down before continuing into the ventricles, an electrical activity not readily visible on an electrocardiogram.

On the ECG, sinus rhythm is evidenced by a stable heart rhythm with distinct P waves (Figure 1.8).

1.4 Supraventricular arrhythmia

In the case of malfunction in the electrical conduction system of the heart, the result may be a disorganized conduction and, subsequently, irregular heart rhythm, a cardiac arrhythmia. The mechanisms involved in an arrhythmia are either disturbances in impulse initiation, referred to as automaticity, or in impulse conduction, referred to as re-entry [20].

Supraventricular arrhythmias may, in the automatic case, be the result of faulty impulses initiated in the atrial tissue, the AV node or blood vessels communicating with the atria such as the pulmonary veins. In this case, the automaticity of the tissues involved may be higher than that of the sinus node, thus 'taking over' the heart rhythm. In the case of re-entrant impulse conduction, a normally initiated

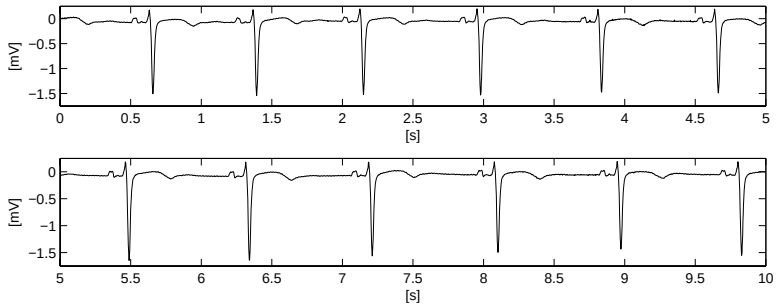

Figure 1.8: Sinus rhythm, lead V_1. A stable rhythm showing distinct P waves.

impulse returns from the ventricles back to the atria through the AV node or other pathways between atria and ventricles. The impulse may then travel in a circuit, resulting in repetitive excitation, again with a higher rate than that of the sinus node. [20]

1.5 Atrial fibrillation

Atrial fibrillation is a supraventricular arrhythmia, and the most common cardiac arrhythmia that needs medical attention [21, 22]. In Sweden, an estimated 100,000 people of a population of 9 million have atrial fibrillation in its chronic form, and an additional 50,000 may have intermittent, self-terminating attacks [23]. Atrial fibrillation is uncommon in people younger than 50 years, but in elderly the occurrence rate may be as high as 10 % [23].

Atrial fibrillation is characterized by a disorganized electrical activation of the atria resulting in uncoordinated contraction leading to loss of efficiency in the blood pumping functionality [22].

Atrial fibrillation is, in itself, not immediately lethal, but is associated with increased long-term morbidity and mortality. The medical conditions most commonly associated with atrial fibrillation are hypertension, thromboembolism possibly leading to stroke, and heart failure [24]. In everyday life, a person with atrial fibrillation may experience for example palpitations, chest pain, and fatigue [22]. There may also be shortness of breath and discomfort due to the deteriorated mechanical function and the, compared to sinus rhythm, often high and irregular heart rhythm.

1.5.1 Electrocardiographic evidence

In the case of atrial fibrillation, the sinus node is no longer initiating the impulse. Instead, the conduction in the atria is seemingly disorganized, possibly with several impulses propagating within, and between, the two atria. The AV node is no longer activated once per cardiac cycle only, it is constantly being bombarded by impulses due to the electrical disorder in the atria. The AV node transmits several of these

impulses to the ventricles, resulting in a heart rate that is no longer stable, but on the contrary has a great variability and, in most cases, is higher than the heart rate during sinus rhythm. Hence, the irregular heart rhythm is the result both of the high rate of impulses reaching the AV node, and of the conduction properties of the AV node itself.

On the ECG, atrial fibrillation is characterized by the absence of P waves and an irregular heart rate. The P waves are missing due to the lack of organized atrial electric activity, instead the ECG baseline is constantly fluctuating with waves of low amplitude (Figure 1.9) [25]. During sinus rhythm, the heart rate is stable with

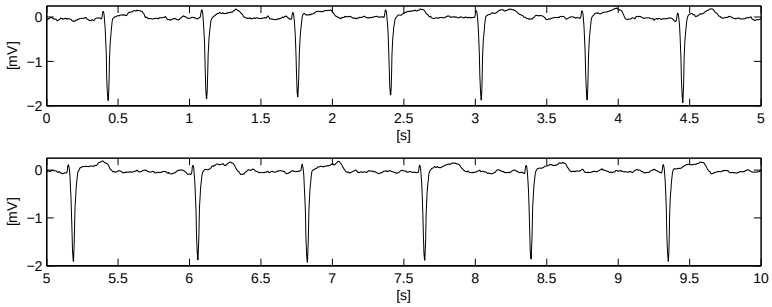

Figure 1.9: Atrial fibrillation, lead V_1. An irregular rhythm with differences in RR interval length. The P waves are missing, instead the baseline is constantly fluctuating with a low amplitude.

small variations synchronized with the breathing frequency, whereas during atrial fibrillation, it is increased and irregular (Figure 1.10) [25].

1.5.2 Classification of atrial fibrillation

Clinically, atrial fibrillation presents itself in two ways: a patient may have atrial fibrillation all the time, or not. In the case where atrial fibrillation is present at all times, it may be classified as continuous, otherwise as intermittent [26]. This simple classification allows focusing on the underlying mechanisms of the arrhythmia. Intermittent atrial fibrillation is connected to the initiating factors since it needs to repeatedly induce new episodes; continuous atrial fibrillation no longer needs initiating and is therefore more related to the factors that allow the arrhythmia to sustain [26].

Clinically, the continuous form of atrial fibrillation may be possible to terminate or not, therefore classification of atrial fibrillation has been proposed to be [22]:

Paroxysmal Intermittent episodes that terminate spontaneously;

Persistent Continuous atrial fibrillation that does not self-terminate but is possible to end pharmacologically or electrically;

Permanent Continuous atrial fibrillation where attempts to terminate have failed, or have not been made.

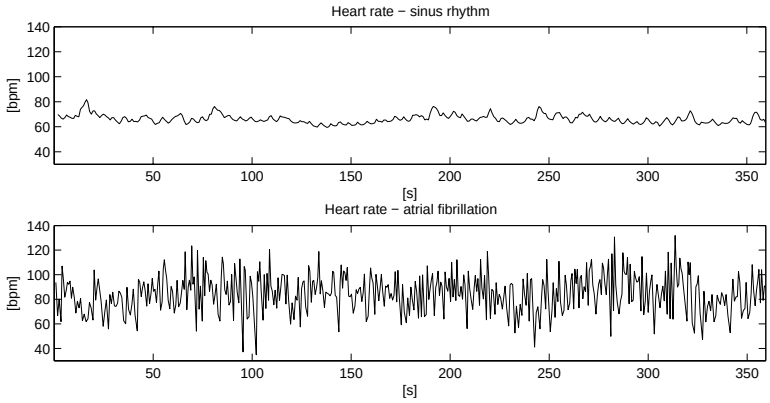

Figure 1.10: Illustration of the differences in heart rate during sinus rhythm (top) and atrial fibrillation (bottom). The fluctuations seen during sinus rhythm, of comparatively lower amplitude and frequency, are due to breathing.

1.5.3 Physiology

In order for atrial fibrillation to initiate, and sustain, there is a need for the electrical conduction properties of the heart to be altered, compared to the healthy case. An initiating factor is needed to start the atrial fibrillation, especially in the paroxysmal case where self-terminated episodes are re-initiated at a later time whereas the persistent and permanent forms of atrial fibrillation need maintaining factors to sustain.

Initiating factors

To initiate atrial fibrillation, there must be a 'trigger', other than the sinus node creating an impulse. It has been suggested that the pulmonary veins may have such properties [27] and that in as many as 9 of 10 patients with atrial fibrillation, such triggers are located in the orifices of the pulmonary veins [28], although this high figure may be challenged [29]. Impulses initiated from this location would propagate into the left atrium and further towards the right, inducing atrial fibrillation.

Patients with paroxysmal atrial fibrillation not based on triggers located at the pulmonary veins may have a similar kind of trigger, located elsewhere in the atria [26]. Other suggested possibilities are re-entry of the impulse via the boundaries between the atria and the ventricles, or via the AV node [26]. Other supraventricular arrhythmias may also deteriorate into atrial fibrillation [23].

Maintaining factors

In order to make atrial fibrillation persistent or permanent, there has to be a maintaining factor, preventing the fibrillation from self-terminating.

One such factor is re-entry, a disorder of impulse propagation, occurring when an impulse repetitively travels around an erroneous circuit [30]. Re-entry may be divided into two different cases: anatomic re-entry and functional re-entry. Anatomic re-entry is present when the path of the erroneous circuit is defined by physical cardiac structures, or anatomical obstacles. Functional re-entry occurs when the electrical conduction properties of the tissue serves as the boundaries for the circuit [30].

Besides being the primary location of triggers initiating atrial fibrillation, the pulmonary veins and their electrophysiological properties [27, 31, 32] may also play a role in the maintenance and sustaining of the arrhythmia.

Atrial fibrillation, in itself, is another maintaining factor. During fibrillation, an electrophysiologic process is active, changing the conduction properties of the heart in such a way that the fibrillation is more easily sustained ("Atrial fibrillation begets atrial fibrillation" [33]). This process is called 'remodeling' [33, 34] and incorporates electrical and structural changes of the atria. Electrical remodeling is linked to the functional re-entry where the electrical changes of atrial tissue enable creation of erroneous, repetitive, impulse conduction circuits [35]. Thus, episodes of paroxysmal atrial fibrillation may, although self-terminated, facilitate the onset of later episodes and eventually enable persistent or permanent atrial fibrillation.

Remodeling will also occur if a trigger, such as those located at the pulmonary veins, initiates repeated impulses rapidly. This kind of 'focal' activity will, in itself, cause atrial arrhythmia and promote the atrial remodeling required to enable re-entry and atrial fibrillation [30].

1.6 Analysis of supraventricular conduction

The electrical properties of supraventricular conduction in the context of atrial fibrillation may be studied using a variety of methods, some of which will be described here. Signals may be recorded using invasive techniques, where the use of cardiac catheters is the most common tool although, for example, open-heart surgery may allow a different approach. Signals may also be recorded using non-invasive techniques, in which case the ECG in different forms is the most common.

All recording and analysis techniques play an important role in the research of atrial fibrillation, some allow studying the ongoing fibrillation itself whereas others aim at studying the normal sinus rhythm for comparison. The latter methods may also be used to study conduction between episodes of paroxysmal atrial fibrillation to understand the initiating, and terminating, factors.

1.6.1 Non-invasive techniques

Signal-averaged P waves

The morphologies, or shapes, of the different waveforms present in the ECG may be used in combination with the geometric electrode placement to interpret both the site of origin [36, 37, 38, 39] and the path [40, 41] of the electrical activation

of the heart. The morphology of the P wave could reflect the interatrial as well as intraatrial conduction patterns of the atria [40].

A popular method in Computer-based analysis of P wave morphology is to produce a signal-averaged P wave which is then bandpass-filtered using one of several suggested techniques [42], typically at 40–250 Hz (Figure 1.11) [43, 44, 45]. It is then possible to extract a number of parameters from this filtered wave.

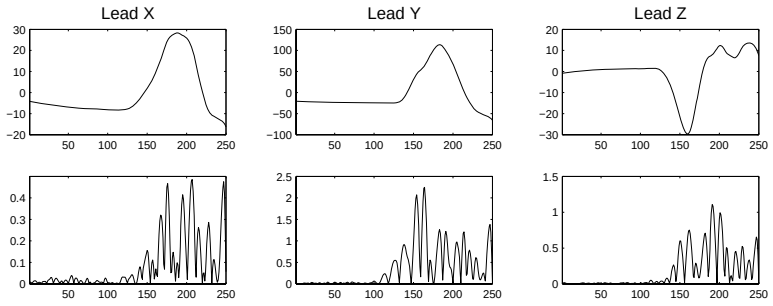

Figure 1.11: Illustration of a bandpass-filtered P wave. The top row shows the unfiltered P wave morphology, the lower shows the result after bandpass filtering at 40–250 Hz and calculating the absolute value of the result.

Most often the duration is used, shown in numerous studies to be prolonged in patients with a history of atrial fibrillation compared to healthy individuals [46, 47, 48] and also in patients with persistent atrial fibrillation compared to those with paroxysmal [49], observations suggested to be linked to an enlargement of the atria [50]. Variations of the method include examining differences between the duration measured in different leads [46] or studying the signal segment at the end of the P wave [43, 44, 45].

The use of the bandpass-filtered P wave excludes the analysis of the true morphology, in this case an 'unfiltered' approach is needed. Such an analysis has the advantage that it, combined with orthogonal lead recordings may provide the possibility of a geometrical interpretation of the underlying atrial excitation [51].

From a signal processing point of view, the P wave in the ECG is a small waveform that has a poor signal-to-noise ratio. In the clinical setting, the possibility of detailed analysis of the the P wave is therefore limited. In order to look at the morphology of the P wave, it needs to be 'magnified', and the noise level reduced. Based on the assumptions that the noise is not statistically correlated with the P waves and that several P waves are of similar shape, signal averaging would be a suitable approach. The advantage of signal averaging is that by averaging n waves, the amplitude of uncorrelated noise will be reduced by $\sqrt{n}$ while leaving the signal unaffected [52]. Its disadvantage is that the result can only show an average wave, it does not allow analysis of the individual waves.

Frequency analysis of atrial fibrillation

As illustrated in Figure 1.9, an ECG recording of atrial fibrillation displays no P waves but instead a constant electrical activity in the atria. One way of charac-

terizing this activity is to perform a spectral analysis of the atrial signal [53, 54].

The first step is to reduce the QRST waves [55, 56], since their large amplitude would affect the subsequent spectral analysis. The frequency at the spectrum peak is used as a measure of the dominant atrial fibrillation frequency of the recording. If short segments of the ECG are used, it would be possible to perform an analysis of the variation of the atrial fibrillation frequency over time [57].

The method offers an attractive, non-invasive way of characterizing atrial fibrillation using techniques readily available at almost any clinical location, i.e., a recorded standard ECG and an analysis computer. The method has been applied in several studies, for example [58, 59, 60, 61].

RR interval analysis

The distribution of RR intervals has been shown to vary when heart range changes [62, 63]. By taking sequences of 64 RR intervals and drawing different histograms, according to the mean heart rate of the individual sequences, the distribution of RR intervals during different heart rates could be visualized. The analysis revealed that during atrial fibrillation, as opposed to sinus rhythm, changes in heart rate are not produced by one single RR interval distribution moving, but instead of the increase or decrease of two distributions at fixed positions, one with long RR intervals and one with short (Figure 1.12).

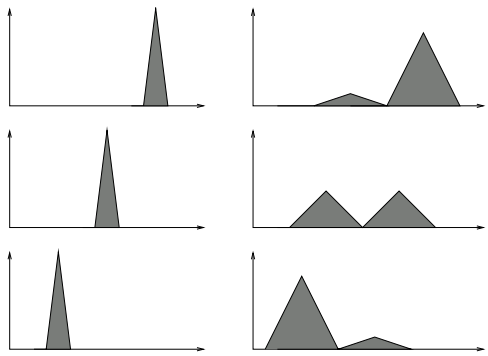

Figure 1.12: Schematic illustration of the two different mechanisms of changes in RR interval distribution during increasing heart rate. Left column shows the healthy case where a stable rhythm results in a single, narrow distribution moving toward shorter RR intervals. Right column shows the mechanism found in the case of atrial fibrillation, where heart rate changes as a result of two RR interval populations increasing or decreasing. Note that the peak locations move in this case as well.

The two distributions of RR intervals are believed to be the result of the AV node having two different entries within the right atrium, both with different electrical conduction properties. The entries are named the 'slow' and 'fast' pathways, where the slow pathway is characterized by a short refractory period and low conduction velocity and the fast pathway of long refractory period and

high conduction velocity. The slow pathway would then be the cause of the short RR intervals and the fast pathway the cause of the long RR intervals.

By using medical intervention, the bimodal distribution may be affected and an RR interval analysis allows investigation of whether the two distributions are equally affected or if the different pathways of the AV node respond in different ways to the treatment.

Alternatively, modification of the inputs to the AV node by ablation procedures shows altered patterns of the RR interval distribution, and may transform a double distribution of RR intervals into a single [64].

An alternative way of presenting the RR interval information would be to use a Lorenz plot [65], a '2-dimensional' histogram of observations of consecutive pairs of RR intervals. Some additional information may be extracted from this, compared to the histogram analysis described above. However, the analysis does not include information on the RR interval distribution changes that are connected to changes in heart rate.

By calculating the difference between two consecutive RR intervals, a difference histogram may be created. Combined with the RR interval histogram, it may give information about the structure of different heart rhythm patterns [66].

1.6.2 Invasive techniques

Catheter recordings

Analysis of recordings made using cardiac catheters in an electrophysiology laboratory perhaps provides the most direct and accurate results of atrial conduction. The ECG has a drawback in that an electrode will always record an 'average' signal from a larger area of the heart compared to the catheter which measures a more local signal. The sacrifice is obviously the invasive nature of the catheter procedures. Another advantage of the catheter technique is that it does not only allow recordings of signal, it also allows electrical interventions, such as paced stimulation, and ablation. A few catheter-based studies from our group are [67, 68, 69].

A drawback of the catheter based techniques is that it is difficult to orient inside the heart. This has been overcome by new techniques that combine the catheter with different techniques of localization, examples of such systems are CARTO [70], LocaLisa [71], and EnSite NavX [72]. A few studies from our group using the CARTO system are [73, 74, 75].

Open-heart surgery recordings

Catheter-based techniques are aimed at recording signals from the inside of the heart. During open-heart surgery, there is an opportunity to record signals from the outside. Using an electrode array, positioned on the heart, our group has previously identified atrial conduction patterns [76, 77, 78].

Chapter 2

Aims

2.1 Outline of the study

The aim of the study presented in this dissertation was to implement, evaluate, and describe selected methods for exploration of the supraventricular conduction, in healthy people and those with a history of atrial fibrillation. Supraventricular conduction is, obviously, conduction in the parts of the heart that are not the ventricles. Figure 2.1 shows an outline of those; the sinus node, right and left atria, and the AV node. Figure 2.1 also indicates the parts that are covered in

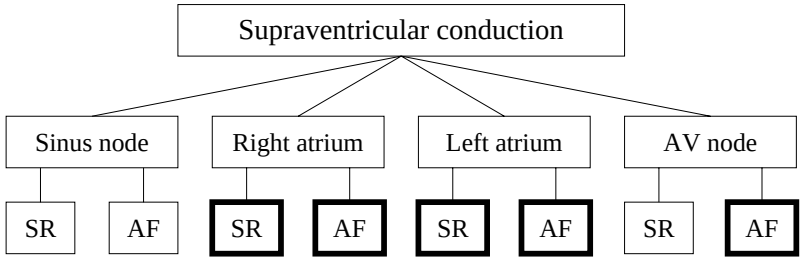

Figure 2.1: Supraventricular conduction, i.e., conduction in the sinus node, right and left atria, and the AV node. The study described in this dissertation covers the parts surrounded by thick solid lines. 'SR' and 'AF' denotes studies on healthy subjects and those with a history of atrial fibrillation, where the latter may be made both during sinus rhythm and atrial fibrillation

this study, using thick solid lines. The abbreviations 'SR' and 'AF' should in this case be understood as investigations made on healthy people and those with a history of atrial fibrillation, respectively. In the the latter case, subjects may not necessarily be in the state of atrial fibrillation at the time of the recording.

2.2 Aims

Study of AV-nodal conduction properties

During atrial fibrillation, the atrial activation rate is much higher than the ventricular. The difference between them, and the irregularity of the ventricular rate, is attributed to the conduction properties of the AV node. These may be analyzed by the distribution of RR intervals at specific heart rates.

The aim of the study (Paper I) was

- to further develop the method of heart rate-stratified histogram analysis [62, 63] to allow a more detailed analysis;
- to apply the method to study the effect of RR interval distribution following a medical intervention.

Study of atrial conduction

The conduction of the right and left atria may be studied using the morphology of signal-averaged P waves. The morphology enables interpretation of the direction of conduction and the comparison between recordings during sinus rhythm in healthy volunteers and patients with a history of atrial fibrillation. By using orthogonal VCG leads, it may also be possible to identify the part of the atria responsible for differences in morphology.

The aim of the study was

- to further develop the method to allow analysis of parameters describing the morphology of signal-averaged P waves [51];
- to further develop the method to allow analysis of P waves of different morphologies in the same recording to assess the variability of atrial conduction.

Modeling of P waves using linear systems

The complexity of signal-averaged P waves may be described in different ways. A low level of complexity may be chosen, describing P waves simply as 'positive', 'negative', or a combination of the two. At a higher level of complexity, different parameters may be used, such as locations and amplitudes of local maxima and minima.

A different approach is to use system identification and create a model that will reproduce the P wave. The properties of the model may then be used to assess the complexity of the signal-averaged P wave.

The aim of the study (Paper II) was

- to model signal-averaged P waves using linear systems;
- to evaluate the complexity of signal-averaged P waves based on the modeling results.

Classification of different P wave morphologies

When comparing signal-averaged P waves from healthy volunteers and patients with a history of atrial fibrillation, characteristic differences may be seen. Describing such differences in intuitive and directly observable parameters have proved difficult.

The aim of the study (Paper II) was

- to implement and evaluate a method to classify any choice of parameters into either of two groups;
- to apply the method to the problem of classifying two different kinds of P wave morphologies using different choices of parameters.

Evaluation of mathematical lead conversion

The differences in signal-averaged P wave morphology associated with propensity to atrial fibrillation may be easily detected in recordings of VCG performed using an orthogonal lead system. In the clinical routine however, the dominant system is the 12-lead ECG.

The aim of the study (Paper III) was

- to implement and evaluate a method to mathematically transform a recorded 12-lead ECG into orthogonal vectors;
- to evaluate whether signal-averaged P wave morphology parameters associated with atrial fibrillation are preserved in the transform.

Study of left atrial conduction patterns

Previously, atrial fibrillation was recognized as a random conduction pattern in the atria. This has later been questioned and the conduction is instead characterized as having preferential patterns.

The aim of the study (Paper IV) was

- to further develop and evaluate a method to allow analysis of conduction patterns along a multipolar cardiac catheter [67];
- to apply the method to signals recorded with a catheter placed inside the coronary sinus, allowing analysis of the left atrial conduction patterns.

2.3 Outline of the dissertation

The **Introduction** contains a background to the analysis of supraventricular conduction, with overviews of the function of the heart, electrocardiography, sinus rhythm, and atrial fibrillation. The **Introduction** also contains an overview of the analysis of supraventricular conduction with an introduction to the methods described in this dissertation.

The **Methods** chapter contains a concise description of the various different methods used in the study.

The **Results** chapter contains the results of both the evaluation of the different methods and the analyses of data.

The **Discussion** contains methodological aspects of the different methods used in the study.

The appendices contain detailed descriptions of the methods used in the study. **Appendix A** is a description of the heart rate-stratified histogram analysis used in analysis of AV-nodal conduction properties. **Appendix B** is a description of the method used to extract signal-averaged P waves, and analyze their variability and morphology. **Appendix C** is a description of the inverse Dower transformation used to mathematically convert 12-lead ECG recordings into orthogonal leads. **Appendices D** and **E** are descriptions of the methods used for automatic classification of signal-averaged P wave morphology and the P wave modeling used to create the parameters used in the classification algorithm. **Appendix F**, finally, is a description of the correlation function analysis used to assess the similarity and time propagation of the catheter signals recorded inside the coronary sinus.

Chapter 3

Methods

3.1 Data acquisition

3.1.1 Ambulatory ECG

Ambulatory ECG recordings were performed using a Model 423 Dynacord Cassette Holter Recorder (DelMar Avionics, Irvine, CA, USA). The cassette was then read using a Model 263 StrataScan Holter Analysis System (DelMar Avionics, Irvine, CA, USA) where automatic extraction of RR interval information was performed. The RR intervals were denoted as their length, in milliseconds, or as 0 or 9999 if any of the corresponding QRS-complexes were classified as something other than 'narrow QRS-complex'.

The sampling frequency of the tape reader was 128 Hz but for interval information only 64 Hz resolution was used, resulting in an RR interval resolution of 15.625 ms, although only the truncated, integer values of the RR intervals were recorded. Only RR intervals with length between 200 and 1500 ms (40-300 bpm) were included. The possible values of RR-intervals are

$$\{203.125, 218.750, 234.375, 250.000, 265.6250 \ldots\}$$

which, truncated, yields

$$\{203, 218, 234, 250, 265 \ldots\}$$

The 'true' resolution is 15.625 ms but after the truncation becomes

$$\{15, 16, 16, 15, \ldots\}$$

The RR interval information was exported as an ASCII text file for further analysis.

3.1.2 ECG and VCG

Collection of data was performed using an internal ISA A/D card in an ordinary PC, connected to the study subject via a standard ECG cable and electrodes.

The electrode configuration could be the standard 12-lead ECG or the Frank-lead VCG. The A/D card samples ECG with the frequency 1000 samples per second and channel using 16 bits at a resolution of 0.625μV. The A/D-card, drivers and acquisition software was supplied in a research cooperation with Siemens Elema AB.

All ECG and VCG recordings were performed with the subjects at rest.

Frank-lead electrode placement

Frank-lead vectorcardiograms are calculated from unipolar signals recorded from seven positions of the body [18], five on the torso, one on the back of the neck, and one on the left foot. However, the equipment used in this study, described above, is designed to record 12-lead ECG and can only record six unipolar signals and the three bipolar limb leads. This was solved by recording Frank-lead VCGs using the electrode positioning shown in Figure 3.1, where the six unipolar inputs record the signals from the torso and the back of the neck, whereas the limb leads are used to calculate the signal from the left foot.

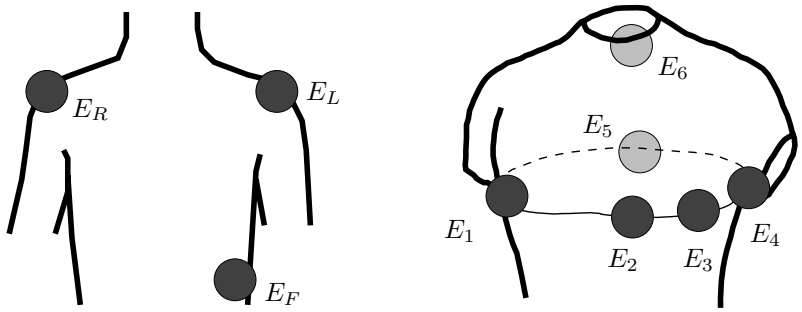

Figure 3.1: Electrode placement, Frank-leads. Due to the acquisition equipment not recording the left foot signal of Frank's equations, the standard limb lead electrodes, E_R, E_L, and E_F needs to be recorded (Left, see text). Additionally, the six unipolar leads defined by Frank should be recorded from positions E_1–E_6 (Right). Signals from both sets of electrodes should of course be recorded simultaneously but the sets have been separated to simplify the description.

The six electrodes E_1–E_6, usually used to record the 12-lead ECG chest leads V_1–V_6, were positioned at the locations named I, E, C, A, M, and H by Frank. The signal from the left foot, the position named F by Frank, may be calculated using Einthoven's limb lead equations and Einthoven's law (Equations (1.1) and (1.2)) as:

$$V_F = \frac{II + III}{3} = \frac{2II - I}{3}$$

The original term in Frank's equations, $0.655V_F$, may then be substituted for $0.437II - 0.218I$, and the resulting equations used to calculate Frank-lead VCG

in this study would then be:

$$\begin{aligned} X &= -0.781V_1 + 0.171V_3 + 0.610V_4 \\ Y &= 0.345V_5 - V_6 - 0.218I + 0.437II \\ Z &= -0.264V_1 - 0.374V_2 - 0.231V_3 + 0.133V_4 + 0.736V_5 \end{aligned} \tag{3.1}$$

where V_1 would, in this case, denote the signal recorded from the electrode at position E_1 as shown in Figure 3.1, etc.

It should be noted that, in difference to the 12-lead ECG in Figure 1.5, the Frank lead system includes one electrode positioned on the back, which may record local information not readily available in the ECG.

3.1.3 Electrogram recordings

Electrograms were recorded from the coronary sinus using a 10-pole catheter (Dynamic XT 201-101, Bard Electrophysiology, Lowell, MA, USA). Pole 1, the tip of the catheter, was in the distal coronary sinus and pole 10 at the orifice.

The electrodes on the catheter are 1 mm wide and positioned in pairs, with 5 mm spacing between the pairs and 2 mm between the electrodes in each pair. In total, a distance of 40 mm may be covered by the electrode.

The signals were recorded using a BARD Cardiac Mapping System (BARD LabSystem DUO, Bard Electrophysiology, Billerica, MA, USA). Ten unipolar electrograms and a 12-lead ECG were recorded simultaneously using a sampling speed of 1 kHz per channel and a resolution of 16 bits.

The electrograms and Lead V_1 of the ECG were exported as a binary file for subsequent analyses.

3.2 Analysis tools

The methods described in Appendices A, B, C, D, E, and F were all implemented using contemporary versions of MATLAB (www.matlab.com). To increase speed of execution, some parts were written in C [79], and compiled with gcc (gcc.gnu.org) to create MATLAB-compatible mex-files. All programs were intended to be run on a GNU/Linux workstation. In the present study, contemporary versions of RedHat Linux (www.redhat.com) and later Fedora Core (www.redhat.com/fedora) were used.

ECG and VCG recordings were transformed into the wfdb format used by Physionet [80]. This was not needed for analysis purposes but allows the use of a wide range of software developed for the purpose of processing ECG files, for example WAVE. A set of mex-wrappers for the wfdb software routines were created to allow data handling directly in MATLAB. These wrappers are freely downloadable from Physionet's homepage (www.physionet.org).

3.3 Statistical analyses

3.3.1 Paper I

Comparisons between observations from two groups were performed using the Wilcoxon signed rank test. Statistical significance was defined at the level $P < 0.05$.

3.3.2 Paper II

Evaluation of whether parameters were normally distributed was performed using the Kolmogorov-Smirnov test. Comparisons of parameters from two different groups were performed using the Wilcoxon rank sum test[1], calculated using the MATLAB function ranksum. Statistical significance was defined at the level $P < 0.05$.

3.3.3 Paper III

Paired comparisons of parameters obtained from one group were performed using the Wilcoxon signed rank test. Comparisons between parameters from two different groups were performed using the Wilcoxon rank sum test. Comparisons between parameter sets and a scalar were performed using the Wilcoxon signed rank test. Calculations were performed using the MATLAB functions ranksum and signrank. Statistical significance was defined at the level $P < 0.05$.

3.3.4 Remarks

Besides comparisons between two observations from one group, or between observations from two groups, several methods used in this study are based on a statistical approach. The maximum correlation coefficient calculated from correlation function analysis described in Appendices B and F is based on the covariance between signals. The Fisher linear discriminant described in Appendix E is based on the distribution of multidimensional parameter sets.

3.4 Analysis of AV-nodal conduction during atrial fibrillation

The properties of AV-nodal conduction during atrial fibrillation were studied using heart rate-stratified histograms of RR interval distribution. The method is described in detail in Appendix A.

3.4.1 Creating heart rate-stratified histograms

RR interval information was extracted from ambulatory ECG recordings. From each recording, a number of histograms were created, illustrating the distribution of RR intervals at specific heart rate intervals. The histograms were created by

[1] In Paper II referred to as the Mann-Whitney U test

taking sequences of 20 RR intervals, calculating the mean heart rate and adding the 20 RR intervals to the histogram with the corresponding heart rate interval.

From previous studies [62, 63] it was known that such histograms often reveal two distinct distributions, with long and short RR intervals. To find the peaks of such distinct distributions, the histograms were smoothed using a 3-term simple moving average filter, applied repeatedly until no peaks were found closer to each other than 50 ms.

To increase resolution beyond the 15.625 ms of the recording system, a second-order polynomial was fitted to the middle bar of a peak and the two adjacent bars on each side. This would allow an arbitrary resolution of peak location, which was chosen to 1 ms.

3.4.2 Measured histogram parameters

When two or more distributions were observed in the histograms, a heart rate level might be observed where a distribution of shorter RR intervals takes precedence over a distribution with longer ones, i.e., the peak amplitude became higher. This heart rate level was defined as PDC (peak dominant change).

To characterize the histograms, four parameters were used. PV(s) (peak value, slow heart rate) was the peak location of the major distribution of long RR intervals; PV(f) (peak value, fast heart rate) was the corresponding value of the short RR intervals; PG (peak gap) the difference between the two, and PVR (peak value ratio) the ratio between them. In Paper I, the parameters were only calculated from the PDC histogram.

If only one RR interval distribution was observed in the histograms, this was treated as two superimposed distributions with parameter values PDC=NA (Not Applicable), PG=0, PVR=1.00, PV(f) and PV(s)=NA.

3.4.3 Study material

Ambulatory ECG recordings were performed on 24 patients, suffering from persistent atrial fibrillation. The patients were divided into two groups, A and B, with 11 patients in Group A and 13 in Group B. In Group A, one 24-hour long control recording and one 24-hour long intervention recording were made on each patient. In Group B, one 12-hour long recording was made, where the first part served as a control for the second, intervention, part. In both groups, the intervention consisted of infusion of magnesium, glucose, insulin, and potassium [81]. The patients and the background of the specific interventions are described in detail in Paper I.

Three comparisons were made:

- In group A, comparison between the control recording and the intervention recording;
- In group A, comparison between the first and last seven hours of the intervention recording;
- In group B, comparison between the first and last four hours of the recording.

3.5 Analysis of right and left atrial conduction during sinus rhythm

Non-invasive analysis of the right and left atrial conduction during sinus rhythm was performed using Frank-lead VCG recordings, where signal-averaged P waves were used to interpret the underlying atrial electrical excitation. The method used to extract signal-averaged P waves is described in detail in Appendix B.

3.5.1 Extracting P waves

P waves generally have too low SNR (signal-to-noise ratio) in order to be directly extracted from the VCG. To increase SNR, signal-averaging of several P waves was performed.

Under the assumption that P waves precede the ventricular activity, the first step was to detect the QRS complexes and to create groups of QRS complexes with similar morphology. This enabled a 'filtering' of erroneous beat detection, QRS-like artifacts, and exclusion of non P wave-preceded ventricular activity, e.g. ventricular ectopic beats.

Signal segments preceding a chosen group or groups of QRS complexes were extracted and groups of such segments with similar morphologies were created. For each individual group, the signal average was calculated and each individual signal segment in the group was time-shifted and compared with the group's average to find an offset creating maximal agreement. Using the time-shifted signal segments, the group's signal average was then recalculated.

The onset and end of each group of QRS complexes and P waves were set manually. The definition of a P wave was then the part of a signal average between the manually defined onset and end.

3.5.2 Evaluation of manual setting of P wave onset and end

In order to evaluate the reproducibility of the manual setting of onset and end of the signal averaged P waves, three different individuals each performed two blinded settings on a test set containing 47 Frank-lead VCG recordings of healthy subjects and patients with a history of atrial fibrillation. All P waves were presented in random order in each test.

The different observers were:

Physician A cardiologist, well acquainted with the method, considered being the 'golden standard';

Engineer Not trained in clinical interpretation of ECG, well acquainted with the method;

EP nurse Nurse with ECG experience from an electrophysiology lab, unfamiliar with the method.

Evaluation was performed both between the different settings of each observer, and between the different observers.

3.5.3 Analysis of morphology

Before extracting parameters describing P wave morphology, the signal-averaged P waves were smoothed to reduce noise further. A smoothing filter was applied iteratively until no local maxima or minima were found closer than 20 ms (i.e., the period of 50 Hz powerline interference).

The morphology of the P waves were then described using the location and amplitude of the remaining local maxima and local minima, and the location of zero crossings. In order to produce comparable values for these parameters, the amplitude was set to 0 at the onset of the P wave.

In the study described in Paper III, a vector magnitude was calculated to enable analysis of overall atrial activation, regardless of direction of activation spread. The magnitude, conventionally defined as [40, 82, 83, 84]:

$$SM = \sqrt{X^2 + Y^2 + Z^2} \tag{3.2}$$

and named 'Spatial magnitude', would only be applicable in analyses of orthogonal lead recordings.

3.5.4 Analysis of variability

The variability of P wave morphology was evaluated by the number of groups found with different P wave morphologies, the number of members in each group, the differences in morphologies between the groups, and the switching between groups of individual, consecutive, P waves.

3.6 P wave modeling

Modeling of signal-averaged P waves was performed to evaluate feasibility and to assess the complexity of such signals. P waves were approximated as the atrial electrical response to an external or internal stimuli and modeled as the impulse response of a linear system. The details of the modeling algorithm are described in Appendix D.

3.6.1 System identification

Each P wave was treated as the output, y, of a linear system

$$\left\{ \begin{array}{rcl} x_{k+1} & = & Ax_k + Bu_k \\ y_k & = & Cx_k + Du_k \end{array} \right.$$

The system matrices A, B, C, and D were estimated from data using the theory developed by Ho and Kalman [85], and further by Kung [86].

Two model orders were used, the most appropriate as indicated by the modeling algorithm, and order 5, for comparison of performance.

3.6.2 Analysis of residuals

Evaluation of the performance of the system identification was made by means of residual analysis, i.e., the difference between the original signal and the output of the modeled system. To quantify the difference, the residual magnitude was calculated by dividing the 2-norm of the residual with the 2-norm of the original signal.

3.6.3 Study material

Frank-lead recordings from 52 healthy subjects and patients with a history of atrial fibrillation were used. Signal-averaged P waves were extracted using the method described in Appendix B, except for the smoothing procedure.

3.7 P wave classification

Based on a previous study [40], the morphology of signal-averaged P waves were classified as either 'normal' or 'possible interatrial conduction defect'. The Fisher linear discriminant, described in detail in Appendix E, was calculated, and its performance in automatically classifying P waves was evaluated.

3.7.1 Fisher linear discriminant

Classification into one of two possible groups was made using the Fisher linear discriminant [87]. The method uses projection to reduce a multi-dimensional parameter set into a one-dimensional number. The discriminant was calculated using two groups of parameter sets with known classification.

To evaluate the performance, a retrospective analysis was performed by comparing each individual set of parameters to the previously defined classification.

A prospective test was performed by applying the discriminant on data not included in its calculation.

3.7.2 Parameter sets

A number of different choices of parameter sets were evaluated as input data to the Fisher linear discriminant. In the study described in Paper II, three different parameter sets were tried, all from the P wave modeling described in Section 3.6:

- the absolute values of the eigenvalues of the matrix A;
- the coefficients of the denominator polynomial of the transfer functions;
- the coefficients of the numerator polynomial of the transfer function of Lead Z.

Beside these, the signal itself was used as a parameter set, with different degrees of decimation. The decimation factors 1 (i.e., the original signal), 5, 10, and 20 were evaluated in an attempt to reduce the amount of data.

3.7.3 Study material

Frank-lead VCG recordings from 52 subjects were used, 27 from healthy subjects and 25 from patients with a history of atrial fibrillation. In a first experiment, twenty recordings from each group were used as a 'training set' and the remaining 12 as an 'evaluation set'. Additionally, different sizes of the training and evaluation sets were used.

P waves were extracted from leads X, Y, and Z using the method described in Appendix B, except for the smoothing procedure. The P waves of each individual recording were then classified manually as belonging to either of two classes; 'normal' or 'possible interatrial conduction defect' based on their morphologies [40].

3.8 Lead conversion

Signal-averaged P waves from Frank-lead VCG recordings may be used to geometrically interpret the underlying atrial conduction pattern. Since the normal clinical procedure is to record 12-lead ECG, the inverse Dower transform was used to evaluate whether derived VCG contains the same information as recorded VCG. The inverse Dower transform is described in detail in Appendix E.

3.8.1 Study material

Two groups were studied, healthy subjects and patients with a history of atrial fibrillation. The latter were verified to be in sinus rhythm at the time of recording.

Recordings were performed on 25 patients. Unfortunately, four of these had to be excluded due to either the ECG or VCG recording being faulty, leaving 21 cases. To match these, the first 21 recordings in a database of healthy subjects were used.

One 12-lead ECG and one Frank-lead VCG were recorded in each study case. Eight leads of the ECG; V_1–V_6, I, and II, were transformed into a derived VCG by using the inverse Dower transform. Using the method described in Appendix B, signal-averaged P waves were then extracted from the ECG, recorded VCG, and derived VCG.

3.8.2 Comparison between ECG and derived VCG

The morphologies of the signal-averaged P waves from the analyses of ECG and derived VCG were not compared directly, because of the difference in lead configuration. Instead, only indirect measures were used in the comparison. The parameters used were:

- number of P wave groups found;
- number of members in the largest P wave group found;
- P wave duration;
- PQ time.

In the ideal case, all these parameters should have equal outcome in both analyses.

3.8.3 Comparison between recorded VCG and derived VCG

The same parameters as described in the previous section were used as an initial comparison between recorded and derived VCGs. Additionally, the morphology of the signal-averaged P waves from the recorded and derived VCG were compared in two ways: by correlation coefficient, and by residual analysis. Before comparison, the amplitude scaling and offset parameters of the derived VCG were adjusted to minimize the difference between the recorded and derived VCG by means of least-squares fitting.

To compare P wave morphologies, several parameters were evaluated (Figure B.1):

- location and amplitude of maximum in Lead X, $X_{\max}$;
- location and amplitude of maximum in Lead Y, $Y_{\max}$;
- location and amplitude of minimum in Lead Z, $Z_{\min}$;
- location and amplitude of first zero crossing in Lead Z located after $Z_{\min}$, Z_{zero};
- location and amplitude of maximum in Lead Z located after Z_{zero}, $Z_{\max}$;
- distance between two peaks in the Spatial magnitude, SM_{diff}.

3.9 Analysis of left atrial conduction during atrial fibrillation

To assess the similarity between electrograms recorded using a catheter, and the direction of conduction along the catheter, correlation function analysis was used. The method is described in detail in Appendix F.

3.9.1 Study material

Fourteen patients admitted for clinical electrophysiologic examinations were included in the study. Of these, seven[2] were diagnosed with paroxysmal atrial fibrillation, three with ectopic atrial tachycardia, two AV reentrant tachycardia, and two AV-nodal reentrant tachycardia.

In each patient, at least 60 s long recordings of unipolar electrograms were performed.

Eighteen recordings were performed on the 14 patients, with multiple recordings made on two patients with ectopic atrial tachycardia (recordings both during sinus rhythm and atrial tachycardia), and two patients with paroxysmal atrial fibrillation (recordings both during sinus rhythm and atrial fibrillation).

[2]Not six as stated in Paper IV

3.9.2 Signal preprocessing

Low-frequency distortions were reduced in the electrograms and lead V_1 by calculating the component and then subtracting it. The distortion was calculated using a 3^{rd} order Butterworth low-pass filter with cut-off frequency 0.5 Hz by means of the MATLAB functions butter and filtfilt.

Powerline (50 Hz) interference was reduced using a subtraction algorithm [88].

3.9.3 Removal of ventricular artifacts

Electrogram segments distorted by ventricular activity were removed by performing a linear interpolation of the signal. The segments of ventricular activity were identified using automatic detection of QRS complexes [89] in ECG Lead V_1. All signals were inspected manually to assure that all artifacts emanating from ventricular activity were minimized.

3.9.4 Correlation function analysis

Electrograms were pairwise time-shifted ± 20 ms in steps of 1 ms, and for each step the correlation coefficient was calculated. In each of the nine possible pairwise comparisons, the maximum value of the correlation coefficient and its corresponding time-shift were recorded. From the sign of the time-shift parameter, the conduction direction was derived, and from the value of the correlation coefficient, the similarity of the activation patterns in the two electrograms was evaluated.

Chapter 4

Results

4.1 Heart rate-stratified histogram analysis

Unfortunately, no evaluation could be made of the performance of the R wave detection. The DelMar system is based on proprietary software and file formats. The system has a feature to allow manual correction of the classification of, for example, ventricular ectopic beats, but the numerical accuracy of the wave detection could not be examined. It was noted that most recordings contained periods without RR intervals detected.

4.1.1 Evaluation of sequence length

The length of the RR interval sequences was not seen to significantly alter the appearance of the histograms. Using longer sequences would produce fewer histograms, resulting in loss of information of the RR interval distribution at low and high heart rates. Shorter sequences would, accordingly, produce more histograms with information at more heart rates but at the cost of losing information of the double-peaked RR interval distribution in individual histograms. An example of the differences between two analyses using sequences of different length is illustrated in the following example:

> **Example 4.1.** From one recording of ambulatory ECG, two HRSH analyses were performed, one using sequences of length 5 and another using sequences of length 250 (length of step is one in both cases). The result is shown in Figure 4.1. In the case of length 5, sequences were found with mean heart rates between 50 and 190. With length 250, heart rates were between 75 and 155. The histograms in Figure 4.1 made from sequences of length 5 contained 33045, 34250, and 33885 RR intervals which is equal to 6609, 6850, and 6777 sequences. The histograms made from sequences of length 250 contained markedly more RR intervals: 1926500, 2664000, and 2436250 although the number of sequences were of the same order of magnitude: 7706, 10656, and 9745.

In the study described in Paper I, a number of different lengths of sequences were evaluated. A sequence length of 20 was chosen as an empirically obtained

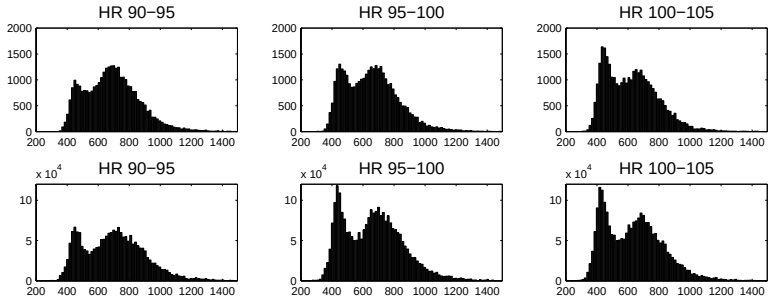

Figure 4.1: Example of the difference between HRSH analysis using sequence length 5 (top) and 250 (bottom). Histograms are shown before smoothing is applied. The histograms from sequences of length 250 are made from markedly higher numbers of RR intervals.

value for the analysis, including the consideration that shorter sequences take less time to analyze.

4.1.2 Evaluation of step length

The length of the step between two consecutive sequences of RR intervals was not seen to make any difference in the analysis results. Using a step length of less than the sequence length would mean that some RR intervals are included two or more times in different histograms, while a step length longer or equal to the sequence length results in single RR intervals being used only once. The differences between two analyses using step lengths 1 and 20 are illustrated in the following example:

> **Example 4.2.** From one recording of ambulatory ECG, two HRSH analyses were performed, one using step length of 1 and another using step length of 20 (the length of the sequences is 20 in both cases). The result is shown in Figure 4.2.
> Using step length 1 resulted in histograms made from a much higher number of both RR intervals and sequences; 168380, 176720, and 169780 compared to 8740, 9280, and 7960 RR intervals, or 8419, 8836, and 8489 compared to 437, 464, and 398 sequences. The histograms had smoother contours in the case of step length 1.

In the study described in Paper I, a step length of 1 was chosen after empirical testing of several values.

4.1.3 Evaluation of heart rate range

The heart rate range used to separate the different histograms should be as low as possible to allow the highest resolution when determining the heart rate interval at which PDC occurs. However, lowering the heart rate range will also reduce the number of RR intervals in the individual histograms which, in turn, would affect the analysis negatively. For the study in Paper I, heart rate range was chosen

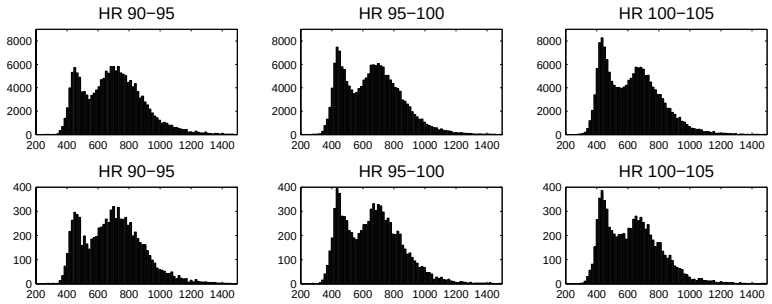

Figure 4.2: Example of the difference between HRSH analysis using step length 1 (top) and 20 (bottom). Histograms are shown before smoothing is applied. The histograms from step length 1 are made from markedly higher numbers of RR intervals.

empirically to 5 bpm.

4.1.4 Peak dominant change

PDC was found in 9 of 11 patients in the control recording of Group A when analyzing the whole 24-hour recording. When analyzing the first and last 7-hour long segments, in one patient the heart rate variability during the first 7-hour interval was too low to include the PDC interval although two distributions were observed.

In the intervention recording of Group A, PDC was found in the same 9 of 11 patients as in the control recording.

In the recordings of Group B, PDC was found in 12 of 13 patients. When analyzing the first and last four hours of the recording, one patient of those 12 was found to have a single-peak distribution of RR-intervals in the 0–4 hr interval and a double-peak distribution in the 8–12 hr interval.

4.1.5 Group A, comparison between beginning and end of control recording

To evaluate the reproducibility of the analyses, the first and last seven hours of the 24-hour long control recordings were compared. The patient where PDC could only be observed in the second 7-hour segment was excluded from this analysis.

Numerical values of the comparisons are shown in Table 4.1.

No statistically significant differences were seen in any of the recorded parameters. PDC was, surprisingly, found at different heart rates in all comparisons, but the differences were not consistent.

The observations of each individual case can be seen in Table 1 of Paper I.

	PDC [bpm]		PG [ms] at PDC		PVR at PDC	
	0–7 hr	17–24 hr	0–7 hr	17–24 hr	0–7 hr	17–24 hr
Median	110	115	157	159	1.37	1.37
Mean (SD)	111 (8)	110 (10)	135 (89)[1]	146 (85)	1.33 (0.22)	1.35 (0.20)
P-value	0.56		0.64		0.95	

	PV(f) [ms] at PDC		PV(s) [ms] at PDC	
	0–7[2]hr	17–24 hr	0–7[3]hr	17–24 hr
Median	429	434	599	589
Mean (SD)	419 (27)	423 (24)	588 (58)	601 (54)
P-value	0.25		0.25	

Table 4.1: Values of the comparisons between the first and last seven hours of the 24-hour control recordings of Group A. Based on Table 1 in Paper I. Values of the individual cases have been omitted and P-values are stated with their exact values.

4.1.6 Group A, comparison between control and intervention recordings

Comparisons between control and intervention in Group A were made using the whole 24-hour recordings. Numerical values of the comparisons are shown in Table 4.2.

	PDC [bpm]		PG [ms] at PDC		PVR at PDC	
	Control	Interv.	Control	Interv.	Control	Interv.
Median	115	110	147	156	1.36	1.31
Mean (SD)	113 (10)	104 (16)	132 (84)	146 (88)	1.32 (0.21)	1.33 (0.22)
P-value	0.08		0.03		0.63	

	PV(f) [ms] at PDC		PV(s) [ms] at PDC	
	Control	Interv.	Control	Interv.
Median	417	440	558	604
Mean (SD)	413 (25)	455 (94)	574 (60)	633 (108)
P-value	0.20		< 0.01	

Table 4.2: Values of the comparisons between the 24-hour control and intervention recordings of Group A. Based on Table 2 in Paper I. Values of the individual cases have been omitted and P-values are stated with their exact values.

Though not statistically significant, PDC was seen to move towards lower heart rates in the intervention recordings. This effect is due to the statistically significant

[1] Not 122 (93) as stated in Paper I
[2] Not 5 as stated in Paper I
[3] Not 5 as stated in Paper I

change of PV(s) towards longer RR intervals and the resulting increase of PG.

The observations of each individual case can be seen in Table 2 of Paper I.

4.1.7 Group B, comparison between beginning and end of recording

In Group B, comparisons were made between the first and last four hours of each individual recording, where the first four hours served as a control for the last. Numerical values of the comparisons are shown in Table 4.3.

	PDC [bpm]		PG [ms] at PDC		PVR at PDC	
	0–4 hr	8–12 hr	0–4 hr	8–12 hr	0–4 hr	8–12 hr
Median	95	87.5	140	167	1.30	1.36
Mean (SD)	97 (8)	90 (14)	143 (86)	178 (86)	1.32 (0.21)	1.37 (0.21)
P-value	0.03		< 0.01		0.04	

	PV(f) [ms] at PDC		PV(s) [ms] at PDC	
	0–4 hr	8–12 hr	0–4 hr	8–12 hr
Median	449	485	632	709
Mean (SD)	459 (45)	513 (92)	628 (50)	706 (79)
P-value	< 0.01		< 0.01	

Table 4.3: Values of the comparison between the first and last four hours of the 12-hour recordings of Group B. Based on Table 3 in Paper I. Values of the individual cases have been omitted and P-values are stated with their exact values.

Statistically significant changes were seen in all parameters. PDC moved towards lower heart rates, both PV(s) and PV(f) moved towards longer RR intervals, PG and PVR increased. Since PVR is increased, PV(s) is proportionally more affected than PV(f).

The observations of each individual case can be seen in Table 3 of Paper I.

4.1.8 Changes in RR interval distribution with increasing heart rate

By combining all RR interval histograms into a composite graph, three-dimensional images could be created where the heart rate-related changes of RR interval distribution may be studied. One example of such a graph is shown in Figure 4.3. The graph clearly shows how RR interval distribution is made up of two separate distributions, corresponding to PV(s) and PV(f). With increasing heart rate, the change in RR interval distribution consists of a decrease in the distribution of long RR intervals and an increase in the one with short.

An additional observation is that, with increasing heart rate, the locations of peaks move towards shorter RR intervals.

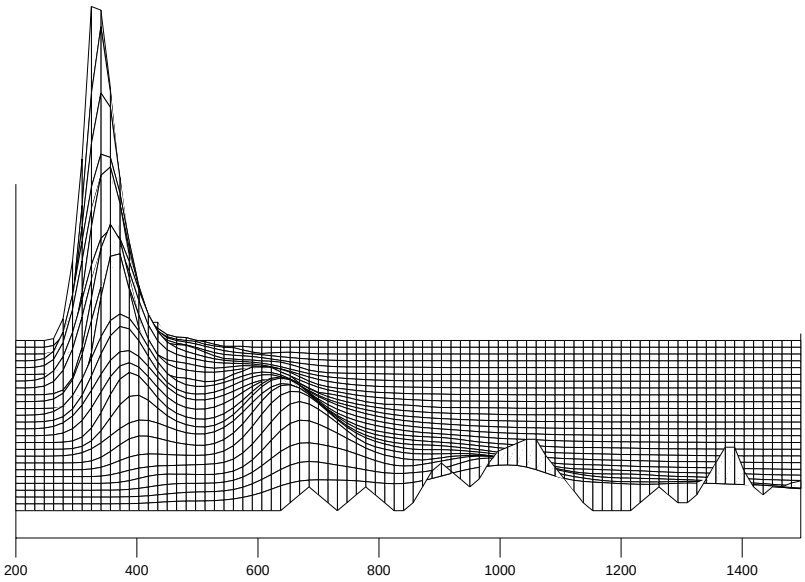

Figure 4.3: Example of three-dimensional graph of RR interval distribution, with increasing heart rate 'into' the graph. With increasing heart rates, two mechanisms can be observed: the shift between the two separate distributions, and the peak of each distribution moving towards shorter RR intervals.

4.2 Signal-averaged P waves

Figure 4.4 shows an illustration of the result after the QRS-detection and P wave extraction.

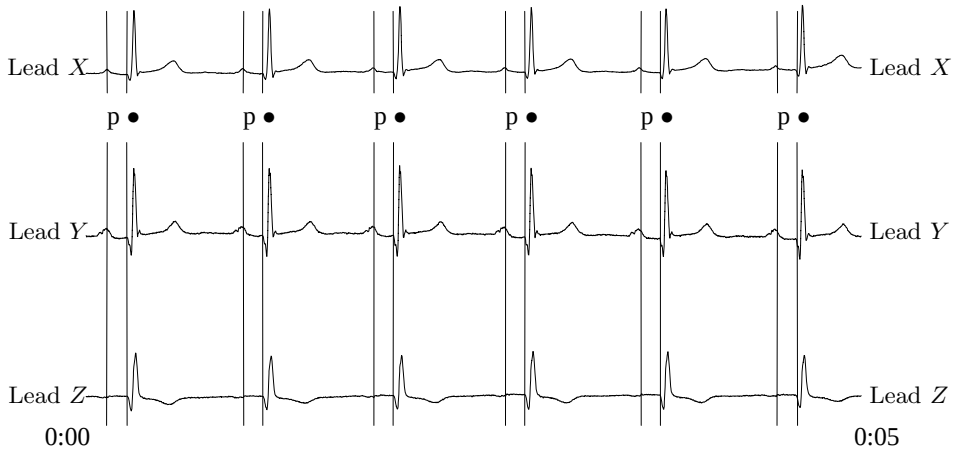

Figure 4.4: Example of the QRS and P wave detection on the first 5 seconds of a Frank-lead recording. The lines indicate P waves and onsets of the detected QRS complexes, 'p' indicates P wave, and • indicates classification as 'normal QRS'. The graph is produced using pschart [80].

4.2.1 Evaluation of QRS detection

An illustration of the performance of the QRS detection is shown in Table 4.4, where the results after analyzing recordings from five healthy cases and five with a history of atrial fibrillation have been verified manually.

The QRS complexes missed in cases 2 and 6 were not detected due to them being located too closely to the beginning and end of the recording, which did not allow the QRS detection algorithm to recognize them. The four beats marked as 'other' in cases 7, 8, and 10 were all detected correctly but in the manual procedure of defining onset and end it was obvious that these were not 'normal' QRS, but rather ventricular ectopic beats. The three missed beats in Case 9 were due to a sudden step-like fluctuation of the ECG 'baseline' near the QRS complexes. This made the detection algorithm leave these QRS complexes undetected. No false detections of QRS complexes were made in any of the ten recordings evaluated.

4.2.2 Evaluation of user-defined signal window

The position of the user-defined signal window defining the P wave was important. Since the Q wave might have a much steeper slope and higher amplitude than the P wave, it was necessary for the performance of the P wave signal averaging that the end of the signal window was positioned before the QRS onset. If the Q wave

Healthy

Case	Found QRS	Note
1	374	
2	365	1 missed (at beginning of record)
3	401	
4	420	
5	369	
Total	1929	1 missed

History of atrial fibrillation

Case	Found	Note
6	496	1 missed (at end of record)
7	341	1 'other'
8	315	2 'other'
9	372	3 missed (step-like baseline)
10	454	2 'other'
Total	1978	4 missed, 5 false detections

Table 4.4: Result of QRS detection algorithm on recordings from five healthy cases and five with a history of atrial fibrillation.

was included, the result would not be 'P wave triggered' signal averages but instead 'Q wave triggered'.

Having a fully user-defined window enabled signal-averaging of any part of the cardiac cycle besides the P wave, such as QRS complex or T wave, or waves in the previous or following cycle.

4.2.3 Evaluation of signal averaging of P waves

Signal averaging of the P waves reduced noise and created different groups of P waves with different morphologies. The result of signal averaging is illustrated using the following example:

Example 4.3. A 21-minute-long VCG recording from a healthy individual was analyzed in parts of different length. Figure 4.5 shows one single P wave in comparison to averages of 11, 31, and 103 P waves, created using 14.5, 45, and 120-seconds long sequences, respectively. The averages shown all belong to the group with the largest number of members.
Noise was reduced significantly already in the case of 11 averaged P waves and the morphology did not change in the cases of 31 and 103 P waves.
The manual setting of onset and end was somewhat ambiguous in the cases with 11 and 31 P waves due to remains of low-frequency noise whereas the case with 103 P waves had a very stable 'baseline'. For a reliable analysis, a recording length of at least a minute or 'some minutes' would be desired, depending on signal quality and P wave variability.
The numbers of P waves in different identified morphologies are illustrated in Table 4.5.

Length of sequence	Number of members in P wave groups
14.5 s	11, 2, 2
30 s	20, 4, 2
45 s	31, 9, 2
60 s	42, 13, 2, 2
120 s	103, 17, 6, 2
6 min	222, 113, 24, 17, 17, 6, 4
21 min	808, 327, 112, 42, 27, 21, 17, 9, 9, 8, 4, 3, 3, 3, 2

Table 4.5: Number of P waves with different morphologies found when analyzing segments of different lengths in a 21-minute-long VCG recording. Groups with only one member are not shown. It was obvious that the longer the recording, the more P wave groups were found.

4.2.4 Evaluation of setting of P wave onset and end

Intra-observer comparison

Figure 4.6 shows the results of comparing the two subsequent settings of P wave onset and end of each observer. The results of those trained in the method were well within ±5 ms for both onset and end, whereas the observer not trained had a markedly wider distribution. In all cases, the results were centered around 0.

Inter-observer comparison

Figure 4.7 shows the results of the comparison between the settings of the three observers. The agreement between the trained observers was within ±5 ms in both onset and end, and centered around 0, indicating similar settings in both parameters.

The comparison between the Physician and the EP nurse in onset settings showed a wider distribution, moved towards negative values indicating lower agreement between the observers and the Physician's onset settings being earlier in the signal window. Similarly, the comparison of end settings showed a wider distribution, this time moved slightly towards positive values indicating the Physician's setting being later in the signal window.

Resulting P wave duration

Figure 4.8 shows a Bland-Altman plot [90] of the comparisons of resulting P wave duration when calculated from the onset and end settings of the three observers. The difference in P wave duration in the comparison between the trained observers was 4 ± 18 ms (mean ± two standard deviations).

One possible outlier was removed from the comparison between Physician and EP nurse (duration 145 ms vs. 272 ms). The distribution was 0 ± 25 ms (mean ± two standard deviations) without the outlier and -2 ± 45 ms with the outlier included.

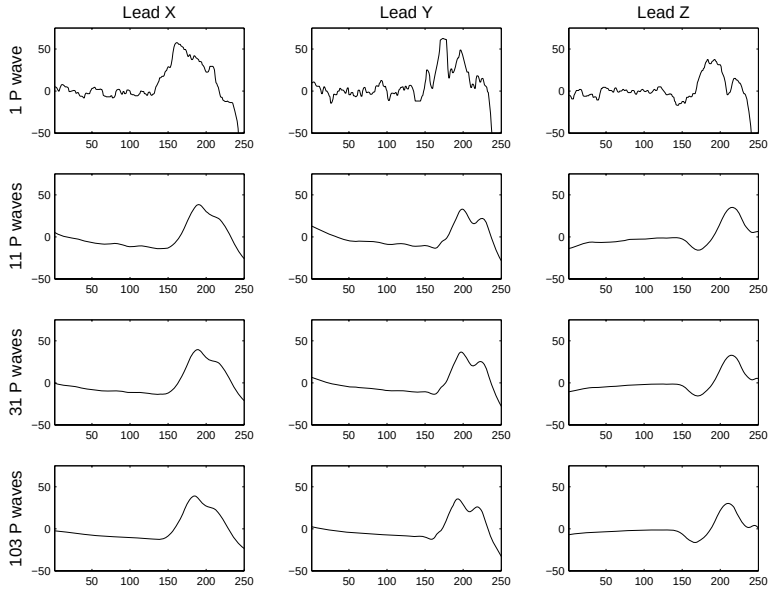

Figure 4.5: Example of signal-averaging of different numbers of P waves. The top row shows one single P wave before low-pass and powerline frequency filtering. The other rows show the result after filtering and signal averaging of 11, 31, and 103 P waves. Noise is reduced significantly already in the case of 11 averaged P waves but not until the case with 103 averaged P waves the onset and end may be reliably defined. All signals are shown before smoothing was performed.

4.2.5 Analysis of variability

To illustrate the results of a P wave variability analysis, the study material described in Paper III was used. This contained Frank-lead recordings from 21 healthy subjects and 20 patients with a history of atrial fibrillation.

Number of P wave groups

The number of groups of P waves identified in each study subject is illustrated in Figure 4.9. Only groups with more than one member were included under the assumption that groups with just one member were the results of noise or other artifacts in the recordings. No statistically significant difference was found when comparing the number of different P wave morphologies found in healthy people compared to those with a history of atrial fibrillation ($P = 0.15$, Wilcoxon rank sum test).

Figure 4.9 also shows the relation between the number of members in the found groups compared to the number of members in the largest group. It was seen that in healthy cases, no group exceeded 40%, i.e., in all recordings, the largest group contained at least 2.5 times as many P waves as the second largest. In the AF

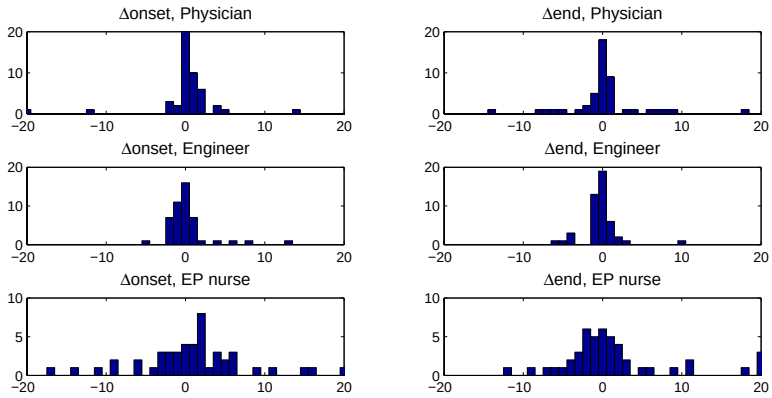

Figure 4.6: Intra-observer variability of settings of P wave onset and end

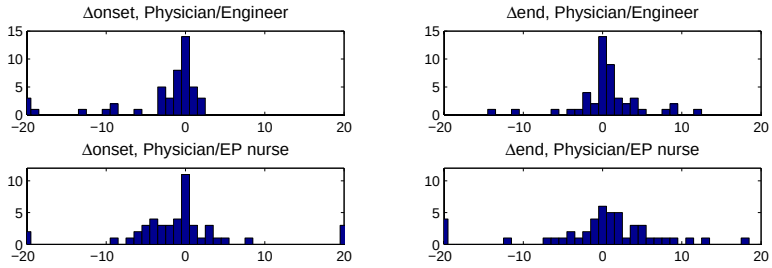

Figure 4.7: Inter-observer variability of settings of P wave onset and end

cases, the second largest group contained at most 20% of the number of P waves in the largest.

Correlation between groups

The correlations between the morphology of the largest group, Group 1, and the other groups found were calculated in each individual recording. The result is shown in Figure 4.10. It was observed that in several cases, groups had a correlation close to, or even above, the similarity criterion 0.9, when compared to Group 1 of the recording. Among the AF cases, there were more observations of negative correlation values than among the healthy ones.

Switching between groups

Consecutive P waves were found to change between different morphologies. Two variants of such switching was found, as illustrated in the following example:

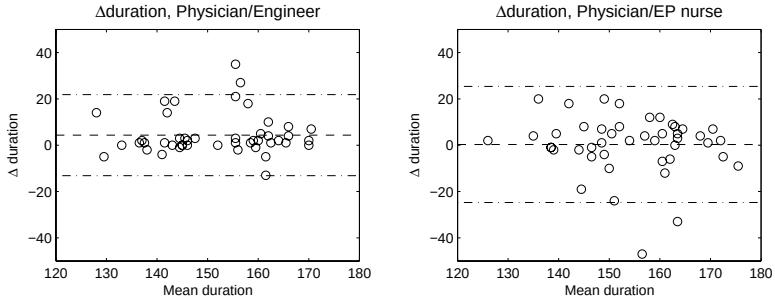

Figure 4.8: Inter-observer variability of P wave duration. Lines indicate mean ± two standard deviations. One possible outlier value in the right plot at (208.5,-127) is not shown and not included in the calculation of the mean and standard deviation.

Example 4.4. Two Frank-lead VCG recordings from healthy subjects were analyzed, denoted as Case A and Case B. Case A had six groups with 390, 14, 10, 3, 2, and 1 members. Case B had 4 groups with 249, 83, 8, and 2 members. Figure 4.11 shows a graphical illustration of the switching between P wave groups in consecutive P waves. Table 4.6 shows numerical values of the same analysis.
It was seen that in both cases, the highest probability was found when conduction was of 'Group 1' type with probability of the next P wave also being of Group 1 morphology of 0.93 and 0.98, respectively. This agreed with the information in Figure 4.9 where it was seen that the number of members of Group 1 in all cases were much larger than in any other.
The graph of Case A in Figure 4.11 shows that a majority of P waves belonged to Group 1. It also shows that when there were switches to other morphologies, the return back to Group 1 occurred within a few beats. This can also be seen numerically in Table 4.6 where the observed probability of switching from Group 2–6 to Group 1 is much higher than to any other.
Studying case B shows that Group 1 morphology was very stable with probability 0.98 to stay in this conduction pattern. However, once conduction switched to Group 2 or 3 morphology, there was only a low probability of returning to Group 1 of 0.01 if in Group 2. This can be seen in Figure 4.11 where there is one longer sequence of Group 2 and 3 P waves around P wave number 50 and another at the end of the recording from P wave 300 and forward.

Morphology differences

When different morphologies were found in a recording, they could be interpreted as originating from the same underlying atrial conduction pattern, or not. In some cases, differences were only subtle, whereas in other cases, they were more prominent. An illustration of this is shown in the following example:

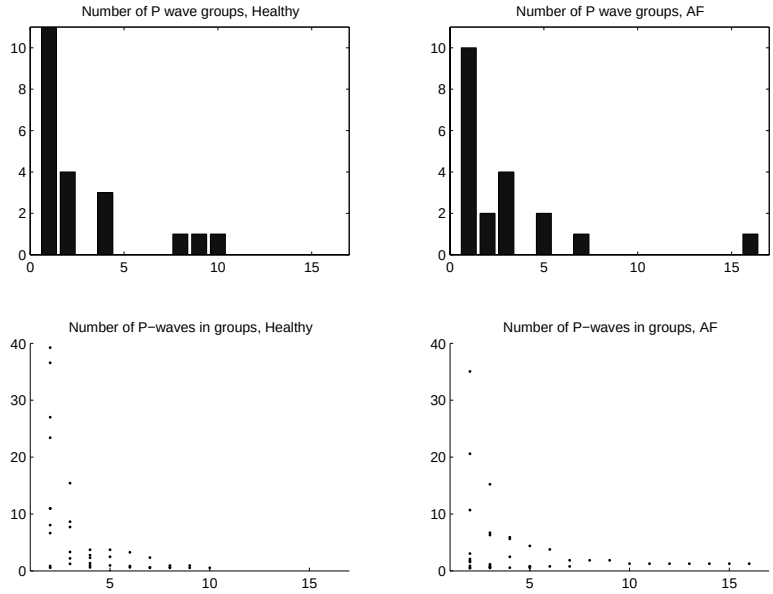

Figure 4.9: Illustration of the variability of P wave morphology. The two figures at the top show the number of cases where different numbers of P wave groups with more than one member was found. The two lower figures show the number of members in groups expressed as a percentage of the number of members in the largest group.

Example 4.5 (Example 4.4 continued). The four morphologies with largest number of members found in Case A are shown in Figure 4.12 and those found in Case B are shown in Figure 4.13.
It was seen that the differences between the morphologies in Case A were small and it could be argued that they belonged to the same underlying pattern of conduction since the difference between them could be explained by a low-frequency artifact in Leads X and Y.
Case B showed a more visible difference in morphologies where Group 1 and 4 seemed to belong to the same underlying conduction pattern and Group 2 and 3 to another.
Combining the information of Figures 4.11, 4.12, and 4.13 suggested that the variability of Case A was only due to low-frequency artifacts not removed in the filtering whereas the variability of Case B was a true change in underlying conduction pattern.

Change of dominant morphology

Besides the observation of the different mechanisms of changes in P wave morphology found, as illustrated in Figure 4.11, another observation was made in a recording where the dominant morphology changed when analyzing longer segments.

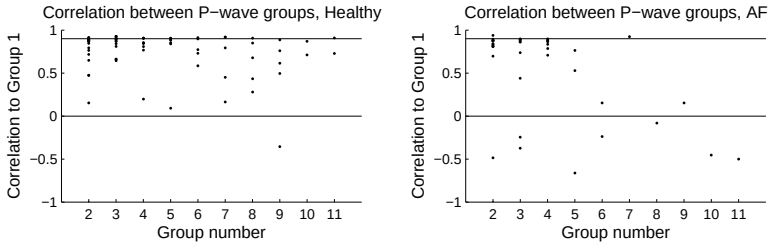

Figure 4.10: Correlation between Group 1 and other groups with more than one member. Each dot represents an observation from an individual recording. The threshold of the similarity criterion, 0.9 is indicated with a line. Note that some groups actually exceed the threshold.

Case A

	1	2	3	4–6
1	0.93	0.03	0.02	0.02
2	0.86	0.07	0.07	0
3	0.90	0.10	0	0
4–6	1	0	0	0

Case B

	1	2	3	4
1	0.98	0.01	0.01	0.01
2	0.01	0.90	0.08	0
3	0	1	0	0
4	1	0	0	0

Table 4.6: Two examples of P wave variability expressed as the observed probability of switching group in two healthy cases with four and six observed groups with more than one member. The row number indicates the group of the 'present' P wave and the column number the group of the 'following' P wave.

Example 4.6 (Case observation). A 21-minute-long VCG recording was made on a healthy individual. When analyzing, an observation of change of dominant morphology was made when including longer segments of the recording (Figure 4.14). The switch is illustrated in Figure 4.15. It was seen that among the first 150 P waves (120 seconds), there was a dominant P wave morphology, seen in the top row of Figure 4.14. From P wave 150 and on, the dominant morphology was replaced by another, illustrated in the middle and bottom row of Figure 4.14, which remained dominant through the remainder of the recording. It can be seen in Figure 4.15 that the dominant morphology of the first part of the recording did not exist in the last, and the dominant morphology of the last part of the recording did not exist in the first part.

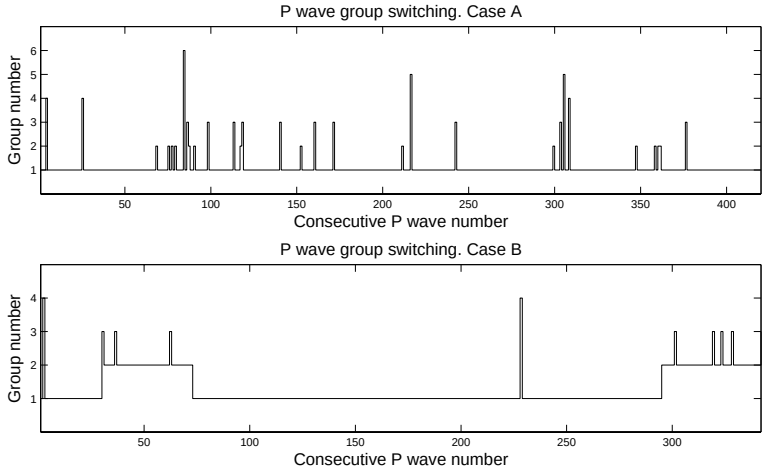

Figure 4.11: Examples of switching between P wave groups in two healthy cases. In Case A, the morphology of Group 1 is dominant, P waves of other morphologies only appear in very short sequences, after which P wave morphology returns to Group 1. In Case 2, longer sequences of P waves with Group 2 and 3 morphology exist.

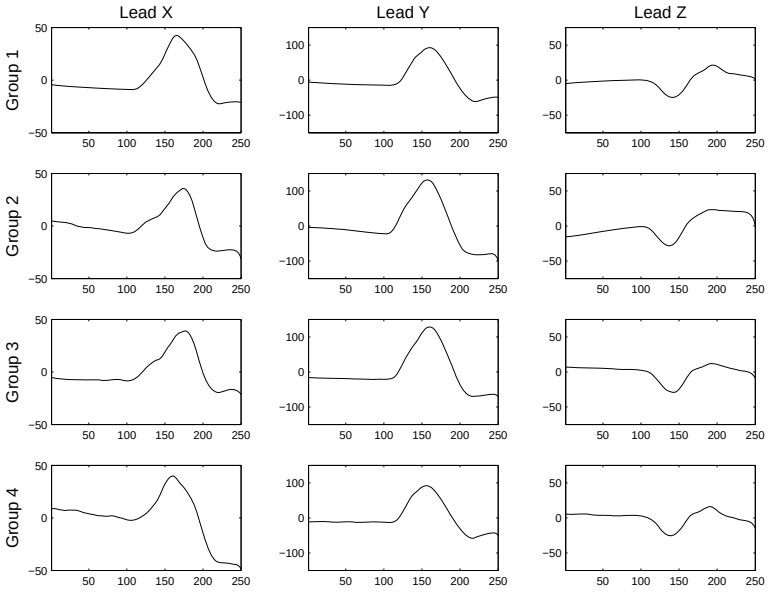

Figure 4.12: The four most common morphologies found in Case A (Example 4.4). The similarity criterion, correlation coefficient greater than 0.9, in this case results in groups with only subtle differences, most visible in the form of a leaning baseline in Leads X and Z.

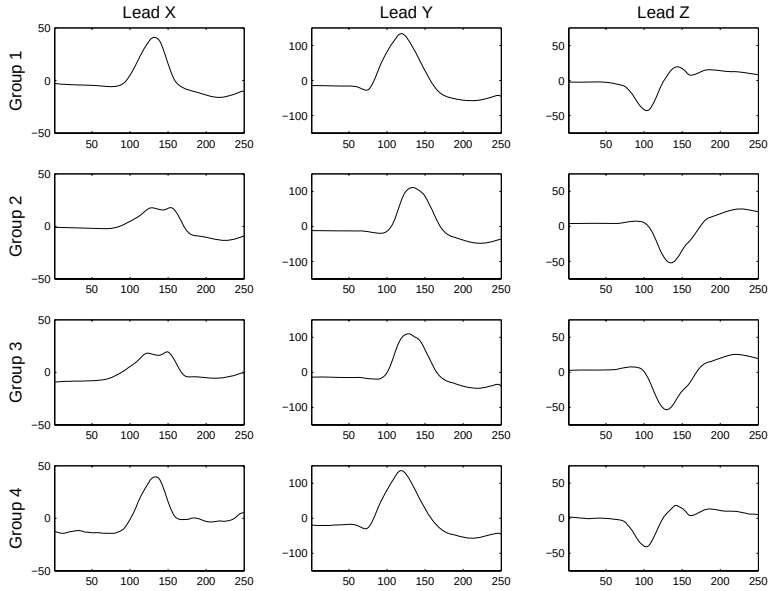

Figure 4.13: The four different morphologies found in Case B (Example 4.4). The similarity criterion correlation coefficient larger than 0.9 results in two slightly different morphologies, one in Groups 1 and 4, and one in Groups 2 and 3.

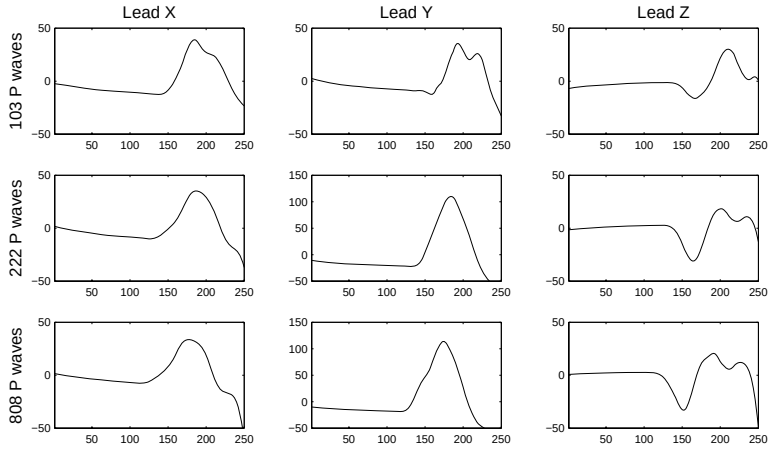

Figure 4.14: Change of dominant P wave morphology when including more P waves in the signal averaging. The top row shows the dominant morphology of the first 2 minutes of the recording and the middle and bottom line shows the dominant morphology of the first 6 minutes and the whole 21 minutes of the recording, respectively. Note change of amplitude in Lead Y.

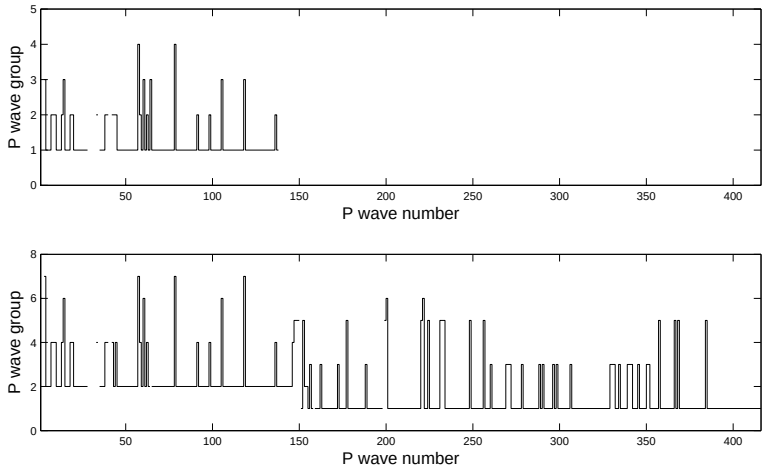

Figure 4.15: Change of dominant P wave morphology. Top row shows P wave morphologies found in the first 120 seconds of the registration. Bottom row shows morphologies found in the first six minutes. At P wave 150 there is a change from one dominant morphology to another. Neither morphology exists in the other part of the recording.

4.3 P wave modeling

4.3.1 Model order

An appropriate model order was chosen from the singular value decomposition in Equation (D.4). These were presented in plots like Figure 4.16. After inspection

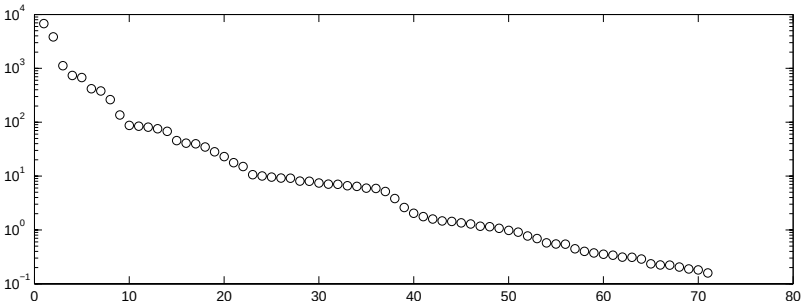

Figure 4.16: Example of the result of the singular value decomposition in Equation (D.4). A notch can be seen between the x-axis values 9 and 10 suggesting a model order of $n = 9$.

of these plots, model order 9 was chosen as the cut-off between signal and noise and used in the P wave modeling.

4.3.2 System identification

The distributions of the residuals calculated from Equation (D.7), using model order 9 and 5, are shown in Figure 4.17.

An illustration of the best and worst result of the system identification using model order 9 is shown in Figure 4.18 where the MATLAB function dimpulse was used to calculate the impulse response from the matrices A_n, B_n, C_n, and D_n of Equation (D.5).

4.4 P wave classification

4.4.1 Classification of the training set

The results of the Fisher linear discriminant analysis applied to parameters from models of order 9 can be seen in Figure 4.19. The separation between the groups was best when using the Lead Z numerator polynomial coefficients, where 37 of 40 cases were classified correctly.

The result of the Fisher linear discriminant analysis applied to the P wave signals with different decimation factors is shown in Figure 4.20. The best separation was achieved when using decimation factor 10, although all values produced a fully correct classification.

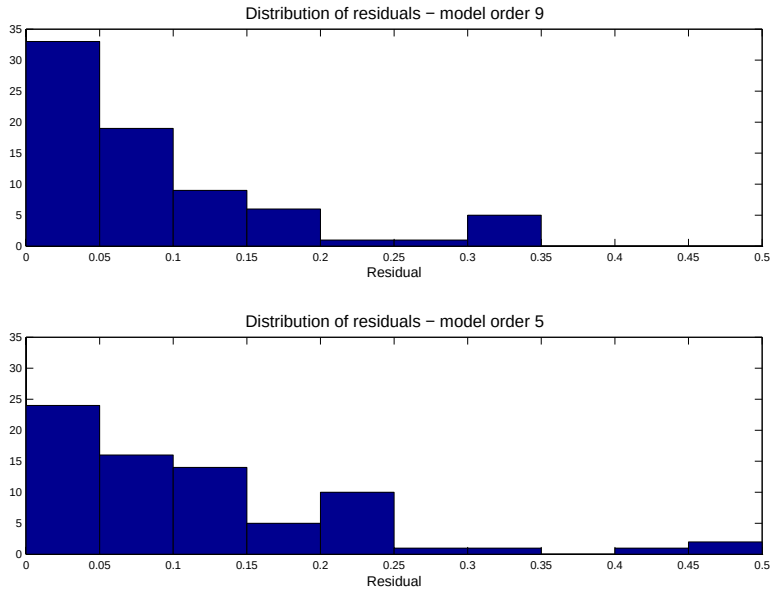

Figure 4.17: Distribution of residuals when comparing modeled P waves with recorded.

4.4.2 Alternative choice of threshold

It can be seen in Figure 4.20 that the performance of the discrimination threshold in Equation (E.4) was not optimal, especially in the case of decimation factor 5. This is not obvious in Figure 4.19 and was not discovered in the preparation of Paper II. An improved performance of the threshold could be achieved by switching place of m_A and m_B in the numerator. Equation (E.4) then became

$$\vartheta = \frac{\left(\sqrt{(\lambda^T R_A \lambda)}\lambda^T m_B + \sqrt{(\lambda^T R_B \lambda)}\lambda^T m_A\right)}{\sqrt{(\lambda^T R_A \lambda)} + \sqrt{(\lambda^T R_B \lambda)}} \tag{4.1}$$

The result when applying Equation (4.1) on data from the Fisher linear discriminant analysis of P waves decimated a factor 10 is shown in Figure 4.21. The threshold moved closer to the distribution of '×' (cases with possible interatrial conduction defect) which had a lower standard deviation than the distribution of '○' (healthy cases). This result agreed better with an intuitive setting of the threshold and made the discrimination better, although both Equation (E.4) and (4.1) created a correct classification. The result was similar for other choices of decimation factors. The classification results stated in Paper II did not change with this other choice of threshold, the reason being that the standard deviations of both groups were in this case of the same magnitude, which can be appreciated in Figure 4.19.

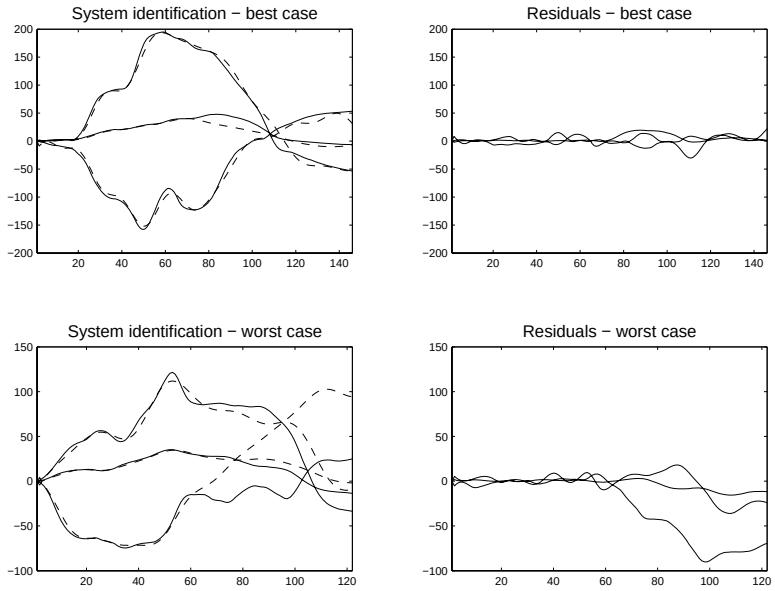

Figure 4.18: Result and residuals of the best and worst case of the system identification using model order 9. The left column shows the original (solid line) and modeled (dashed line) of the best (top) and worst (bottom) cases. The right column shows the corresponding residuals. The residual magnitude was 0.010 in the best case and 0.341 in the worst.

4.4.3 Classification of the evaluation set

Figure 4.22 shows the result of classification of the evaluation set. Six of the seven healthy cases, and five of the five cases with possible interatrial conduction defect were classified correctly.

Figure 4.23 shows the classification results when using different numbers in the training set groups. When using two groups of 15, 16, 17, or 18 cases each, the results of the evaluation set classification were about 70%. Using two groups of 19, 20, 21, or 22 cases each, classification was fully correct except when 20 cases were used, as described above.

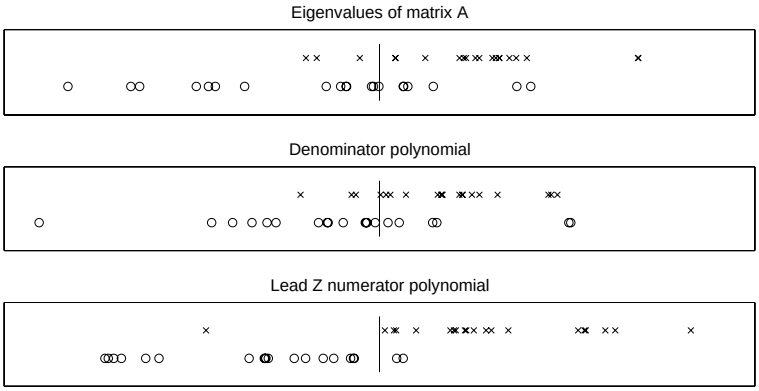

Figure 4.19: Results of the Fisher linear discriminant on separating the two types of P waves using three different sets of test parameters (○: healthy, ×: interatrial conduction defect). The parameters of the two different groups have been separated vertically for a better view, the vertical line indicating the threshold chosen.

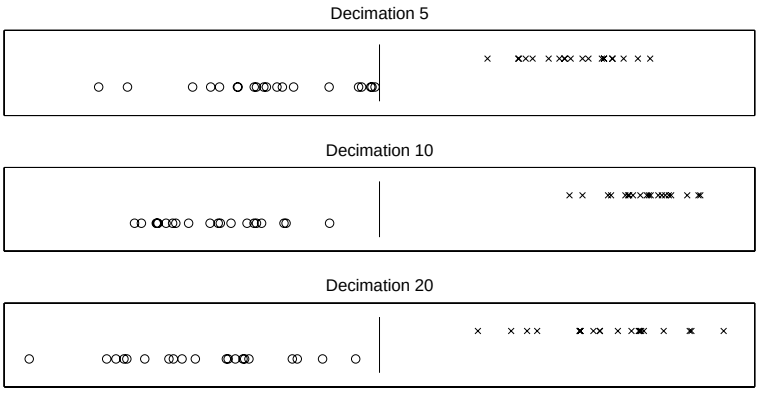

Figure 4.20: Results of the Fisher linear discriminant on separating the two types of P waves using the (decimated) signal itself as the parameter set (○: healthy, ×: interatrial conduction defect). The parameters of the two different groups have been separated vertically for a better view, the vertical line indicating the threshold chosen.

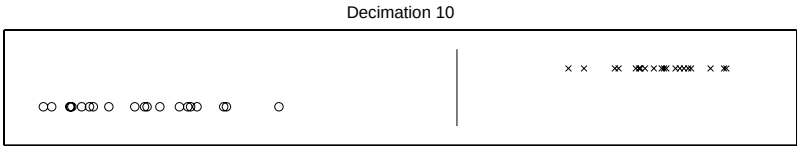

Figure 4.21: Result of the alternative threshold in Equation (4.1). Compare with Figure 4.20.

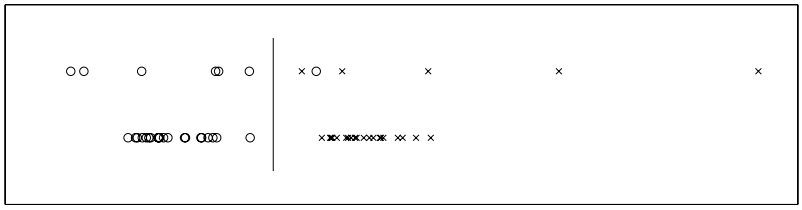

Figure 4.22: Result of classification of training set (two groups of 20 cases, lower part) and evaluation set (7 healthy cases and 5 cases with interatrial conduction defect, upper part). ○: healthy cases, ×: cases with interatrial conduction defect.

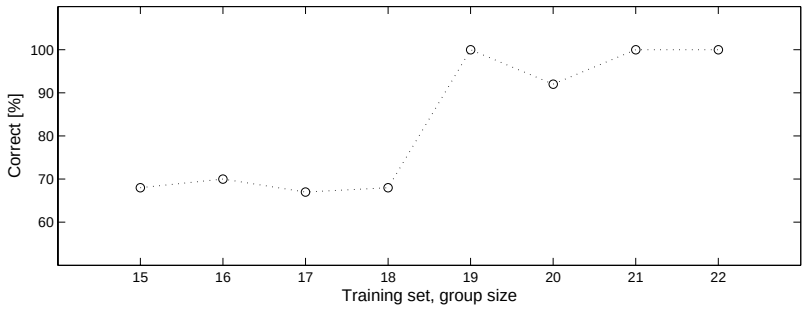

Figure 4.23: Result of classification of evaluation set when using different numbers of cases in the two groups in the training set. When groups of 18 recordings or less were used, the classification of the evaluation set was around 70% correct. With more than 18 in each training set group, the evaluation set was almost fully correctly classified.

4.5 Lead conversion

One recording from a patient with history of atrial fibrillation had to be excluded due to a too high noiselevel to allow any analysis. Thus, 21 healthy cases and 20 with a history of atrial fibrillation were included in the results.

4.5.1 Errata: Frank-lead electrode placement

Unfortunately, for reasons unknown, the electrode placement used in the study described in Paper III was not exactly the one described in Figure 3.1. The electrode at location E_1 was positioned at the lower left abdomen, and the electrode at location E_6 was positioned at the front of the neck.

The influence of these position changes on the VCG is at this time not fully understood, and the results of Paper III should be interpreted with care.

4.5.2 Comparison between ECG and derived VCG

Preservation of variability

Figure 4.24 shows the difference in number of groups found and difference in number of members in the largest group found, using Bland-Altman [90] plots.

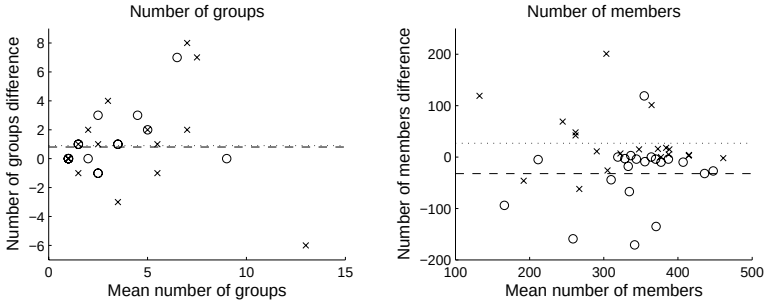

Figure 4.24: Analysis of preserved variability between ECG and derived VCG expressed as (left) number of P wave groups with more than one member, and (right) number of members in the largest group. ○: healthy cases, ×: cases with history of atrial fibrillation. Dashed line is mean of healthy cases, dotted line is mean of cases with history of atrial fibrillation.

The mean difference of number of groups found was 0.9 in the healthy cases and 0.8 in those with a history of atrial fibrillation, indicating that ECG recording analysis yields more groups than derived VCG recordings ($P = 0.04$ and $P = 0.14$, respectively).

The mean difference of number of members in the largest group found was -32 in the healthy cases and 27 in those with history of atrial fibrillation. Thus, the largest group of P waves found has less members in ECG recordings from healthy subjects, and more in recordings from patients with a history of atrial fibrillation, than their derived VCG counterparts ($P < 0.01$ and $P = 0.03$, respectively).

Preservation of duration and PQ time

Figure 4.25 shows the mean differences in P wave duration and PQ time, using Bland-Altman [90] plots.

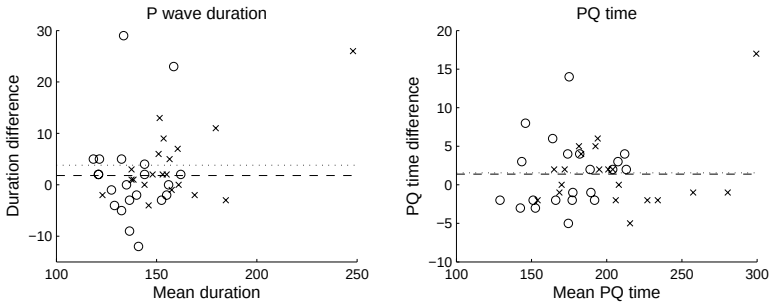

Figure 4.25: Analysis of differences in (left) P wave duration and (right) PQ time between ECG and derived VCG. ○: healthy cases, ×: cases with history of atrial fibrillation. Dashed line is mean of healthy cases, dotted line is mean of cases with history of atrial fibrillation.

The mean difference of P wave duration was 1.8 in the healthy cases and 3.8 in those with a history of atrial fibrillation, indicating longer P wave duration in the ECG recordings ($P = 0.67$ and $P = 0.03$, respectively).

The mean difference of PQ time was 1.4 in the healthy cases and 1.6 in those with a history of atrial fibrillation, indicating longer PQ time in the ECG recordings ($P = 0.20$ and $P = 0.15$, respectively).

4.5.3 Comparison between VCG and derived VCG

Preservation of variability

Figure 4.26 shows the difference in number of groups found and difference in number of members in the largest group found, using Bland-Altman [90] plots.

The mean difference of number of groups found was 0.5 in the healthy cases and -0.2 in those with a history of atrial fibrillation, indicating that VCG recordings yield more groups than derived VCG recordings in healthy cases and less in those with a history of atrial fibrillation ($P = 0.52$ and $P = 0.39$, respectively).

The mean difference of number of members in the largest group found was -9 in the healthy cases and 31 in those with history of atrial fibrillation. Thus, the largest group of P waves found has less members in VCG recordings from healthy subjects and more members in recordings from patients with a history of atrial fibrillation compared to their derived VCG counterparts ($P = 0.06$ and $P = 0.04$, respectively).

Preservation of duration and PQ time

Figure 4.27 shows the mean differences in P wave duration and PQ time, using Bland-Altman [90] plots.

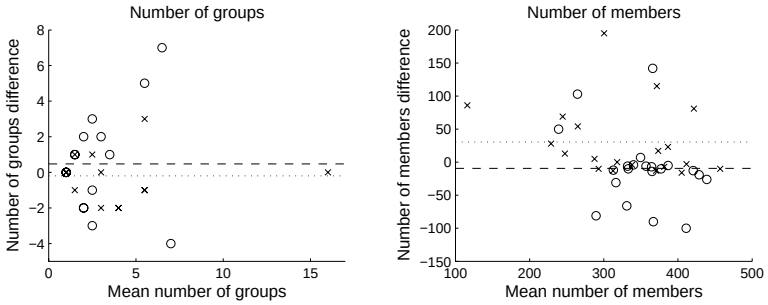

Figure 4.26: Analysis of preserved variability between recorded VCG and derived VCG expressed as (left) number of P wave groups with more than one member, and (right) number of members in the largest group. ○: healthy cases, ×: cases with history of atrial fibrillation. Dashed line is mean of healthy cases, dotted line is mean of cases with history of atrial fibrillation.

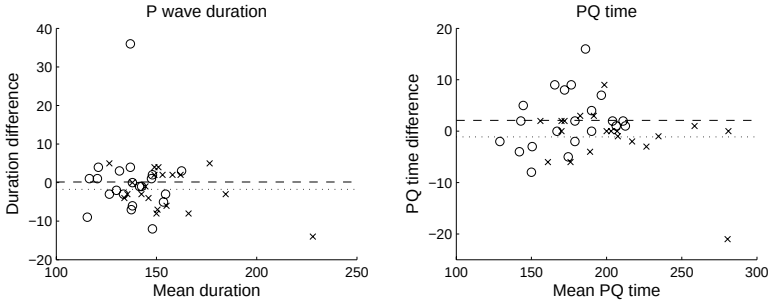

Figure 4.27: Analysis of differences in (left) P wave duration and (right) PQ time between recorded VCG and derived VCG. ○: healthy cases, ×: cases with history of atrial fibrillation. Dashed line is mean of healthy cases, dotted line is mean of cases with history of atrial fibrillation.

The mean difference of P wave duration was 0.1 in the healthy cases and -1.8 in those with a history of atrial fibrillation, indicating longer P wave duration in VCG recordings from healthy subjects and shorter in recordings from patients with a history of atrial fibrillation, compared to their derived VCG counterparts ($P = 0.40$ and $P = 0.18$, respectively). In Figure 4.27, a possible outlier is seen at (137,36), with this excluded, the mean P wave duration difference of the healthy recordings would be -1.7 (and the P value changed to $P = 0.19$).

The mean difference of PQ time was 2.1 in the healthy cases and -1.1 in those with a history of atrial fibrillation, indicating longer PQ time in VCG recordings from healthy subjects and shorter in recordings from patients with a history of atrial fibrillation, compared to their derived VCG counterparts ($P = 0.14$ and $P = 0.60$, respectively). In Figure 4.27, a possible outlier is seen at (280,-21), with this excluded, the mean PQ time difference of the atrial fibrillation recordings would be -0.1 (and the P value changed to $P = 0.92$).

Mathematical comparison

The results of the different mathematical comparisons between VCG and dVCG are shown in Table 4.7.

Correlation

	Healthy		History of AF	
Lead X	0.95	(0.82–1.00)	0.95	(0.61–1.00)
Lead Y	0.95	(0.66–1.00)	0.95	(0.80–0.99)
Lead Z	0.92	(0.15–0.99)	0.95	(0.76–0.99)

Scaling parameter

	Healthy		History of AF	
Lead X	0.88	(0.46–1.24)	0.96	(0.52–1.24)
Lead Y	1.37	(0.53–1.66)	1.32	(0.61–2.53)
Lead Z	0.92	(0.28–1.88)	1.02	(0.74–1.33)

Residual magnitude

	Healthy		History of AF	
Lead X	0.23	(0.06–0.49)	0.23	(0.06–0.73)
Lead Y	0.24	(0.06–0.68)	0.17	(0.06–0.48)
Lead Z	0.38	(0.12–0.91)	0.32	(0.15–0.57)

Table 4.7: Results of mathematical comparisons between P waves from VCG and derived VCG. Numbers are given as: median (min–max).

The correlation was generally found to be high, indicating good agreement between the morphology of the different P waves, when amplitude was not considered.

The amplitude scaling parameter found by least-squares fitting should ideally have the value 1, in the case of agreement in amplitude. In the healthy cases, the scaling parameters of Leads X and Y were significantly different from 1 ($P < 0.01$ in both cases, $P = 0.54$ in Lead Z). In those with a history of atrial fibrillation, Lead Y was significantly different from 1 ($P < 0.01$, $P = 0.52$ in Lead X, and $P = 0.49$ in Lead Z). Comparisons were made using the Wilcoxon signed rank test.

Analysis of residuals

Numerical values of the magnitudes of the residuals according to Equation (C.6) are presented in Table 4.7.

An overall image of the residuals of each sample is shown in Figure 4.28. The image was produced by extracting, for example, the value of sample number 1 of all residuals from the comparisons of Lead X in the healthy cases and calculating the median and 10^{th} and 90^{th} percentiles, then from sample number 2 and so on. This created an image of the overall residuals, useful to evaluate possible systematic errors in the inverse Dower transform.

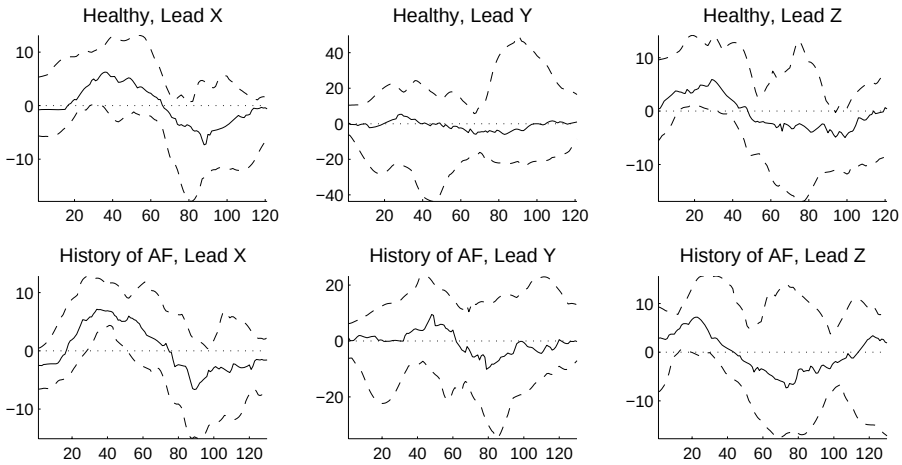

Figure 4.28: Overall residuals of the comparison between recorded and derived VCG. Figures show median (solid line), and 10^{th} and 90^{th} percentile (dashed lines) of residuals for each time instant of all comparisons. A systematic appearance can be seen where the residuals are generally positive in the first half of the P waves and negative in the second.

Figure 4.28 shows that residuals were generally positive in the first half of the P waves, and negative in the second half, indicating a possible time-dependent systematic error.

4.6 Correlation function analysis

4.6.1 Recording quality

In one recording performed during atrial fibrillation, the signal from pole number 10 (coronary sinus orifice) had to be excluded due to a too high noise level.

In another recording performed during atrial fibrillation, the signal from pole number 1 (tip of the catheter) had to be excluded due to the signal being saturated.

4.6.2 QRS detection and removal

All QRS complexes in Lead V_1 of the recordings were detected correctly. The amount of signal needing to be removed by linear interpolation was verified in each individual recording to assure that only signals emanating from atrial activity remained (Table 4.8).

Sinus rhythm

	Recording number				
	1	2	3	4	5
Diagnosis	AVRT	AVRT	AVNRT	PAF	PAF
Heart rate	66	93	88	40	64
Signal removed	24%	16%	17%	12%	15%

	Recording number				
	6	7	8	9	10
Diagnosis	AVNRT	PAF	EAT (LA)	EAT (RA)	PAF
Heart rate	97	78	61	70	54
Signal removed	22%	23%	11%	16%	8%

Atrial fibrillation

	Recording number				
	1	2	3	4	5
Diagnosis	PAF	PAF	PAF	PAF	PAF
Heart rate	111	119	105	106	91
Signal removed	19%	18%	15%	20%	26%

Ectopic atrial tachycardia

	Recording number		
	1	2	3
Diagnosis	EAT (LA)	EAT (LA)	EAT (RA)
Heart rate	91	88	133
Signal removed	13%	16%	25%

Table 4.8: The amount of signal lost due to removal of ventricular artifacts in the electrograms. AVRT: AV reentrant tachycardia, AVNRT: AV-nodal reentrant tachycardia, PAF: paroxysmal atrial fibrillation, EAT (LA): left atrial ectopic atrial tachycardia, EAT (RA): right atrial ectopic atrial tachycardia.

4.6.3 Correlation values and electrogram shape

An example, illustrating the connection between correlation values and electrogram shape in a recording made during atrial fibrillation is shown in Figure 4.29. A similar example, but from a recording made during sinus rhythm is shown in Figure 4.30.

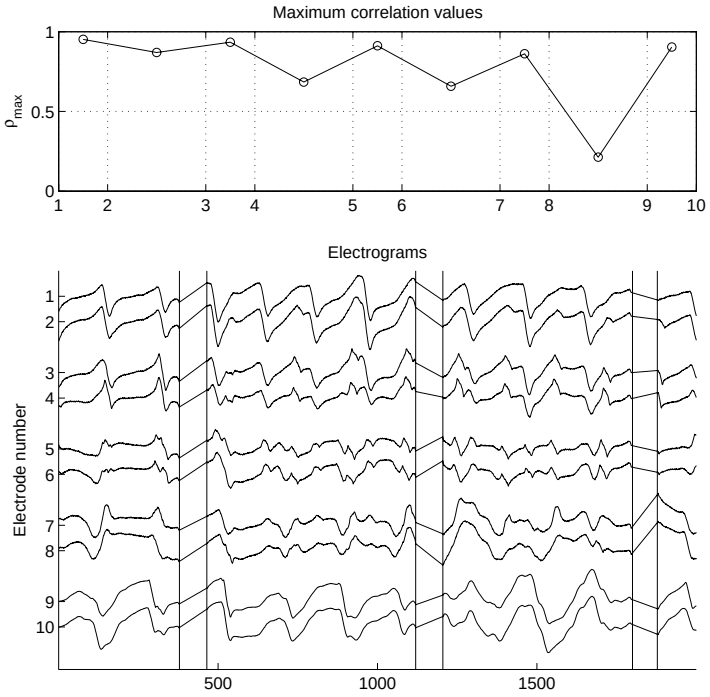

Figure 4.29: Example of the connection between correlation values and electrogram shapes in an atrial fibrillation recording. Top: correlation values between electrogram pairs. The x-axis scale indicates electrode placement on the catheter. Bottom: 2-second segment of the electrograms. Electrograms 1–4 are similar as indicated by high correlation, Electrograms 5–10 are pairwise similar with high correlation in each pair but with differences between the pairs. The lowest correlation is found between Electrograms 8 and 9 which is also where the signals have the most obvious change in shape. The vertical lines indicate the segments where ventricular artifacts were removed by linear interpolation.

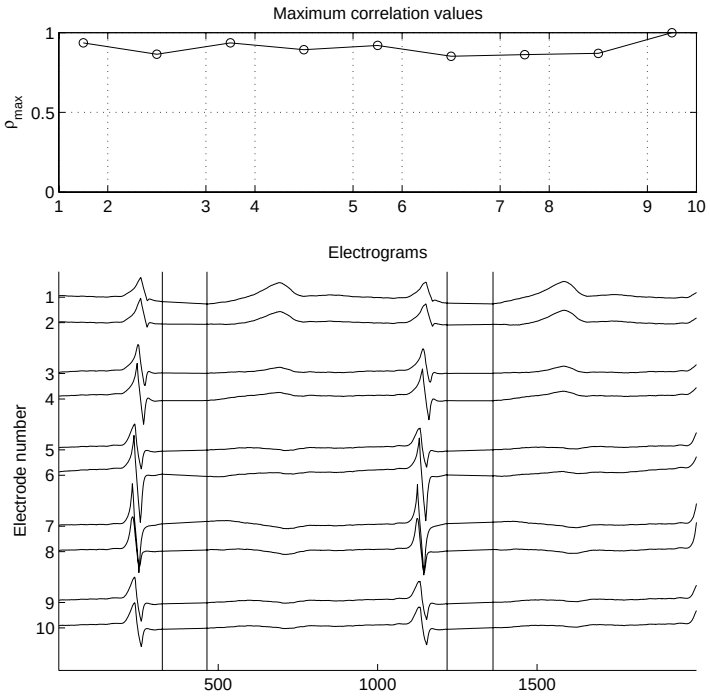

Figure 4.30: Example of the connection between correlation values and electrogram shapes in a sinus rhythm recording. Top: correlation values between electrogram pairs. The x-axis scale indicates electrode placement on the catheter. Bottom: 2-second segment of the electrograms. The shapes of the recorded electrograms change gradually along the catheter, resulting in high correlation in all pairwise comparisons. The vertical lines indicate the segments where ventricular artifacts were removed by linear interpolation.

4.6.4 Correlation

The maximum correlation values in each recording are plotted in Figures 4.31 (ectopic atrial tachycardia), 4.32 (sinus rhythm), and 4.33 (atrial fibrillation), where it is seen that correlation values are generally found to be higher during sinus rhythm than during atrial fibrillation or tachycardia.

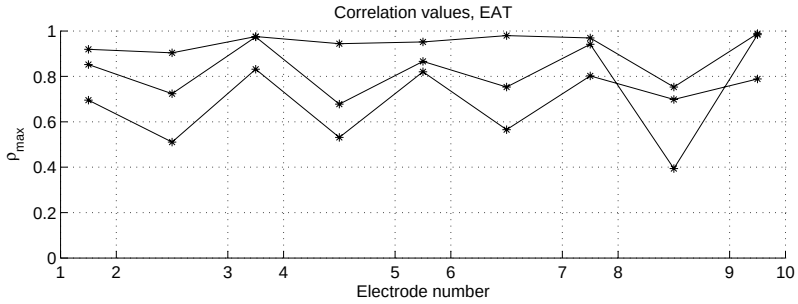

Figure 4.31: Correlation values, recordings made during ectopic atrial tachycardia.

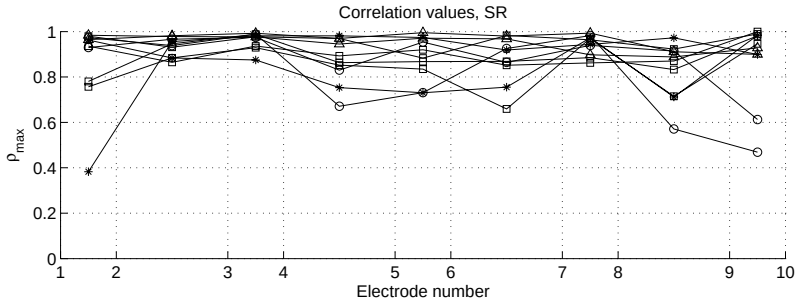

Figure 4.32: Correlation values, recordings made during sinus rhythm. Symbols denote recordings from patients with history of □: atrial fibrillation, ∗: ectopic atrial tachycardia, △: atrioventricular reentrant tachycardia, and ○: AV-nodal reentrant tachycardia.

4.6.5 Time delay and conduction direction

The cumulative time delays for each recording are plotted in Figures 4.34 (ectopic atrial tachycardia), 4.35 (sinus rhythm), and 4.36 (atrial fibrillation).

Figure 4.34 shows that in the two recordings made in cases with left atrial ectopic focus, the impulses were moving from left to right. In the recording made in the case with right atrial ectopic focus, the impulses were moving from right to left.

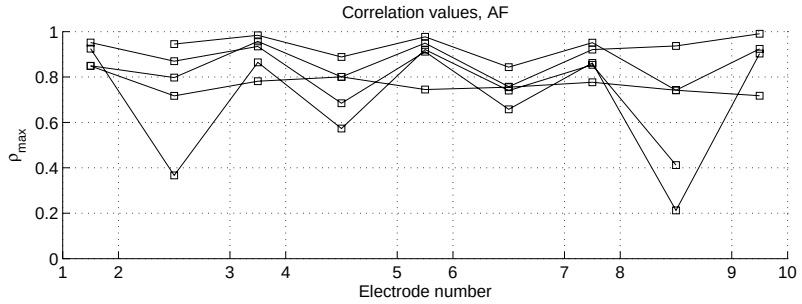

Figure 4.33: Correlation values, recordings made during atrial fibrillation.

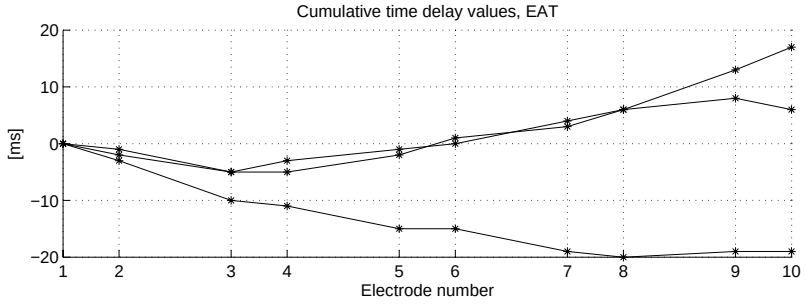

Figure 4.34: Cumulative time delay, recordings made during ectopic atrial tachycardia.

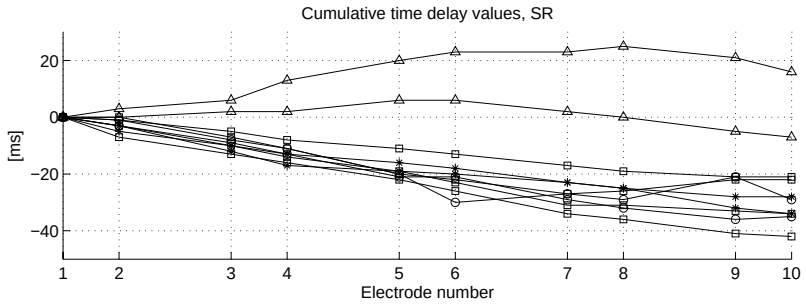

Figure 4.35: Cumulative time delay, recordings made during sinus rhythm. Symbols denote recordings from patients with history of □: atrial fibrillation, ∗: ectopic atrial tachycardia, △: atrioventricular reentrant tachycardia, and ○: AV-nodal reentrant tachycardia.

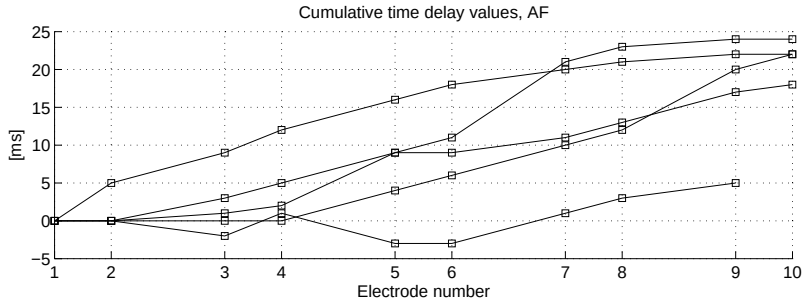

Figure 4.36: Cumulative time delay, recordings made during atrial fibrillation.

Chapter 5

Discussion

5.1 Signal acquisition and preprocessing

5.1.1 Analog input characteristics

According to the recommendations of AHA (American Heart Association) [15, 91], the input frequency characteristics of equipment acquiring ECG should be at least 0.05–150 Hz. The lower cut-off at 0.05 Hz would prevent any induced artifacts of the ECG likely to occur if higher frequencies were used [91]. The A/D (analog-to-digital) conversion should be performed at a minimum sampling rate of 500 Hz and minimum resolution of 10 μV.

The Siemens system used to record ECG and VCG well met the latter criteria with its 1000 Hz, 0.625 μV A/D conversion. Unfortunately, the input filter characteristics of the equipment were not known. However, since the hardware was equivalent to that used in Siemens' commercial electrocardiographs, it was assumed that the recommendations were met.

The BARD system also meets the required sampling rate, using 1000 Hz. The A/D conversion and input filtering may be chosen in different steps. In the electrogram recordings performed in this study, a maximum input voltage of 2 mV was chosen, with 16-bit A/D conversion, and input filters set at 0.01–500 Hz.

5.1.2 Low-frequency artifact filtering

In all recordings of ECG, VCG, and electrograms, low frequency artifacts were present and necessary to be removed before subsequent analyses. The activity of the heart was assumed to be a repetitive pattern of the, serial, waveforms PQRST. The lowest frequency component of the signal would then correspond to the interval between each PQRST. With a lower bound for the heart rate of 30 bpm, an appropriate low-pass filter would have the cut-off frequency 0.5 Hz, such a filter would, however, induce serious distortions in the ECG [91].

Since no analyses in this study were performed in real-time, the low-frequency artifacts could be filtered by applying a 0.5 Hz low-pass filter twice, forward and backward. The second, reverse time-filtering would then remove the distortions

induced by the first [92, 93]. This technique was applied to all ECGs, VCGs, and electrograms recorded in this study. Although electrograms have a different morphology that ECGs and VCGs, the same 0.5 Hz low-pass filter would be appropriate since, during sinus rhythm, the lowest frequency is determined by the heart rate and during atrial fibrillation, is much higher (compare Figures 4.29 and 4.30).

Throughout the study, no recordings were found that came even close to a heart rate of 30 bpm, thus no need for lowering the 0.5 Hz cut-off was present.

5.2 Heart rate-stratified histogram analysis

5.2.1 The effect of non-narrow QRS-complexes

One prerequisite of heart-rate stratified histogram analysis is that only atrial fibrillation with narrow QRS-complexes should be included. In the output of the DelMar analysis system, the series of RR intervals, other types of beats are marked with 9999 or 0. The MATLAB program discards these as if they were not present which will introduce an artifact; sequences that are not true. The result is illustrated in Figure 5.1, where it can be seen that the narrow QRS-complexes before and after the deviant beat or beats will actually be treated as if they were the same.

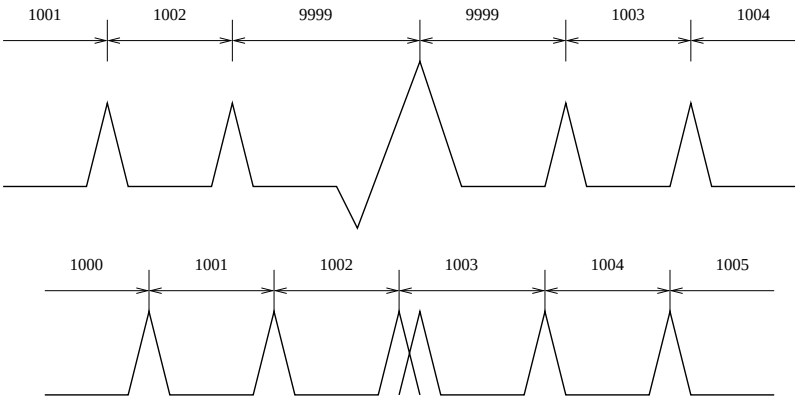

Figure 5.1: Illustration of what happens when beats are discarded. The rejected beat is identified by the two '9999' in the RR interval series. If these are simply removed, the RR interval series will look as if the second beat of interval '1002' and the first beat of interval '1003' are actually the same. The result would be a false series of the intervals '1000'–'1005'.

The influence of this artifact on the result of the analysis depends on the number of rejected beats. This number varied among the cases, as can be seen in Figure 5.2.

The results from Paper I were not seen to change when attempts were made to correct the analyses and only include true RR interval sequences. This may be

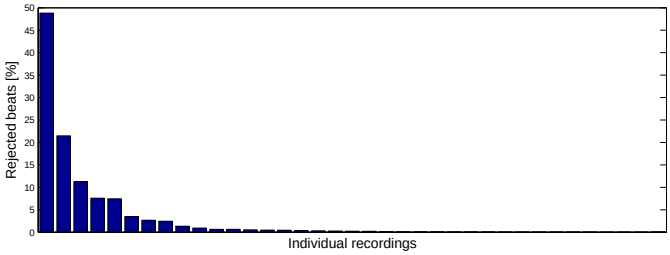

Figure 5.2: The amount of rejected beats of each individual ambulatory ECG recording, i.e., the number of rejected beats compared to the total number of beats, expressed as a percentage. Recordings are sorted, starting with the one with the highest amount of rejected beats. If rejected beats are not handled correctly, they may introduce erroneous RR interval sequences (see text and Figure 5.1).

referred to the fact that parameters were only measured at the heart rate level where PDC occurred, and the number of RR intervals sufficient to produce a reliable distribution. The effect of excluding rejected beats was seen in the histograms produced at the lowest and highest heart rates of an individual recording, where the number of RR interval sequences was too low to create reliable distributions.

5.2.2 The effect of smoothing

Histogram smoothing was performed by repeatedly applying a moving average filter, with the purpose of removing all local maxima except those belonging to the different distributions of RR intervals. This would in effect be equal to low-pass filtering, with the difference of using the smallest distance between two peaks as the criterion to continue smoothing rather than a cut-off frequency. Due to the ripple of the histogram bars at the tails of the distribution, the moving average had to be applied a large number of times, even if the two, or more, dominant RR interval distributions did not need further smoothing. The result is illustrated in Figure 5.3, where it can be seen that the amplitudes of the peaks have decreased significantly, most noticeable in the narrow peak of shorter RR intervals.

An alternative way of smoothing the histograms would be to use a moving median filter instead of a moving average. One advantage would then be that individual bars with higher values than the adjacent bars would be decreased in the first pass of the filter instead of, in the moving average case, being smoothed and possibly introducing an artificial peak. Such effects could be seen in the histograms created using RR interval sequences with low heart rate where, due to the overlap of the sequences, individual bars could become dominant.

Figure 5.3 also shows an example of median filter smoothing and the combination of first applying a moving median and then a moving average filter. The differences compared to the moving average filter used in Paper I is that the amplitudes of the peaks are better preserved and the minima between two peaks look more like the unfiltered histogram.

The results of Paper I would probably not be affected of a different smoothing

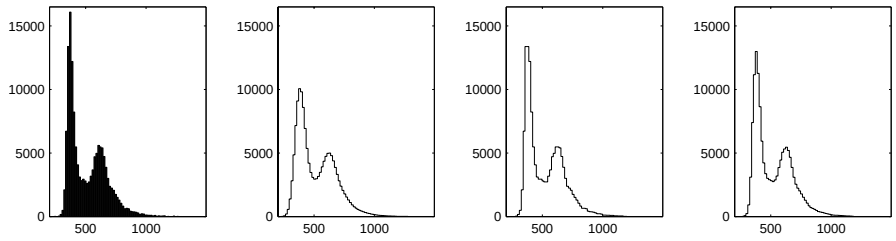

Figure 5.3: The effect on histogram morphology using different smoothing methods. First: original histogram. Second: after moving average only, the histogram is smoother but both peaks have become lower and wider. Third: after moving median only, peak amplitudes are better preserved and the minimum between the peaks looks more like the original histogram. Fourth: after moving median applied once followed by moving average, height and morphology are well preserved, but widening of the peaks can still be observed.

method, since only PDC and peak values at PDC were recorded. In almost all recordings, PDC occurred at a heart rate interval where many RR intervals were included in the histogram, requiring less iterations of the filter and thus reducing the risk of inducing artifacts. However, if a more detailed analysis was to be made, of all heart rate intervals, for example the '3D' version shown in Figure 4.3, the smoothing method should be evaluated more in detail.

5.2.3 The effect of polynomial fitting

Fitting second order polynomials to the histogram peaks allowed a resolution of 1 ms instead of the 15–16 defined by the output of the DelMar system. Figure 5.4 illustrates the performance of the peak detection in two cases, one with a single-bar peak and one with a double-bar peak.

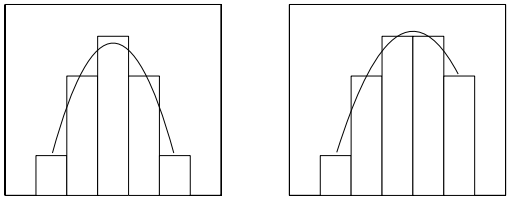

Figure 5.4: Illustration of the effect of fitting a second order polynomial to the RR interval histogram peaks. In the left case, the original value of the peak's position and that of the fitted polynomial will be equal. In the right case, the difference may be 7–8 ms. Intuitively, the fitted polynomial returns a more true result.

In the case where the peak is a single bar, the original value and that of the fitted polynomial will be the same, albeit the amplitude is slightly decreased. In the case where the peak is made of two bars, the polynomial will provide a

more correct peak value since, intuitively, the correct value should be positioned between the two bars. The difference between the original value and that of the fitted polynomial will in this case be 7–8 ms.

A drawback of the polynomial fitting is that a second order polynomial will always create a symmetric peak and it can be seen in the histograms that the two RR interval distributions are skewed with a longer tail on the side with longer RR intervals. The second order polynomial fitting probably works best on the distribution with longer RR intervals, since it is wider and the fitting is made on just five bars which may, locally, be approximated as a symmetrical peak. However, the distribution of short RR intervals is often very narrow (Figure 5.3) and the five bars may, in the histograms made at the highest heart rate levels, cover the peak and make the approximation bad. A more advanced peak identification could therefore be desired.

5.2.4 Peak values without unimodals

The results shown in Tables 4.1, 4.2, and 4.3 were calculated using PG of 0 and PVR of 1.00 in the cases where only one RR interval distribution was found. This was justified by the hypothesis that these cases were regarded as having two distributions of RR intervals, located at the same position. However, since the analysis did not provide proof of this, the numerical values of the analyses with these cases excluded are presented in Table 5.1. The statistical P values do not change since ties are discarded.

Completing Table 4.1

	PG [ms] at PDC		PVR at PDC	
	0–7 hrs	17–24 hrs	0–7 hrs	17–24 hrs
median	162	165	1.38	1.38
mean	168 (60)	178 (51)	1.41 (0.16)	1.42 (0.12)

Completing Table 4.2

	PG [ms] at PDC		PVR at PDC	
	Control	Interv.	Control	Interv.
median	153	173	1.36	1.31
mean	161 (59)	178 (57)	1.32 (0.21)	1.33 (0.22)

Completing Table 4.3

	PG [ms] at PDC		PVR at PDC	
	0–4 hrs	8–12 hrs	0–4 hrs	8–12 hrs
median	154	177	1.33	1.36
mean	155 (78)	192 (71)	1.35 (0.19)	1.40 (0.18)

Table 5.1: Numerical values of Tables 4.1, 4.2, and 4.3 with cases with only one RR interval distribution excluded instead of being recorded with PG of 0 and PVR of 1.00

5.2.5 Additional considerations of the comparison between control and intervention in Group A

In Paper I, it was stated that PV(f) and PVR "were unaffected". This statement is true in the sense that no statistical significances were found but somewhat unfortunate since, based on the definitions in Section A.3, PVR cannot be unaffected if PG has changed as a result of increasing PV(s) and unaffected PV(f). It can be seen from the individual values of Table 2 of Paper I that PV(f) is increased in six cases, decreased in two and unaffected in one. Maybe, had the material been larger, the results would show that both PV(s) and PV(f) move towards longer RR intervals by the same amount (calculated as percent). This would then leave PVR unaffected and PG would increase.

5.2.6 Relation between histogram peaks and AV-nodal function

The two peaks found in most of the HRSH analyses agree well with the hypothesis of the AV node having two inputs, or pathways, with different electrophysiological properties [64, 94]. However, it does not readily explain the cases where only one peak is found and not those where a third, or even fourth, peak is seen (Figure 5.5).

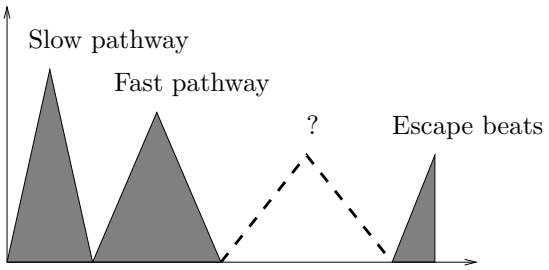

Figure 5.5: Schematic illustration of the peaks found in HRSH analyses. The two leftmost peaks are believed to belong to the slow and fast pathways of the AV node. The peak to the right is positioned at about 1500 ms, equal to 40 bpm, and may therefore be explained by escape beats initiated from the automaticity of the AV node. The fourth peak may have different explanations, see text.

In the cases of 'multimodal' distribution of RR intervals, one peak was often seen at the rightmost end of the histogram, at 1500 ms or 40 bpm. This was considered to be the rate of the automaticity of the AV node, the RR intervals of this peak are then not the result of the electrophysiological properties of the AV-nodal inputs, but rather of the AV node itself.

Following the theory of multiple peaks in the RR interval distribution correlating to multiple AV-nodal pathways, the fourth peak may be the result of multiple pathways [95], possibly even located in the left atrium [96].

It should be remembered that analyzing AV-nodal properties by RR interval-based methods is to use circumstantial evidence. It is an indirect way of assessing the number of pathways and their relation to ventricular rate. Direct input-output measurements of the AV node is probably not possible. However, using catheter based techniques, manipulating the supposed AV-nodal pathways produces a direct result on the RR interval distribution [64, 94], supporting the method.

5.3 Signal-averaged P waves

5.3.1 Similarity criterion

In this study, the criterion used to define whether two P waves were equal, was that the correlation coefficient found, possibly after time-shifting, should exceed 0.9 in all leads. Correlation seems to be the most common methodology used, although other studies present higher values of the threshold, e.g. 0.95 [44], 0.97 [50], 0.98 [97], or even 0.99 [49]. Based on the findings in this study (Figures 4.10 and 4.12), these higher thresholds may discard too many P waves, as even the value 0.9 used here can be argued against as being too high.

Other criteria than correlation may be suggested, for example residual analysis similar to that described in Appendix C.4. However, the need for a threshold will probably remain, regardless of the similarity criterion chosen, and although the exact pattern of P wave variability may be altered, the different morphologies found should stay the same.

5.3.2 P wave grouping methodology

Different methods of extracting the dominant P wave morphology have been suggested. Template matching using a similarity criterion is the basis but the methodology used when choosing the template can vary. Suggested methods are to use the first 10 P waves [44], the first 8 seconds [50], or just one single P wave chosen at random [97] or by an operator [49].

The method presented in this dissertation attempts to identify all morphologies of a recording, using an iterative template matching algorithm. In a sense, all P waves of the recording are then included in the creation of the different templates, making the method computationally heavy. An aspect that needs to be addressed in the future, is that this method does not allow signal-averaging of a fixed number of P waves or continuous adding of P waves to the average until the noise level is below a specified threshold.

5.3.3 P wave signal averaging and smoothing

Signal averaging of P waves offers some attractive features. Unlike filtering, it does not introduce any phase shift, and may remove artifacts in the same frequency range as the desired signal, in this case the P wave. In the ideal case, P waves should be aligned according to the initiating impulse, but since that is not known, time-shifting and correlation calculations are performed. Since it is

hard to perform an exact alignment of P waves, a low-pass filter effect will be introduced.

Since noise is decreased proportional to the square-root of the number of P waves included in the average, it will never be completely removed. In this study, this was not found to be a problem in the P wave group with the largest number of members, but noticeable in the other groups, introducing ambiguity in the parameters used to describe P wave morphology. To avoid this, smoothing was performed after signal averaging, by means of repetitive application of a moving average filter. This was found to be very efficient and allowed determining the morphology parameters in groups with quite few P waves. It should, however, be remembered that smoothing offers only a cosmetic improvement of the signal. Both the noise and the desired signal, the P wave, are affected. Specifically, amplitude measurements should be interpreted carefully.

5.3.4 Manual interaction

The method for analysis of signal-averaged P waves described in Appendix B contains a number of instances where a manual input is needed.

User-defined parameters

Two user-defined values are the thresholds of the similarity criteria used in creating different QRS complex and P wave groups, based on differences in morphologies. The values, throughout this study both chosen to be 0.9, would affect the analysis results; if high, more groups will be created with less different morphologies, if lower, less groups will be created. Neither of these cases can be said to be more correct than the other and the manual choice of these parameters can therefore be used to create different analyses that may eventually provide different, but still correct and valuable results.

The user-defined length and position of the signal window preceding each QRS complex in which P waves are believed to exist, are other parameters requiring human interaction. These are crucial for the analysis, since the similarity criterion of the P wave grouping is based on correlation. The window should be positioned in a way that it covers the whole P wave and have a length such that preferably only the P wave is included in the correlation.

Manual setting of onset and end

A different kind of manual input is that of providing exact settings of the onset and end of QRS complexes and P waves. If these are not made adequately, the result may be erroneous values of morphology parameters. In the work done to develop the P wave analysis method, several ideas of wave delineation were implemented and evaluated. Some worked better than others but none were found to be fully satisfactory to be used as an 'automatic setting' in the sense that it would produce an acceptable result in all cases. The conclusion was then to use manual setting in all cases to assure that all results and comparisons were based on identical analyses.

The answer to the question of whether to use manual or automatic analysis would perhaps be related to whether it is to be used in a clinical or a research situation. In the clinical situation, automated analysis would of course be preferable, even if it is not fully correct in all cases. A decision will never be made without a physician accepting the values from the analysis or discarding them if they are obviously incorrect. Also, the automated analysis has the advantage of being fully reproducible, i.e., given the same input it will always produce the same result. In research however, when applying a method on a new set of data, the results cannot be compared to any previous knowledge and it is therefore important that the values of all parameters can be relied upon to be based on true manifestations of biology, instead of artifacts. Human interaction is then needed to validate the performance of software analysis algorithms before basing findings solely on their output.

For this reason, the manual settings of the method described have been kept throughout the project. Similar to other studies [68, 98], the computer has been used to create a much more extensive analysis on more data than otherwise possible, but the important parameters were left to the human brain, which is still considered superior when it comes to the final touch-up [99].

The major argument against manual setting is that of reproducibility and the risk of 'individual' analysis results. The results of the comparison between the settings of the 'Physician' and 'Engineer', showed that this is probably not an issue. The differences were found to be relatively small, compared to the duration of the P waves and the possible setting resolution, as defined by pixels on the screen. The differences were somewhat larger in the comparison between 'Physician' and 'EP Nurse' but still with a mean close to 0. This indicates that after an initial training period, the 'EP Nurse' will probably perform equally to the 'Physician' and the 'Engineer'. These results show that there exists intuitive positions of P wave onset and end, indicating that analog computer settings should be possible. However, the translation from such intuitive measurements into a working algorithm may prove difficult.

5.3.5 Spatial magnitude

The combined signal, Spatial magnitude (Equations (3.2) and (B.1)), offers some attractive features in the analysis of signal-averaged P waves. By giving an overall view of the atrial activation pattern, independent of conduction direction, it may be possible to identify delays between the activations of the right and left atria. This would show as two distinct peaks separated in time, instead of just one.

However, the Spatial magnitude has some possible drawbacks which must be addressed before interpreting its morphology.

One such drawback, illustrated in Figure 5.6, shows that under certain conditions, the time of onset may be lost compared to the recorded leads, resulting in an erroneous morphology. The situation may be solved by defining the amplitude of all leads to 0 at the P wave onset. Although this may seem a harmless operation, just adding a constant, it will obviously affect the values of the morphology parameters defining amplitudes of local maxima and minima, and the location of zero crossings. Also, it will not allow the calculation of Spatial magnitude until

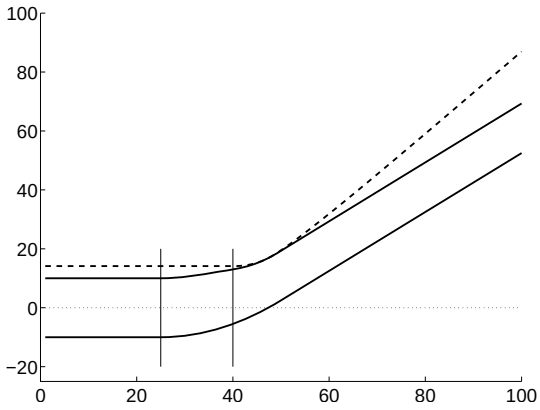

Figure 5.6: Illustration of a possible artifact in the Spatial magnitude. The onset, which in the two leads (solid lines) is located at $t = 25$, is in the Spatial magnitude (dashed line) not identifiable until at $t = 40$. Only two leads are included for simplicity but the example may easily be extended to three leads.

after the P wave onset has been defined, i.e., after signal-averaging and, possibly, smoothing of the individual leads.

Another drawback is that the morphology of the Spatial magnitude is highly dependent of the amplitudes of the recorded leads, as illustrated in Figure 5.7. The morphologies of the recorded leads are obviously the same in both cases, and the interpretation of atrial conduction pattern would be the same in both cases. However, due to the differences in amplitudes, the Spatial magnitude has one peak in the first case but two in the second.

5.3.6 Analysis of variability

In Figures 4.12 and 4.13 it was illustrated that the algorithm creating P wave groups can produce differences that in some cases may not be relevant, they are just variations of the same conduction pattern. For a more accurate analysis, it would therefore be desirable to reduce these groups into one.

The immediate way to do this would be to lower the threshold of the similarity criterion from 0.9 to a value that produces only one group. However, since the same value should be used in all analyses, there may be a risk of also merging groups where a small difference in morphology is relevant and it is desirable to keep the two groups separate.

Another, perhaps more preferable way to reduce the number of groups would be to allow a manual choice of groups to merge by means of some visual, graphic tool. This would have the benefit of allowing a high value of the threshold and still being able to reduce the number of groups created.

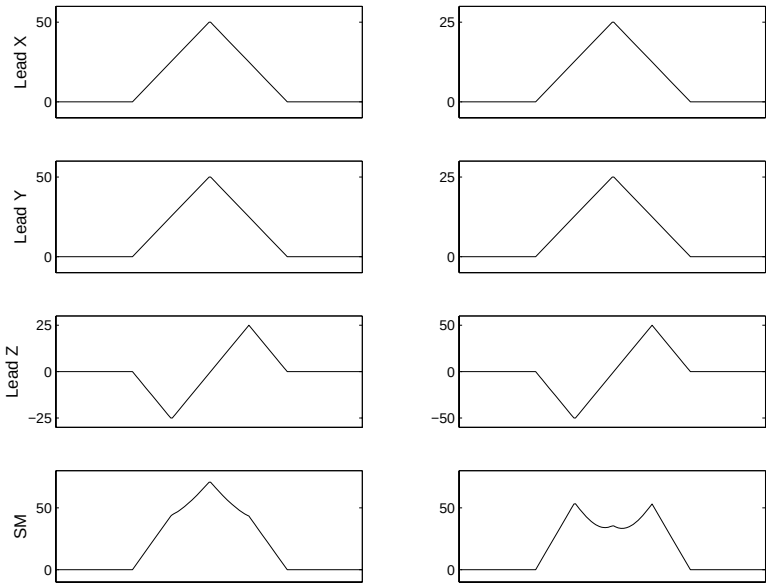

Figure 5.7: Schematic illustration of a possible drawback of the combined signal, SM (spatial magnitude). Using Leads X, Y, and Z of the left column results in a single-peaked SM, using these in the right column results in a double-peaked SM. Although the morphologies of Leads X, Y, and Z would, in both cases, be interpreted as originating from equal underlying atrial conduction patterns, the differences in amplitude changes the appearance, and interpretation, of SM drastically.

5.4 P wave modeling

From the results of the P wave modeling, three conclusions may be pointed out:

- It can be done;
- A linear system is sufficient;
- The system may be of low order.

The first point is by no means obvious, and shows that the atrial conduction follows a predictable pattern. The second and third point gives information on the complexity of the atrial activation, with a linear system being the simplest form of model, and the low order found to be sufficient (9, in this study), indicating that the P wave is a signal of low complexity.

5.4.1 Factors affecting signal approximation

Before accepting the P wave modeling results based on the simplified analysis of P wave complexity above, the implication of the expression "it can be done" needs

to be considered. According to Figures 4.17 and 4.18, residuals did persist, but were, in this study, considered to be acceptable. In another context, such residuals may be considered too large and the above conclusions not possible.

When analyzing the needed, and possible, level of signal approximation, electronic resolution and system-induced artifacts should be considered, as well as biological resolution and biological artifacts.

Electronic resolution

The Siemens equipment used in this study to record ECG and VCG appears quite capable with its 1 kHz, 0.625μV sampling resolution. The quantification effect in a 150 ms, 0.1 mV P wave would hardly be noticeable without magnification, with the resolution being 150 time instants and 160 amplitude levels.

When the recorded signals are then subjected to subsequent analysis, the amplitude resolution following signal-averaging and possibly smoothing, will be equal to that of the computer system, i.e., practically negligible.

Biological resolution

Different from the acquisition equipment, the heart may be considered to be 'analog'.[1] This would then imply the need of an analysis of the 'morphology resolution': what parts of the morphology belong to the overall conduction pattern and what parts are the result of variation between individual beats. In previous studies [40, 83], the resolution considered in making conclusions was limited to just a few local maxima and minima.

Electronic artifacts

Artifacts that may be equipment-associated are different kinds of electrical noise, such as powerline interference or higher frequencies emanating from lights or other electrical equipments positioned near the recording device. The acquisition equipment may also have inherent noise that may be seen as bitripple in signals that should be steady.

A common electric artifact encountered in ECG analysis, though not presented or dealt with in this study, is the impulse of an artificial pacemaker. These impulses are very short and have a large amplitude which creates problems in the alignment of waves, when performing signal-averaging.

Biological artifacts

Biological artifacts seen in an ECG or VCG may be originating from other sources than the heart. One example being low-frequency artifacts, 'baseline wander', often due to study subjects moving. Another example is higher frequency artifacts believed to emanate from muscle control signals, also often due to study subjects moving.

[1] Of course, since there is a quantum charge, that of the electron, $-1.6 \cdot 10^{-19}$ As, the whole nature may be regarded as 'quantified' in a sense. However, reflecting on such a resolution, or even the currents moving in or out of individual cells, would be way beyond the scope of this discussion.

There may also be artifacts in the recorded signal itself. Breathing causes the study subjects to move and will change the signal morphology over the breathing cycle because the geometrical relation between the electrode location and the position of the heart may vary slightly. There may also be a variation of morphology between individual beats due to the conduction pattern not being completely identical from beat to beat.

5.4.2 P wave complexity

All of the above mentioned properties of recording and analyzing biological signals such as ECG and VCG should be considered when choosing an appropriate level of acceptable signal approximation.

In the case of modeling P waves, the first question is what kind of model to choose. In this study, an impulse response model was chosen under the assumption that the P wave is initiated by an impulse. A linear, state-space realization of the model was then chosen as the initial approach, for reasons of simplicity. The second question in the modeling regards appropriate model order. It is desirable to produce an as accurate result as possible without including electrical or biological artifacts. In this study, specifically, it would also be desired to avoid modeling signal components that may be attributed to biological variation, i.e., variations that would probably not be seen if another recording was performed on the same subject. Hence the complexity needed in the modeling could be kept low.

An additional consideration, also supporting the choice of low-complexity modeling, was that the modeling was performed on signal-averaged P waves, a technique which primarily is aimed at reducing stochastic, uncorrelated noise but in addition acts like a low-pass filter reducing not only noise but possibly also P wave components of higher frequencies.

The model order was chosen from empirical evaluation of all the plots like the one shown in Figure 4.17, where the desired cut-off between singular values correlated to signal and those correlated to noise was not obvious in all cases. Model order 9 was then chosen as the lowest value that would be acceptable in all modeling experiments.

During the analyses of P waves throughout this study, there has been a number of situations where the level of detail in the results needs consideration. A few examples are:

- The reproducibility of manual setting of P wave onset and end was shown to be in the order of a few ms. Can that be accepted considered that the P wave, especially after signal-averaging, has onset and end that is quite smooth?
- Is a resolution of P wave duration of 1 ms realistic? It is possible that such a detailed analysis provides an unnecessary impression of exactness, leading to expectations of for example reproducibility that are impossible to meet.
- What level of the similarity criterion should be used to obtain only 'true' changes of morphology in the analysis of variability? Perhaps 0.9 is too high if the analyses of morphology only concern a few peaks, or classification as 'unimodal' or 'bimodal'.

- When comparing different lead systems, recorded or derived, what accuracy should be demanded from the comparison results? There may be biological variations in individual recordings making a perfect comparison impossible. It should also be remembered that Frank's model was built around a 175 lbs, 5 foot $10^1/_2$ inches male subject [100] and, although proved to work well even in infants [101], theoretically limited in its versatility.

5.5 P wave classification

5.5.1 Choice of parameters

The three parameter sets used in Paper III are all based on data obtained from the modeling of the P wave, either state-space (eigenvalues of matrix A) or transfer function (denominator and lead Z numerator polynomials). The reason for this was previously encountered problems when trying to identify intuitive and visual ways of separating the two different kinds of P waves. However, since the initial classification is made by manual definition of a P wave being either 'normal' or 'possible inter-atrial conduction defect' based on its general morphological appearance, the signal itself may be used as a parameter set.

5.5.2 Classifying as uncertain

The classification in Equation (E.3) will only produce two results, correctly or incorrectly classified parameter sets. In a clinical situation, it would be of great value to avoid the incorrectly classified P waves by expanding the threshold ϑ to an interval where parameter sets are classified as 'uncertain'. This may avoid the incorrectly classified data at the price of some correctly classified being changed to the group 'uncertain'. With this change, Equation (E.3) would be

$$\hat{\theta} \in \begin{cases} A, & \lambda^T\hat{\theta} > \vartheta + \delta \\ \text{uncertain}, & \vartheta - \delta \leq \lambda^T\hat{\theta} \leq \vartheta + \delta \\ B, & \lambda^T\hat{\theta} < \vartheta - \delta \end{cases}$$

where δ is the, symmetric, distance on either side of the threshold ϑ that defines the interval of uncertainty. If the symmetry is not desired, for example if the covariances of the groups are very different, the interval may instead be defined by two different distances, δ_1 and δ_2. Equation (E.3) would then be

$$\hat{\theta} \in \begin{cases} A, & \lambda^T\hat{\theta} > \vartheta + \delta_1 \\ \text{uncertain}, & \vartheta - \delta_2 \leq \lambda^T\hat{\theta} \leq \vartheta + \delta_1 \\ B, & \lambda^T\hat{\theta} < \vartheta - \delta_2 \end{cases}$$

5.6 Electrocardiographic lead conversion

5.6.1 Evaluation of influence of erroneous electrode positioning

In an attempt to evaluate the influence of the erroneously positioned electrodes in the Frank-lead recordings, five of the healthy subjects were selected for repeated recordings. Two new recordings were performed on each of them, one with correct positioning of the electrodes and one with the erroneous positions previously used.

From an immediate eyeball inspection, it seemed like the morphology of the P waves did not change at all. With good approximation, the two newly made recordings looked the same. The same observation was made when comparing with the previously performed erroneous Frank-lead recording.

When analyzing amplitudes, differences were found between the two recordings, shown in Table 5.2. From these five cases, it was obvious that the amplitude

	Max, Lead X	Max, Lead Y	Min, Lead Z	Max, Lead Z
Case 1	$44 \rightarrow 42$	$156 \rightarrow 99$	$-35 \rightarrow -36$	$20 \rightarrow 23$
Case 2	$43 \rightarrow 41$	$193 \rightarrow 138$	$-55 \rightarrow -55$	$3 \rightarrow 10$
Case 3	$49 \rightarrow 48$	$147 \rightarrow 107$	$-46 \rightarrow -46$	$10 \rightarrow 11$
Case 4	$37 \rightarrow 35$	$186 \rightarrow 131$	$-44 \rightarrow -36$	$29 \rightarrow 30$
Case 5	$69 \rightarrow 72$	$56 \rightarrow 46$	$-8 \rightarrow -15$	$42 \rightarrow 41$

Table 5.2: Changes in amplitude between the erroneously recorded VCG and the correctly recorded. Differences are small in Leads X and Z but obvious in Lead Y where a decrease is seen. All values are μV.

of Lead Y is smaller in the correctly recorded Frank leads. This agrees with the observation of Paper III, where the least-squares fitting showed amplitude differences in both the healthy cases and those with a history of atrial fibrillation (Table 4.7).

Frank's equation to calculate Lead Y (Equation (3.1)) is based on the electrodes on the back of the neck and the foot [18]. The misplacement of the neck electrode (Figure 3.1, Electrode E_6) on the front instead of on the back may alone be accounted for the amplitude differences, since the other misplaced electrode is not included in the Lead Y equation.

The effect of the other misplaced electrode (Figure 3.1, Electrode E_3) was more difficult to observe. It is included in the equations of both Leads X and Z but is, according to Frank, in both cases mostly used for purposes of correction [18]. Some effect of the amplitudes were seen (Table 4.7), especially on Lead X in the healthy cases, which may be attributed to the misplacement of this electrode. An unavoidable erroneous positioning of electrode E_3 may occur in female subjects, where it might be positioned on, or below, the left breast. According to Frank, "This error is not acute..." [18] since the signal recorded from this electrode is used for correction rather than as a major component of the resulting vector.

Figure 5.8 shows the P wave morphologies of the four different recordings performed on the healthy subject denoted as Case 5 in Table 5.2. The derived VCG

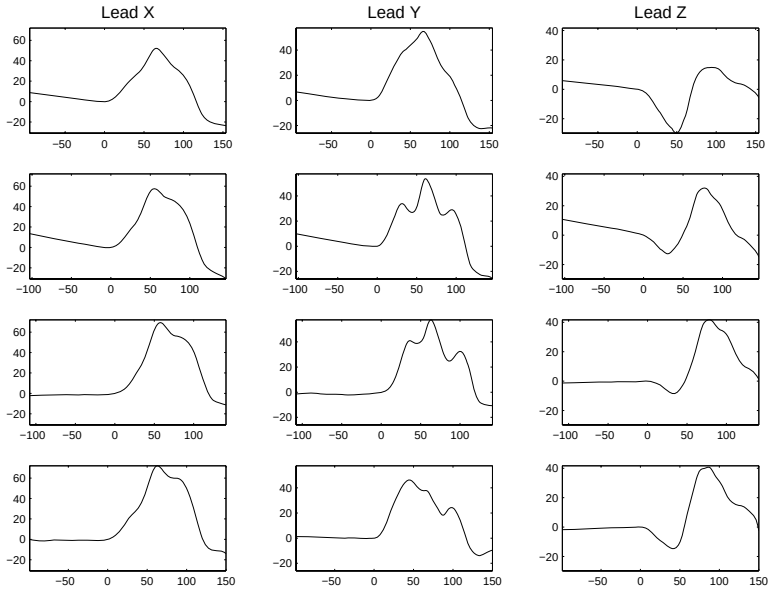

Figure 5.8: Illustration of the effect of erroneously positioned electrodes in a Frank-lead vectorcardiogram recording. First row shows derived VCG, second row shows erroneous VCG, third row shows second recording of erroneous VCG, and fourth row shows the correctly recorded VCG.

and erroneous VCG recorded for the study of Paper III showed a significant difference in morphology of Lead Y, where the VCG had triple peaks. The differences were reproduced in the second erroneous VCG recording, again showing the three peaks. In the correctly recorded VCG, the differences and the peaks are not as obvious.

An additional observation of Figure 5.8 is that Lead Z of all Frank-lead recordings have similar morphology whereas that of the derived VCG differs.

5.6.2 Evaluation of lead transformation

The results presented in Paper III were not unambiguous, the performance of the inverse Dower transform was satisfactory in preserving parameters, when observing the groups. However, in the individual case, the transform performed bad in many cases.

From an engineer's point of view, a much better individual performance would have been desired, in order to accept the derived VCG as a replacement for the recorded VCG. In the field of medical research, however, the most common type of analysis seems to be the comparison between two, or more, groups. In that context, it might be possible to, for example, compare one group with VCG obtained previously using one of the methods with new material obtained using the other method.

5.7 Correlation function analysis

5.7.1 Removal of ventricular artifacts

From Figure F.1, it is obvious that the removal of ventricular artifacts from the coronary sinus recordings is an important step of the analysis. Without removing the artifacts, the correlation function analysis would be dominated by correlation of the artifacts, due to their larger amplitude, instead of the coronary sinus signals. As evidenced in Figure 4.30, this technique is working as intended during sinus rhythm, and probably other regular, organized rhythms. In Figure 4.29, it can be seen that the linear segment resulting from the substitution of the ventricular artifacts is clearly visible, producing a more artificial appearance than in the sinus rhythm case.

To avoid the linear segment influencing the correlation analysis, other approaches may be suggested. The correlation between two signals, $x(t)$ and $y(t)$ is based on the calculation of the empirical covariance:

$$C_{xy} = \sum_i \left(x(i) - \bar{x}\right)\left(y(i) - \bar{y}\right)^T \tag{5.1}$$

One possible alternative to linear substitution of the ventricular artifacts would then be to use the mean of the signals, $\bar{x}$ and $\bar{y}$, instead. According to Equation (5.1), the contribution of those segments would then be 0.

Another alternative would be to choose the values of the indexing variable, i in Equation (5.1), to not be continuous (i.e., include all values 1,2,3,...,N) but instead only include the segments where there is only signal from coronary sinus (for example $i = 1, 2, 3, 6, 7, 8, \ldots$ if indices 4 and 5 contain ventricular artifacts).

However, it is unlikely that either alternative would change the outcome of the analysis. The more important part is the detection of the onset and end of the ventricular artifacts, at the same time leaving as much signal as possible for analysis.

5.7.2 Length of segments in correlation analysis

Figure 4.29 shows that the morphologies of the signals from the coronary sinus are not constant over time but rather variable. Including up to 60 seconds in the correlation function analysis may then be too long segments, producing a result that is too much 'averaged' to reflect the true conduction patterns. In a previous study [76], a "preferential conduction pattern" was assessed by analyzing short segments of atrial signals. Such an approach might had been advantageous in the case of coronary sinus signals as well, since it includes more detailed information on the variability of the conduction pattern compared to the rather crude measure of the whole signal.

5.7.3 Autocorrelation function analysis

A possible future extension of the method would be to include an autocorrelation function analysis to asses the atrial fibrillatory cycle length [102].

Chapter 6

Conclusions

"The ECG is accepted as a useful and important baseline test in all patients with known cardiovascular disease, dysfunction or arrhythmia during the initial evaluation. In some instances more than one ECG is required..."

The American College of Cardiology, 1992 [103]

Conclusions of the study

- Heart rate-stratified histogram analysis provides a way of analyzing the conduction properties of the AV node during atrial fibrillation. The distribution of RR intervals may be affected by medical intervention, indicating an effect on the function of the AV node.
- Signal-averaged P wave morphology provides information about the atrial conduction. By using orthogonal leads, geometrical interpretations may be performed on the direction and pattern of conduction. By looking at differences in P wave morphology, the variability of atrial conduction may be analyzed.
- Signal-averaged P wave morphology may be modeled accurately by using linear system identification. Modeling may be performed using low model order indicating a low complexity of the P wave signal.
- Different signal-averaged P wave morphologies may be automatically classified using the Fisher linear discriminant. The best result is achieved by using the P wave itself as input parameter.
- Mathematical conversion from recorded 12-lead ECG to orthogonal leads may be performed with good accuracy in most cases. Signal-averaged P wave morphology parameters associated with atrial fibrillation are preserved in the transform, provided that comparisons are made on a group basis. Further studies are needed to fully understand the performance of the transform on the individual level.

- Correlation function analysis is a suitable tool to evaluate conduction patterns from cardiac catheter recordings. During atrial fibrillation, consistent conduction directions may be found in signals recorded from the coronary sinus.

Acknowledgments

Financial support

The study was supported financially by grants from the following sources:

- Hjärt-Lungfonden;
- Franke och Margareta Bergqvists stiftelse för främjande av cancerforskning;
- Universitetssjukhusets i Lund stiftelser och donationer;
- Avtal om Läkarutbildning och Forskning (ALF-medel);
- Region Skåne.

Human support

Working as a PhD student means sometimes being alone with thoughts and experiments, other times it means working together with people, struggling towards the common goal.

Alone or together, I have had the pleasure of surrounding myself with just about the best people one could ask for. Below I will mention a few, the others not forgotten.

Evamaria, Tove, Linn You are the most important people to me, providing love and happiness on sunny afternoons as well as cold, rainy mornings. Together, we have embarked on this fantastic journey called Life, where each step is a new experience, and behind every corner there is a place where we have never been before. I could not wish for better travel companions than you.

Bertil Olsson It has been a long time since, in 1995, you asked me if I wanted to be research engineer at the Department of Cardiology. I am grateful that you believed in me and gave me the opportunity to try research and begin the PhD studies that have now resulted in this doctoral dissertation. You have always provided comprehensible explanations of the medical context I work in, and medical 'touch-up' of our manuscripts. Your PhD tutorship ends here, I hope our cooperation does not.

Rolf Johansson My advisor. Somewhere between your skills in Arabic and piloting airplanes, there is a vast knowledge in the field of engineering. I am happy that you have wanted to share that knowledge with me, patiently explaining to me what is obvious to you. I am also happy that our discussions many times have left the actual projects and manuscripts, instead becoming social events filled with stories and anecdotes from many different fields. It is my sincere wish that we can continue our cooperation in future projects.

Max Ingemansson For a while, we were the greatest, literally working day and night. With seven computers running MATLAB analyses and Arnold Schwarzenegger on the video projector, research was at its peak. Unfortunately, those days may never come back, we both have families and you have left the neighborhood. My wish is, that in the future, we will find a way to work together again.

Pyotr Platonov It was a dark and stormy night... when you, The Russian Guy, knocked on my door, looking for a place to stay. This was the beginning of a cooperation that quite fast turned into a deep friendship. You work hard and efficiently, getting things done. I let things take their time and strive for perfection in every detail. There were moments of irritation, but in the end, something good always came out. I am looking forward to our future projects and continued friendship.

Bjarne Madsen Härdig Your contribution to this study is probably bigger than I want to admit and less than you think... It has been invaluable to have you next door, as a colleague and friend, providing an opportunity to leave work for a while and talk about other things. Things like being a husband, becoming a father, being a father, all the things that life is really about. And then some!

Birgit Smideberg Dear Bibi... Yes, I'm afraid you are a poor computer operator. But however limited your skills in that area, just as large is your heart for all of us; those who work here, and those who visit, be they patients or merchants. Without you, our corridors would be a less welcoming place.

Irene Nilsson for sharing everyday computer struggle, and always accepting duty as 'healthy subject', **Lena Lindén** for always being the happy blonde with a smile for everyone, **Fredrik Holmqvist** for scientific and non-scientific discussions, **Monica Magnusson** and **all the people** at *Kardiologens arbetsavdelning* for making it a great place to work.

Bibliography

[1] A.D. Waller. A demonstration on man of electromotive changes accompanying the heart beat. *Journal of Physiology*, 8:229–234, 1887.

[2] W. Einthoven. Galvanometrische registratie van het menschelijk electrocardiogram. In S.S. Rosenstein, editor, *Herinneringsbundel*, pages 101–106. Ijdo Leiden, Leiden Eduard, 1902.

[3] W. Einthoven. Ueber die form des menschlichen electrocardiogramms. *Archiv für die gesammte Physiologie des Menschen und der Thiere*, 60:101–123, 1895.

[4] J.R Henson. Descartes and the ECG lettering series. *Journal of the History of Medicine*, pages 181–186, April 1971.

[5] J.W. Hurst. Naming of the waves in the ECG, with a brief account of their genesis. *Circulation*, 98:1937–1942, 1998.

[6] A.J. Moss. Introductory note to a classic article by Augustus D. Waller. *Annals of Noninvasive Electrocardiology*, 9(2):187–188, April 2004.

[7] W. Einthoven. Die galvanometrische Registerung des menslichen Elektrokardiogram: Zugleich eine Beurtheilung der Anwendung des Capillar-Elektrometers in der Physiologie. *Archiv für die gesammte Physiologie des Menschen und der Thiere*, 99:472–474, 1903.

[8] W. Einthoven. Le telecardiogramme. *Archives internationales de physiologie et de biochemie*, 4:132–164, 1906.

[9] W. Einthoven. The different forms of the human electrocardiogram and their signification. *The Lancet*, 1:853–861, 1912.

[10] W. Einthoven. Nieuwe methoden voor clinisch onderzoek. *Nederlandsch tijdschrift voor geneeskunde*, 29 II:263–286, 1893.

[11] Nobel lectures, physiology or medicine 1922–1941. Elsevier Publishing Company, Amsterdam, 1965.

[12] F.N. Wilson, F.D. Johnston, A.G. Macleod, and P.S. Barker. Electrocardiograms that represent the potential variations of a single electrode. *American Heart Journal*, 9:447–458, 1934.

[13] D.B. Geselowitz. The zero of potential. *IEEE Engineering in Medicine and Biology*, pages 128–132, 136, January/February 1998.

[14] Y. Okamoto and S. Mashima. The zero potential and Wilson's central terminal in electrocardiography. *Bioelectrochemistry and Bioenergetics*, 47:291–295, 1998.

[15] H.V. Pipberger, R.C. Arzbaecher, A.S. Berson, S.A. Briller, D.A. Brody, N.C. Flowers, D.B. Geselowitz, E. Lepeschkin, G.C. Oliver, O.H. Schmitt, and M. Spach. Recommendations for standardization of leads and of specifications for instruments in electrocardiography and vectorcardiography — report of the Committee on Electrocardiography, American Heart Association. *Circulation*, 52(2):*page 11–31*, 1975.

[16] A.R. Barnes, H.E.B. Pardee, P.D. White, F.N. Wilson, and C.C. Wolferth. Standardization of precordial leads. *American Heart Journal*, 15:235–239, 1938.

[17] E Goldberger. A simple indifferent electrocardiographic electrode of zero potential and a technique of obtaining augmented, unipolar, extremity leads. *American Heart Journal*, 23:483–492, 1942.

[18] E Frank. An accurate, clinically practical system for spatial vectorcardiography. *Circulation*, XIII:737–749, May 1956.

[19] H.V. Pipberger, S.M. Bialek, S.M. Perloff, and H.W. Schnaper. Correlation of clinical information in the standard 12-lead ECG and in a corrected orthogonal 3-lead ECG. *American Heart Journal*, 61(1):34–43, January 1961.

[20] C. Blomström-Lundqvist, M.M. Scheinman, E.M. Aliot, J.S. Alpert, H. Calkins, A.J. Camm, W.B. Campbell, D.E. Haines, K.H. Kuck, B.B. Lerman, D.D. Miller, C.W. Shaeffer, W.G. Stevenson, and G.F. Tomaselli. ACC/AHA/ESC guidelines for the management of patients with supraventricular arrhythmias: a report of the American College of Cardiology/American Heart Association Task Force on Practice Guidelines (Writing Committee to Develop Guidelines for the Management of Patients With Supraventricular Arrhythmias). 2003. American College of Cardiology Web Site, http://www.acc.org/clinical/guidelines/arrhythmias/sva_index.pdf.

[21] K.M. Ryder and E.J. Benjamin. Epidemiology and significance of atrial fibrillation. *The American Journal of Cardiology*, 84(9, Supplement 1):131–138, November 1999.

[22] V. Fuster, L.E. Rydén, R.W. Asinger, D.S. Cannom, H.J. Crijns, R.L. Frye, J.L. Halperin, G.N. Kay, W.W. Klein, S. Lévy, R.L. McNamara, E.N. Prystowsky, L.S. Wann, and D.G. Wyse. ACC/AHA/ESC guidelines for the management of patients with atrial fibrillation: a report of the American College of Cardiology/American Heart Association Task Force on Practice Guidelines and the European Society of Cardiology Committee for Practice Guidelines and Policy Conferences (Committee to Develop Guidelines for the

Management of Patients With Atrial Fibrillation). *Journal of the American College of Cardiology*, 38:1266i–lxx, 2001.

[23] Socialstyrelsen. *Socialstyrelsens riktlinjer för hjärtsjukvård 2004. Det medicinska faktadokumentet.* Bergslagens Grafiska AB, Lindesberg, June 2004. Swedish.

[24] A. Hersi and D.G. Wyse. Management of atrial fibrillation. *Current Problems in Cardiology*, 30(4):175–233, April 2005.

[25] S. Goodacre and R. Irons. ABC of clinical electrocardiography: Atrial arrhythmias. *BMJ (Clinical research ed.*, 324(7337):594–597, March 2002.

[26] J.L. Cox. Surgical treatment of atrial fibrillation: a review. *Europace*, 5:S20–S29, 2004.

[27] P. Jaïs, M. Hocini, L. Macle, Kee-Jon Choi, I. Deisenhofer, R. Weerasooriya, D.C. Shah, S. Garrigue, F. Raybaud, C. Scavee, P. Le Metayer, J. Clémenty, and M. Haïssaguerre. Distinctive electrophysiological properties of pulmonary veins in patients with atrial fibrillation. *Circulation*, 106(19):2479–2485, November 2002.

[28] M. Haïssaguerre, P. Jaïs, D.C. Shah, Atsushi Takahashi, M. Hocini, G. Quiniou, S. Garrigue, A. Le Mouroux, P. Le Métayer, and J. Clémenty. Spontaneous initiation of atrial fibrillation by ectopic beats originating in the pulmonary veins. *New England Journal of Medicine*, 339(10):659–666, September 1998.

[29] C. Schmitt, G. Ndrepepa, S. Weber, S. Schmieder, S. Weyerbrock, M. Schneider, M. Karch, I. Deisenhofer, J. Schreieck, B. Zrenner, and A. Schmig. Biatrial multisite mapping of atrial premature complexes triggering onset of atrial fibrillation. *American Journal of Cardiology*, 89(12):1381–1387, June 2002.

[30] G.D. Veenhuyzen, C.S. Simpson, and H. Abdollah. Atrial fibrillation. *Canadian Medical Association Journal*, 171(7):755–760, September 2004.

[31] H. Tada, H. Oral, M. Ozaydin, R. Greenstein, F. Pelosi Jr, B.P. Knight, S.A. Strickberger, and F. Morady. Response of pulmonary vein potentials to premature stimulation. *Journal of Cardiovascular Electrophysiology*, 13(1):33–37, January 2002.

[32] R.J. Hassink, T. Aretz, J. Ruskin, and D. Keane. Morphology of atrial myocardium in human pulmonary veins. a postmortem analysis in patients with and without atrial fibrillation. *Journal of the American College of Cardiology*, 42(6):1108–1114, September 2003.

[33] M.C.E.F. Wijffels, C.J.H.J. Kirchhof, R Dorland, and M.A. Allessie. Atrial fibrillation begets atrial fibrillation. a study in awake chronically instrumented goats. *Circulation*, 92:1954–1968, 1995.

[34] S. Nattel, A. Shiroshita-Takeshita, S. Cardin, and P. Pelletier. Mechanisms of atrial remodeling and clinical relevance. *Current Opinion in Cardiology*, 20(1):21–25, January 2005.

[35] R. Gaspo, R.F. Bosch, M. Talajic, and S. Nattel. Functional mechanisms underlying tachycardia-induced sustained atrial fibrillation in a chronic dog model. *Circulation*, 96(11):4027–4035, December 1997.

[36] C.W. Tang, M.M. Scheinman, G.F. van Hare, L.M. Epstein, A.P. Fitzpatrick, R.J. Lee, and M.D. Lesh. Use of P wave configuration during atrial tachycardia to predict site of origin. *Journal of the American College of Cardiology*, 26(5):1315–1324, November 1995.

[37] K-J. Choi, D.C. Shah, P. Jais, M. Hocini, L. Macle, C. Scavee, R. Weerasooriya, F. Raybaud, J. Clementy, and M. Haissaguerre. QRST subtraction combined with a pacemap catalogue for the prediction of ectopy source by surface electrocardiogram in patients with paroxysmal atrial fibrillation. *Journal of the American College of Cardiology*, 40(11):2013–2021, December 2002.

[38] D. Shah, T. Yamane, K.J. Choi, and M. Haissaguerre. QRS subtraction and the ECG analysis of atrial ectopics. *Annals of Noninvasive Electrocardiology*, 9(4):389–398, October 2004.

[39] P.M. Kistler and J.M. Kalman. Locating focal atrial tachycardias from P-wave morphology. *Heart Rhythm*, 2(5):561–564, May 2005.

[40] P.G. Platonov, J. Carlson, M.P. Ingemansson, A. Roijer, A. Hansson, L.V. Chireikin, and S.B. Olsson. Detection of inter-atrial conduction defects with unfiltered signal-averaged P-wave ECG in patients with lone atrial fibrillation. *Europace*, 2(1):32–41, January 2000.

[41] G. Bagliani, A. Michelucci, F. Angeli, and L. Meniconi. Atrial activation analysis by surface P wave and multipolar esophageal recording after cardioversion of persistent atrial fibrillation. *Pacing and Clinical Electrophysiology*, 26(5):1178–1188, May 2003.

[42] F.A. Ehlert, D. Korenstein, and J.S. Steinberg. Evaluation of P wave signal-averaged electrocardiographic filtering and analysis methods. *American Heart Journal*, 134(6):985–993, December 1997.

[43] N. Hayashida, T. Shojima, Y. Yokokura, H. Hori, K. Yoshikawa, H. Tomoeda, and S. Aoyagi. P-wave signal-averaged electrocardiogram for predicting atrial arrhythmia after cardiac surgery. *Annals of Thoracic Surgery*, 79(3):859–864, March 2005.

[44] A.A. Elesber, A.G. Rosales, W.K. Shen, J.F. Malouf, D.O. Hodge, N.M. Ammash, K. Chadrasekaran, B.J. Gersh, S.C. Hammill, and P.A. Friedman. Noninvasive assessment of acute changes in atrial electrophysiology after cardioversion by signal-averaged P-wave electrocardiography. *Pacing and Clinical Electrophysiology*, 28(2):135–139, February 2005.

[45] A. Dhala, D. Underwood, R. Leman, E. Madu, D. Baugh, Y. Ozawa, Y. Kasamaki, Q. Xue, and S. Reddy. Signal-averaged P-wave analysis of normal controls and patients with paroxysmal atrial fibrillation: a study in gender differences, age dependence, and reproducibility. *Clinical Cardiology*, 25(11):525–531, November 2002.

[46] G.Q. Villani, M. Piepoli, A. Rosi, and A. Capucci. P-wave dispersion index: a marker of patients with paroxysmal atrial fibrillation. *International Journal of Cardiology*, 55(2):169–175, July 1996.

[47] N. Ishimoto, M. Ito, and M. Kinoshita. Signal-averaged P-wave abnormalities and atrial size in patients with and without idiopathic paroxysmal atrial fibrillation. *American Heart Journal*, 139(4):684–689, April 2000.

[48] P.J. Stafford, D. Robinson, and R. Vincent. Optimal analysis of the signal averaged P wave in patients with paroxysmal atrial fibrillation. *British Heart Journal*, 74(4):413–418, October 1995.

[49] F. Santoni-Rugiu, R. Verma, D. Mehta, A. Gopal, E.K.Y. Chan, E. Pe, and A. Gomes. Signal-averaged P-wave ECG discriminates between persistent and paroxysmal atrial fibrillation. *Journal of Electrocardiology*, 34(3):189–195, July 2001.

[50] U. Dixen, C. Joens, B.V. Rasmussen, J. Parner, and G.B. Jensen. Signal-averaged P wave duration and the dimensions of the atria. *Annals of Noninvasive Electrocardiology*, 9(4):309–315, October 2004.

[51] M. Sunemark and L. Bertz. Signalbehandling av EKG. Högupplösning av P-våg genom medelvärdesbildning. Master's thesis, Lund Institute of Technology, Lund, Sweden, 1995. Swedish.

[52] L. Sörnmo and P. Laguna. *Bioelectrical signal processing in cardiac and neurological applications*, chapter 4. Elsevier Academic Press, London, UK, 2005.

[53] M Holm, S Pehrson, M Ingemansson, L Sörnmo, R Johansson, L Sandhall, M Sunemark, B Smideberg, C Olsson, and S.B. Olsson. Non-invasive assessment of the atrial cycle length during atrial fibrillation in man: introducing, validating and illustrating a new ECG method. *Cardiovascular Research*, 38:69–81, 1998.

[54] Qin Xi, A.V. Sahakian, T.G. Frohlich, J. Ng, and S. Swiryn. Relationship between pattern of occurrence of atrial fibrillation and surface electrocardiographic fibrillatory wave characteristics. *Heart Rhythm*, 1(6):656–663, December 2004.

[55] M Stridh and L Sörnmo. Spatiotemporal QRST cancellation techniques for analysis of atrial fibrillation. *IEEE Transactions on Biomedical Engineering*, 48(1):105–111, January 2001.

[56] Qin Xi, A.V. Sahakian, and S. Swiryn. The effect of QRS cancellation on atrial fibrillatory wave signal characteristics in the surface electrocardiogram. *Journal of Electrocardiology*, 36(3):243–249, July 2003.

[57] M. Stridh, L Sörnmo, C. Meurling, and S.B. Olsson. Characterization of atrial fibrillation using the surface ECG: time-dependent spectral properties. *IEEE Transactions on Biomedical Engineering*, 48(1):19–27, January 2001.

[58] C.J. Meurling, M.P. Ingemansson, A. Roijer, J. Carlson, C.J. Lindholm, B. Smideberg, L. Sörnmo, M. Stridh, and S.B. Olsson. Attenuation of electrical remodelling in chronic atrial fibrillation following oral treatment with verapamil. *Europace*, 1(4):234–241, October 1999.

[59] M.P. Ingemansson, B. Smideberg, and S.B. Olsson. Intravenous $MgSO_4$ alone and in combination with glucose, insulin and potassium (GIK) prolong the atrial cycle length in chronic atrial fibrillation. *Europace*, 2(2):106–114, April 2000.

[60] M. Stridh, C. Meurling, S.B. Olsson, and L. Sörnmo. Detection of autonomic modulation in permanent atrial fibrillation. *Medical and Biological Engineering and Computing*, 41(6):625–629, November 2003.

[61] F. Holmqvist, M. Stridh, J.E.P. Waktare, J. Brandt, L. Sörnmo, A. Roijer, and C.J. Meurling. Rapid fluctuations in atrial fibrillatory electrophysiology detected during controlled respiration. *American Journal of Physiology — Heart and Circulatory Physiology*, 289(2):H754–H760, August 2005.

[62] S.B. Olsson, N. Cai, M. Dohnal, and K.K. Talwar. Noninvasive support for and characterization of multiple intranodal pathways in patients with mitral valve disease and atrial fibrillation. *European Heart Journal*, 7:320–333, 1986.

[63] N.S. Cai, M. Dohnal, and S.B. Olsson. Methodological aspects of the use of heart rate stratified RR interval histograms in the analysis of atrioventricular conduction during atrial fibrillation. *Cardiovascular Research*, 21(6):455–462, June 1987.

[64] S. Rokas, S. Gaitanidou, S. Chatzidou, C. Pamboucas, D. Achtipis, and S. Stamatelopoulos. Atrioventricular node modification in patients with chronic atrial fibrillation. role of morphology of rr interval variation. *Circulation*, 103:2942–2948, June 2001.

[65] M. van den Berg, T. van Noord, J. Brouwer, J. Haaksma, D.J. van Veldhuisen, H.J.G.M. Crijns, and I. van Gelder. Clustering of RR intervals predicts effective electrical cardioversion for atrial fibrillation. *Journal of Cardiovascular Electrophysiology*, 15(9):1027–1033, September 2004.

[66] P.M.M. Cashman. The use of R-R interval and difference histograms in classifying disorders of sinus rhythm. *Journal of Medical Engineering and Technology*, 1(1):20–28, January 1977.

[67] S. Santos. System identification applied to cardiac activation. Master's thesis, Lund Institute of Technology, 2001.

[68] Zhen Li, E. Hertervig, J. Carlson, C. Johansson, S.B. Olsson, and Shiwen Yuan. Dispersion of refractoriness in patients with paroxysmal atrial fibrillation. Evaluation with simultaneous endocardial recordings from both atria. *Journal of Electrocardiology*, 35(3):227–234, July 2002.

[69] S. Yuan, O. Kongstad, E. Hertervig, M. Holm, C.M. Pripp, and S.B. Olsson. Recordings monophasic action potentials using a platinum-electrode ablation catheter. *Europace*, 2(4):312–319, October 2000.

[70] L. Gepstein, G. Hayam, and S.A. Ben-Haim. A novel method for nonfluoroscopic catheter-based electroanatomical mapping of the heart. in vitro and in vivo accuracy results. *Circulation*, 95(6):1611–1622, March 1997.

[71] F.H.M. Wittkampf, E.F.D. Wever, R. Derksen, A.A.M. Wilde, H. Ramanna, R.N.W. Hauer, and E.O. Robles de Medina. LocaLisa. new technique for real-time 3-dimensional localization of regular intracardiac electrodes. *Circulation*, 99:1312–1317, March 1999.

[72] C. Tondo, M. Mantica, G. Russo, E. Karapatsoudi, A. Lucchina, F. Nigro, M. Wild, C. Molinaro, and R. Bavila. A new nonfluoroscopic navigation system to guide pulmonary vein isolation. *Pacing and Clinical Electrophysiology*, 28(Supplement 1):S102–S105, January 2005.

[73] Y. Xia, E. Hertervig, O. Kongstad, E. Ljungström, P. Platonov, M. Holm, S.B. Olsson, and S. Yuan. Deterioration of interatrial conduction in patients with paroxysmal atrial fibrillation: electroanatomic mapping of the right atrium and coronary sinus. *Heart Rhythm*, 1(5):548–553, November 2004.

[74] E. Hertervig, S. Yuan, S. Liu, O. Kongstad, J. Luo, and S.B. Olsson. Electroanatomic mapping of transseptal conduction during coronary sinus pacing in patients with paroxysmal atrial fibrillation. *Scandinavian Cardiovascular Journal*, 37(6):340–343, December 2003.

[75] J. Luo, S. Yuan, E. Hertervig, O. Kongstad, E. Ljungström, M. Holm, and S.B. Olsson. Electroanatomic mapping of right atrial activation in patients with and without paroxysmal atrial fibrillation. *Journal of Electrocardiology*, 36(3):237–242, July 2003.

[76] M. Holm, R. Johansson, S.B. Olsson, J. Brandt, and C. Lührs. A new method for analysis of atrial activation during chronic atrial fibrillation in man. *IEEE Transactions on Biomedical Engineering*, 43(2):198–210, February 1996.

[77] M. Holm, R. Johansson, J. Brandt, and C. Lührs. Epicardial right atrial free wall mapping in chronic atrial fibrillation. documentation of repetitive activation with a focal spread — a hitherto unrecognised phenomenon in man. *European Heart Journal*, 18(2):290–310, February 1997.

[78] R. Johansson, M. Holm, S.B. Olsson, and J. Brandt. System identification of atrial activation during chronic atrial fibrillation in man. *IEEE Transactions on Automatic Control*, 43(6):790–799, June 1998.

[79] B.W. Kernighan and D.M. Ritchie. *The C programming language, second edition*. Prentice Hall, Inc., 1988.

[80] A.L. Goldberger, L.A.N. Amaral, L. Glass, J.M. Hausdorff, P.Ch. Ivanov, R.G. Mark, J.E. Mietus, G.B. Moody, C.-K. Peng, and H.E. Stanley. PhysioBank, PhysioToolkit, and PhysioNet: Components of a new research resource for complex physiologic signals. *Circulation*, 101(23):e215–e220, 2000 (June 13). Circulation Electronic Pages: http://circ.ahajournals.org/cgi/content/full/101/23/e215.

[81] M.P. Ingemansson. *Cellular electrophysiological modulation in chronic atrial fibrillation. Studies with magnesium and GIK solution*. PhD thesis, Lund University, 1998.

[82] K. Aytemir, B. Amasyali, G. Abali, S. Kose, A. Kilic, O. Onalan, L. Tokgozoglu, G. Kabakci, H. Ozkutlu, N. Nazli, E. Isik, and A. Oto. The signal-averaged P-wave duration is longer in hypertensive patients with history of paroxysmal atrial fibrillation as compared to those without. *International Journal of Cardiology*, 103(1):37–40, August 2005.

[83] M.P. Ingemansson, J. Carlson, P.G. Platonov, and S.B. Olsson. Effects of $MgSO_4$ and glucose, insulin and potassium (GIK) on atrial conduction during the first 12 hours after DC-conversion of chronic atrial fibrillation. *Scandinavian Cardiovascular Journal*, 35(5):340–346, October 2001.

[84] M. Fukunami, T. Yamada, K. Ohmori, M. Kumagai, K. Umemoto, A. Sakai, N. Kondoh, T. Minamino, and N. Hoki. Detection of patients at risk for paroxysmal atrial fibrillation during sinus rhythm by p wave-triggered signal-averaged electrocardiogram. *Circulation*, 83(1):162–169, January 1991.

[85] B. Ho and R. Kalman. Effective construction of linear state-variable models from input/output functions. *Regelungstechnik*, 14(12):545–548, 1966.

[86] S.Y. Kung. A new identification and model reduction algorithm via singular value decomposition. In *Proceedings of the 12th Asilomar Conference on Circuits, Systems and Computers*, pages 705–714, Pacific Grove, CA, 1978.

[87] R. A. Fisher. The statistical utilization of multiple measurements. *Annals of Eugenics*, 8:376–386, 1938.

[88] I. Christov. Dynamic powerline interference subtraction from biosignals. *Journal of Medical Engineering & Technology*, 24(4):169–172, July/August 2000.

[89] I.K. Daskalov, I.A. Dotsinsky, and I.I. Christov. Developments in ECG acquisition, preprocessing, parameter measurement, and recording. *IEEE Engineering in Medicine and Biology Magazine*, 17(2):50–58, March/April 1998.

[90] J.M. Bland and D.G. Altman. Statistical methods for assessing agreement between two methods of clinical measurement. *The Lancet*, 1(8476):307–310, February 1986.

[91] J.J. Bailey, Berson A.S., A. Garson Jr., L.G. Horan, P.W. Macfarlane, D.W. Mortara, and C. Zywietz. Recommendations for standardization and specifications in automated electrocardiography: Bandwidth and digital signal processing — a report for health professionals by an ad hoc writing group of the committee on electrocardiography and cardiac electrophysiology of the Council on Clinical Cardiology, American Heart Association. *Circulation*, 81(2):730–739, February 1990.

[92] E.W. Pottala, J.J. Bailey, M.R. Horton, and J.R. Gradwohl. Suppression of baseline wander in the ECG using a bilinearly transformed, null-phase filter. *Journal of Electrocardiology*, 22(Supplement):243–247, 1989.

[93] M.E. Cain, J.W. Mason, J.L. Anderson, M.M. Scheinman, M.F. Arnsdorf, and A.L. Waldo. Signal-averaged electrocardiography. *Journal of the American College of Cardiology*, 27(1):238–249, January 1996.

[94] S. Rokas, S. Gaitanidou, S. Chatzidou, A. Agrios, and S. Stamatelopoulos. A noninvasive method for the detection of dual atrioventricular node physiology in chronic atrial fibrillation. *The American Journal of Cardiology*, 84(12):1442–1445, December 1999.

[95] P. Weismüller, C. Braunss, C. Ranke, and H-J Trappe. Multiple AV nodal pathways with multiple peaks in the RR interval histogram of the holter monitoring ECG during atrial fibrillation. *Pacing and Clinical Electrophysiology*, 23(11 Part II):1921–1924, November 2000.

[96] M.D. Gonzalez, L.J. Contreras, F. Cardona, C.J. Klugewicz, J.B. Conti, A.B. Curtis, T.E. Morey, and D.M. Dennis. Demonstration of a left atrial input to the atrioventricular node in humans. *Circulation*, 106(23):2930–2934, December 2002.

[97] P.J. Stafford, J. Cooper, and C.J. Garratt. Improved recovery of high frequency P wave energy by selective P wave averaging. *Pacing and Clinical Electrophysiology*, 19:1225–1229, August 1996.

[98] E.J. Hertervig, Shiwen Yuan, J. Carlson, O. Kongstad-Rasmussen, and S.B. Olsson. Evidence for electrical remodelling of the atrial myocardium in patients with atrial fibrillation. A study using the monophasic action potential recording technique. *Clinical Physiology and Functional Imaging*, 22(1):8–12, January 2002.

[99] A.H. Kadish, A.E. Buxton, H.L. Kennedy, B.P. Knight, J.W. Mason, C.D. Schuger, and C.M. Tracy. ACC/AHA clinical competence statement on electrocardiography and ambulatory electrocardiography: a report of the American College of Cardiology/American Heart Association/American College of Physicians-American Society of Internal Medicine Task Force on Clinical Competence (ACC/AHA Committee to Develop a Clinical Competence

Statement on Electrocardiography and Ambulatory Electrocardiography). *Journal of the American College of Cardiology*, 38(7):2091–2100, December 2001.

[100] E. Frank. The image surface of a homogeneous torso. *American Heart Journal*, 47(5):757–768, May 1954.

[101] L. Edenbrandt, A. Houston, and P.W. Macfarlane. Vectorcardiograms synthesized from 12-lead ECGs: A new method applied in 1792 healthy children. *Pediatric Cardiology*, 15(1):21–26, 1994.

[102] A. Shimizu, Y. Yoshiga, T. Yamagata, M. Esato, M. Doi, H. Kakugawa, R. Kametani, N. Inoue, M. Kanemoto, and M. Matsuzaki. New method of determining the atrial fibrillation cycle length during human atrial fibrillation. *Journal of Cardiovascular Electrophysiology*, 14(9):965–970, September 2003.

[103] R.C. Schlant, R.J. Adolph, J.P. DiMarco, L.S. Dreifus, M.I. Dunn, C. Fisch, A. Garson, L.J. Haywood, H.J. Levine, J.A. Murray, R.J. Noble, and J.A. Ronan Jr. Guidelines for Electrocardiography. A Report of the American College of Cardiology/American Heart Association Task Force on Assessment of Diagnostic and Therapeutic Cardiovascular Procedures (Committee on Electrocardiography). *Journal of the American College of Cardiology*, 19(3):473–481, March 1992.

[104] G.E. Dower, H.B. Machado, and J.A. Osborne. On deriving the electrocardiogram from vectorcardiographic leads. *Clinical Cardiology*, 3:87–95, 1980.

[105] L. Edenbrandt and O. Pahlm. Vectorcardiogram synthesized from a 12-lead ECG: superiority of the inverse dower matrix. *Journal of Electrocardiology*, 21(4):361–367, November 1988.

[106] E.H. Moore. On the reciprocal of the general algebraic matrix. *Bulletin of the American Mathematical Society*, 26:394–395, 1920.

[107] R. Penrose. A generalized inverse for matrices. *Proceedings of the Cambridge Philosophical Society*, 51:406–413, 1955.

[108] R. Johansson. *System Modeling and Identification*. Prentice Hall, Englewood Cliffs, NJ, 1993.

Appendix A

Heart rate-stratified histogram analysis

A.1 Heart rate-stratified histograms

To analyze how RR interval distribution changes with heart rate, the RR interval series was divided into sequences:

$$\begin{aligned} s_1 &= \{R_1, R_2, \ldots, R_n\} \\ s_2 &= \{R_{1+k}, R_{2+k}, \ldots, R_{n+k}\} \\ s_3 &= \{R_{1+2k}, R_{2+2k}, \ldots, R_{n+2k}\} \\ &\vdots \end{aligned}$$

where $R_1, R_2, \ldots$ are the RR intervals, n is the length of the sequence and k is the length of the 'step' taken in the series to begin the next sequence.

For each sequence, the mean of the RR intervals was calculated and converted to heart rate. The mean heart rate of sequence s_1 would be:

$$H(s_1) = \frac{1}{\frac{1}{n}\sum_{i=1}^{n} R_i} \cdot 1000 \cdot 60$$

All RR intervals from sequences with equal mean heart rate were then displayed in a histogram. The histogram distribution would then depend on the length of the sequences, n, the step length, k, and the heart rate range used to define 'equal mean heart rate'.

A.2 Histogram smoothing

As illustrated in Figure A.1, the contours of the histograms are somewhat ragged, more noticeable in histograms made from fewer RR intervals. To smooth the contours, a 3-term simple moving average was applied repeatedly to each histogram,

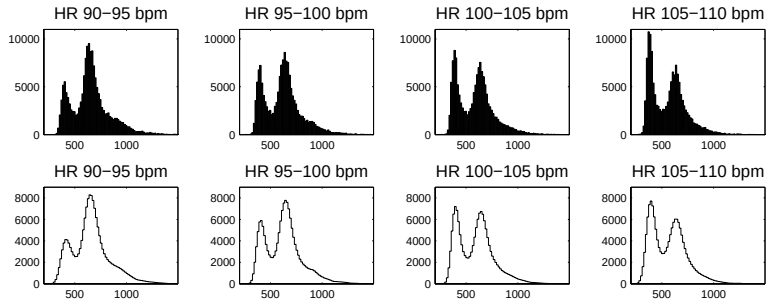

Figure A.1: Top row shows RR interval histograms created from sequences with mean heart rates between 90 and 110 bpm. Bottom row shows the same histograms after applying a 3-term simple moving average filter repeatedly. The result of the filter is a smoother curve and less sharp peaks.

recalculating the bars as:

$$b_{k+1}(n) = \begin{cases} \frac{1}{3}\sum_{i=n-1}^{n+1} b_k(i) & ,2 \leq n \leq N-1 \\ b_k(n) & ;n = 1, n = N \end{cases} \tag{A.1}$$

where $b_k(n)$ is the n^{th} bar of the histogram after k iterations of the filter and N is the total number of bars in the histogram. Each individual histogram was recalculated using Equation (A.1) until no local maxima were found closer to each other than 50 ms, which in effect was the same as four bars. Peaks located closer were considered to be 'noise' due to the statistical variation of the limited series of RR intervals.

A.3 Histogram parameters

In Figure A.1, two peaks are clearly distinguishable. It can also be seen that with increasing heart rate, the relation between the amplitude of the two peaks change, where the distribution of shorter RR intervals increases and the distribution of longer RR intervals decreases. Between the two histograms marked 95–100 bpm and 100–105 bpm, the amplitude of the 'short' distribution becomes higher and the heart rate 100 bpm is called PDC (Peak Dominant Change). PDC was used as the reference heart rate, i.e., the parameters used to characterize the RR interval distribution were calculated in the histogram following it. The characterizing parameters as defined in Paper I[1] were:

- PV(s), location (in ms) of the peak of the distribution of long RR intervals (Peak Value, slow heart rate)

[1] The mathematically oriented reader would probably object to the use of f and s as arguments. However, the notation from Paper I was kept for reasons of continuity.

- PV(f), location (in ms) of the peak of the distribution of short RR intervals (Peak Value, fast heart rate)
- PG = PV(s) − PV(f), difference (in ms) between locations of the two peaks (Peak Gap)
- PVR = $\frac{\text{PV(s)}}{\text{PV(f)}}$, ratio between the locations of the two peaks (Peak Value Ratio)

Figure A.2 shows an example of PV(f) and PV(s).

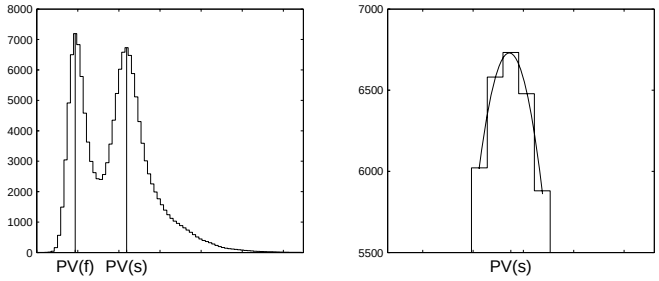

Figure A.2: Example of calculation of the peak locations PV(f) and PV(s) in a histogram. The left plot shows the definitions of PV(f) and PV(s). The right plot shows a magnification of PV(s) with the result after fitting a 2^{nd} order polynomial to the peak to increase resolution

As the resolution of the RR intervals was between 15 and 16 ms (Section 3.1.1), this also defines the resolution at which the peak locations, PV(s) and PV(f) can be observed. To increase the peak location resolution, a 2^{nd} order polynomial was calculated, using the highest histogram bar and the two bars on each side. To find the coefficients of the polynomial, the MATLAB function polyfit was used. The peak location resolution may then be chosen arbitrarily and was set to 1 ms, and the values of the polynomial calculated using the MATLAB function polyval. An example of the polynomial fitting can be seen in Figure A.2.

Appendix B

Signal-averaging P waves

A direct detection of P waves in an electrocardiogram is difficult, due to the poor signal-to-noise ratio. However, under the assumptions that P waves appear just before the much more prominent QRS complexes, and that the noise is uncorrelated to the P waves, signal-averaging would be a suitable tool to extract the P waves from noise.

B.1 Signal preprocessing

Low-frequency artifacts were removed by calculating the disturbance and then subtracting it from the signal. The filter used was a 3^{rd} order Butterworth low-pass filter with cut-off frequency 0.5 Hz, with filter coefficients calculated using the MATLAB function butter. Since all data processing was made on previously recorded signals, zero-phase filtering was feasible by forward and reverse filtering using the MATLAB function filtfilt.

Powerline interference (50 Hz in Sweden) was reduced using a subtraction algorithm [88].

B.2 Similarity criterion

An important feature of a signal-averaging algorithm is the way signal segments are defined as 'equal' or not. Throughout this study, a correlation coefficient greater than 0.9 was used as the similarity criterion.

In order to assess similarity between two signal segments, correlation function analysis was used, where the two segments were time-shifted to find the maximum correlation. If more than one lead was included in the comparison, correlation was calculated leadwise and the lowest value recorded for each time shift, with the end result being the maximum of these values.

B.3 Extraction of QRS complexes

B.3.1 Detection of QRS complexes

An automatic algorithm was used to detect the positions of QRS complexes in the signal [89], giving an estimate of the onset of the Q wave. The QRS complexes were then defined as signal windows from 20 ms preceding, to 99 ms following, each detected onset.

B.3.2 Creation of QRS morphology groups

The purpose of creating different groups of QRS complexes was twofold. First, the use of a similarity criterion would exclude artifacts and erroneous beats since these would form groups with one, or very few, members and may be discarded. Second, it allowed analysis of activation related to only QRS complexes of a certain morphology, by discarding all QRS complexes not belonging to the chosen group(s).

Based on the similarity criterion, all QRS complexes with similar morphology were sorted into the same group using the method described in the following pseudo-algorithm:

1. The first group is created by taking the first detected QRS complex of the recording;
2. Subsequent QRS complexes are compared to the previously defined group(s) and, based on the similarity criterion:
   - Added to a group if it is fulfilled;
   - Used to create a new group if it is not fulfilled.

   This step is repeated until all QRS complexes detected have been analyzed;
3. The signal-averages of the individual groups are calculated;
4. All QRS complexes are compared to the created signal-averages and, as in Step 2, added to a group if the similarity criterion is fulfilled or used to create a new one if it is not;
5. The signal-averages of each individual group is recalculated;
6. Steps 4 and 5 are iterated until the number of groups found and the number of members in each individual group are not changed in two subsequent iterations[1].

In Steps 2 and 4, when calculating the correlation coefficient, a maximum time shift of ± 32 ms was used. In the same steps, the onset of each individual QRS complex was adjusted according to the time shift resulting in the maximum correlation.

[1] As a worst case, this might induce an endless loop, switching between two or more states. However, after several hundred analyses, this has yet to happen.

B.3.3 Manual correction of QRS settings

For each group of QRS found, there was a possibility of adjusting the onset manually, should the automatic result not be satisfactory. The onset and end of each individual QRS group were then defined using a graphical figure in a window on the computer screen, showing all leads, where the user may set marks. This technique, using ginput in MATLAB, limited the possible resolution of the settings to the width of a pixel on the screen. Since the signal segments displayed covered 400 ms (99 ms before and 300 ms after the onset) the settings resolution would be 0.7 ms[2], which is less than the sampling interval of 1 ms and the settings were rounded to the nearest ms value. In the same window, it was also possible to classify the QRS as either 'normal' or other code [80].

B.4 P wave extraction

The same technique used to produce different groups of QRS complexes described above was used to produce groups of P waves with different morphologies, in this case using a maximum time shift of ± 16 ms when calculating the correlation coefficients of the similarity criterion.

Initially, the P waves were defined as signal segments just prior to the onsets of the QRS complexes. In this study, only QRS complexes belonging to the largest group classified as 'normal' were used. As default, the width of the signal windows was set to 250 ms (samples) and the window end at the Q wave onset. However, in cases with unusually long P wave duration or PQ time, it would be necessary to expand and/or move the window to fully cover the P wave.

When more than one group of P waves were observed, the group with the largest number of members was named 'Group 1', the next 'Group 2' and so on.

B.4.1 P wave trigging

The correlation calculations of the similarity criterion were performed on signal segments containing P waves only. The time-shifting and subsequent window position adjustment would then be based on the differences in PQ time in the individual P waves. The resulting signal averaged P waves are referred to as being 'P wave triggered' as opposed to the case where P wave windows are based only on the QRS onset which is called 'QRS triggered'.

P wave trigging enhances the performance of the signal-averaging, and the values of the time shifts found may be interpreted as observations of differences in PQ time.

B.4.2 Manual correction of P wave settings

The onset and end of each individual P wave group average were defined using the same technique as in the QRS complexes. In the P wave case, the length of the signal segments displayed in the window was 250 ms, giving a settings resolution of 0.45 ms. As in the QRS case, the settings were rounded to the nearest ms value.

[2] In the case of a 17-inch monitor, with resolution 1024×768

B.5 Analysis of morphology

B.5.1 Parameters describing morphology

The morphology of a signal-averaged P wave may be described in different ways, the P wave duration could be used as an estimate of the total time of the atrial activation sequence, and the PQ time could provide information on the delay of the impulse conduction between the atria and the ventricles. Additionally, in this study, a number of well-defined points of the P waves in different leads was used (Figure B.1):

- Lead X: location and amplitude of the maximum;
- Lead Y: location and amplitude of the maximum;
- Lead Z: location and amplitude of the minimum, location of the zero-crossing after the minimum, location and amplitude of the maximum after the zero-crossing.

Before measuring the location and amplitude parameters, P waves were smoothed to remove signal ripple and only keep the gross appearance. Smoothing was performed by repeated applying of a 5-term simple moving average until no local maxima were found closer to each other than 20 ms (the period of the 50 Hz powerline interference).

B.5.2 Spatial magnitude

In Paper III, an additional signal was included for compatibility with previous studies [40, 83], the 'Spatial magnitude'. It was derived from the three orthogonal vector leads X, Y, and Z as the vector norm:

$$S_{\mathrm{SM}} = ||S_{\mathrm{vcg}}||_2 \tag{B.1}$$

where

$$S_{\mathrm{vcg}} = \begin{pmatrix} X \\ Y \\ Z \end{pmatrix}$$

In Spatial magnitude, the parameters used to describe morphology was (Figure B.1):

- Locations of local maxima;
- 'Nadir', i.e., the local minimum often present just before the end as defined from Leads X, Y, and Z [40].

B.5.3 Interpretation of conduction pattern

When using Frank lead recordings, the morphologies of the three orthogonal leads X, Y, and Z, may give information on the geometric progression of the atrial activation sequence. Assuming activation initiated from the sinus node at the top, right, back part of the right atrium, the normal morphology would be:

- Lead X positive, activation from right to left;
- Lead Y positive, activation from top to bottom;
- Lead Z negative, activation from back to front.

Deviations from this may then be interpreted as either sinus node initiated activation with deviating atrial conduction pattern or atrial activation not originating from the sinus node.

B.6 Analysis of variability

Different from previous studies of P wave morphology [40, 83], where only one type of morphology was analyzed, the method suggested in the present study allows analysis of P wave variability. The different groups created in the P wave extraction will have differences in their morphologies, indicating differences in the underlying atrial conduction pattern.

Using the created P wave groups, a P wave variability analysis may contain for example:

- The number of groups found, and the number of members in each group, would be an observation of the stability of the atrial activation;
- The different morphologies may, in the case of VCG recordings, allow interpretation of the differences in the underlying atrial activation patterns;
- An observation of which group the individual, consecutive, P waves belong to would indicate how often morphologies change and also how they change.

B.6.1 Remarks

All analyses of P wave variability described above would of course be dependent of the similarity criterion which must be kept the same in all analyses being compared. Also, it must be assured that the variability in P wave morphologies is not simply the result of a noisy recording.

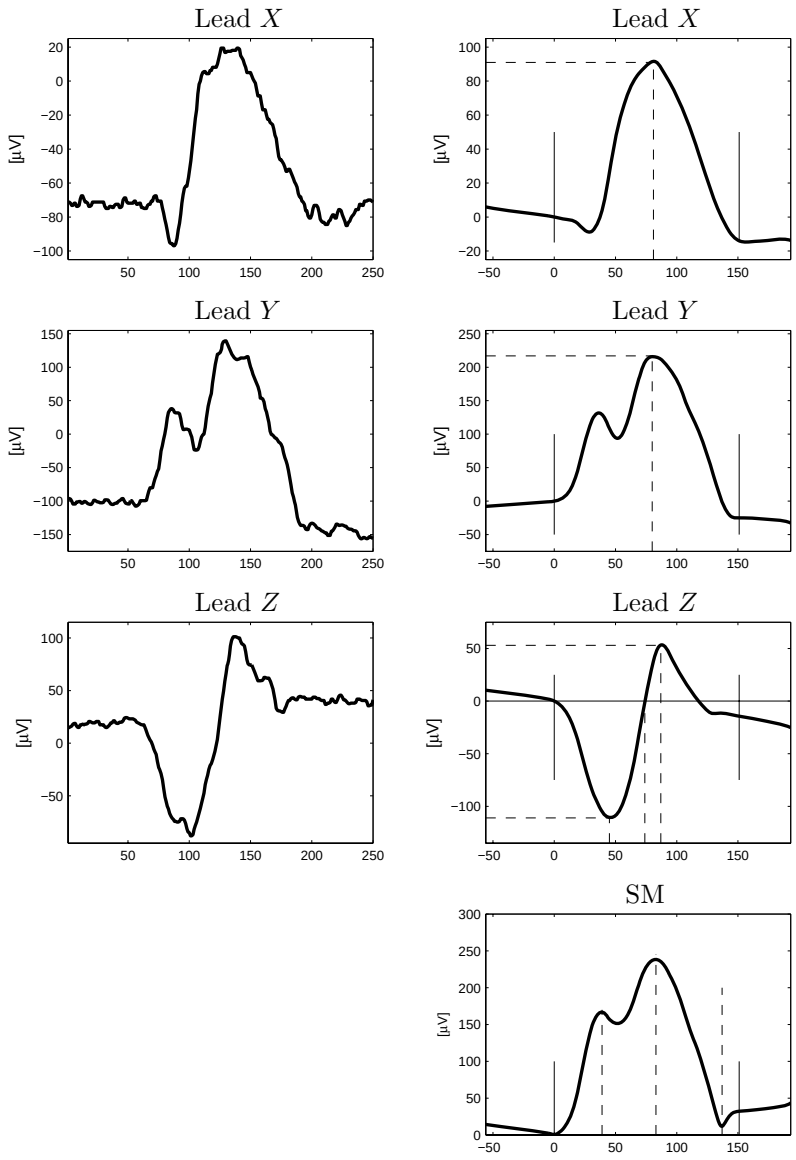

Figure B.1: Illustration of the parameters used to describe P wave morphology. Left column shows an example of the appearance of one single P wave from a Frank-lead recording. The right column shows the result after signal-averaging and smoothing, with the measured morphology parameters (see text) indicated with dashed lines.

Appendix C

Inverse Dower transformation

C.1 The Dower transformation matrix

The Dower transformation matrix [104] is used to calculate the 12-lead ECG from a recorded Frank-lead vectorcardiogram. It is a linear, sample-wise matrix operation which may be used in real-time applications. The matrix has the numerical values

$$D = \begin{pmatrix} -0.515 & 0.157 & -0.917 \\ 0.044 & 0.164 & -1.387 \\ 0.882 & 0.098 & -1.277 \\ 1.213 & 0.127 & -0.601 \\ 1.125 & 0.127 & -0.086 \\ 0.831 & 0.076 & 0.230 \\ 0.632 & -0.235 & 0.059 \\ 0.235 & 1.066 & -0.132 \end{pmatrix}$$

Transformation between the two lead systems is made simply by the matrix operation

$$\begin{pmatrix} V_1 \\ V_2 \\ V_3 \\ V_4 \\ V_5 \\ V_6 \\ I \\ II \end{pmatrix} = D \begin{pmatrix} X \\ Y \\ Z \end{pmatrix}$$

or shorter

$$\hat{S}_{\text{ecg}} = DS_{\text{vcg}} \tag{C.1}$$

where $\hat{S}_{\text{ecg}}$ is the calculated ECG and S_{vcg} is the recorded (Frank-lead) VCG.

C.2 The inverse Dower transformation matrix

In order to calculate VCG from ECG, there is a need to calculate the inverse Dower transformation matrix [105]. Since the matrix D is non-square, no inverse exists and therefore the pseudo inverse, or the Moore-Penrose inverse [106, 107], is used. This inverse would be calculated as

$$D^{\dagger} = \left(D^T D\right)^{-1} D^T$$

The derived VCG, $\hat{S}_{\text{vcg}}$, would then be

$$\hat{S}_{\text{vcg}} = D^{\dagger} S_{\text{ecg}} = \left(D^T D\right)^{-1} D^T S_{\text{ecg}} = \left(D^T D\right)^{-1} D^T D S_{\text{vcg}} = S_{\text{vcg}} \qquad \text{(C.2)}$$

i.e., the calculated and recorded VCG are the same, provided that the Dower transformation matrix is such that the calculated ECG, $\hat{S}_{\text{ecg}}$ of Equation (C.1), is equal to the recorded ECG, S_{ecg}.

The inverse Dower transform may then be performed by calculating

$$\begin{pmatrix} X \\ Y \\ Z \end{pmatrix} = D^{\dagger} \begin{pmatrix} V_1 \\ V_2 \\ V_3 \\ V_4 \\ V_5 \\ V_6 \\ I \\ II \end{pmatrix}$$

where $D^{\dagger}$ has the numerical values

$$D^{\dagger} = \begin{pmatrix} -0.172 & -0.074 & 0.122 & 0.231 & 0.239 & 0.194 & 0.156 & -0.010 \\ 0.057 & -0.019 & -0.106 & -0.022 & 0.041 & 0.048 & -0.227 & 0.887 \\ -0.229 & -0.310 & -0.246 & -0.063 & 0.055 & 0.108 & 0.022 & 0.102 \end{pmatrix}$$

The inverse Dower transform described only uses two of the six limb and augmented leads. By combining Equations (1.1), (1.2), and (1.4) it can be shown that if Leads I and II are recorded, the other may be calculated as

$$\begin{cases} III &= II - I \\ aVL &= \frac{1}{2}(II - 2I) \\ aVR &= \frac{1}{2}(I + II) \\ aVF &= \frac{1}{2}(I - 2II) \end{cases}$$

This means that since Leads III, aVL, aVR, and aVF can all be expressed as functions of Leads I, and II, they do not contain any unique information that will be lost in the transform where they are not included.

C.3 Statistical error analysis

Equation (C.2) shows calculation of VCG from ECG without considering the influence of noise. Before applying the equation, the possible influence of noise needs to be evaluated.

A noise component, ν_{ecg}, is introduced, with the expected value

$$\mathcal{E}\left\{\nu_{\text{ecg}}\right\} = 0$$

and assumed to be uncorrelated with the ECG.

Equation (C.2) would, with noise added, be

$$\hat{S}_{\text{vcg}} = D^{\dagger}\left(S_{\text{ecg}} + \nu_{\text{ecg}}\right) = S_{\text{vcg}} + D^{\dagger}\nu_{\text{ecg}}$$

The expected value of the derived VCG would then be

$$\mathcal{E}\left\{\hat{S}_{\text{vcg}}\right\} = \mathcal{E}\left\{S_{\text{vcg}} + D^{\dagger}\nu_{\text{ecg}}\right\} = S_{\text{vcg}} + D^{\dagger}\mathcal{E}\left\{\nu_{\text{vcg}}\right\} = S_{\text{vcg}}$$

i.e., it is not affected by the noise.

The matrix $D^{\dagger}$ determines the influence of ν_{ecg} on the derived VCG, where the maximum value of ν_{ecg} is found parallel to the singular values of $D^{\dagger}$:

$$\sigma_{D^{\dagger}} = \begin{pmatrix} 0.938 \\ 0.531 \\ 0.396 \end{pmatrix} \tag{C.3}$$

The influence of ν_{ecg} on the variance of $\hat{S}_{\text{vcg}}$ is

$$\mathcal{E}\left\{\hat{S}_{\text{vcg}}\hat{S}_{\text{vcg}}^{T}\right\} = S_{\text{vcg}}S_{\text{vcg}}^{T} + D^{\dagger}\mathcal{E}\left\{\nu_{\text{ecg}}\nu_{\text{ecg}}^{T}\right\}{D^{\dagger}}^{T}$$

where the maximum error is found parallel to the singular values of the matrix $D^{\dagger}{D^{\dagger}}^{T}$:

$$\sigma_{D^{\dagger}{D^{\dagger}}^{T}} = \begin{pmatrix} 0.880 \\ 0.282 \\ 0.157 \end{pmatrix} \tag{C.4}$$

Since all singular values in Equations (C.3) and (C.4) are lower than 1, it can be expected that the inverse Dower transformation matrix is stable in the sense of noise propagation and may be used safely.

C.4 Mathematical comparison between recorded and derived VCG

The differences between signal-averaged P waves obtained from the recorded and derived VCG were assessed in three ways: by means of correlation coefficient, scaling parameters obtained by least-squares fitting, and the magnitude of the residual.

Before comparison, P waves were time-shifted to find maximum correlation in order to avoid differences in setting of onset and end affecting the result.

C.4.1 Correlation coefficient

The first parameter of the comparison was the maximum correlation coefficient found. This was included because the similarity criterion of the P wave extraction (Appendix B) uses a correlation function algorithm to define whether two P waves originate from the same activation pattern or not.

C.4.2 Least-squares fitting

Least-squares fitting was performed to find differences in amplitude scaling and offset, by minimizing the residual calculated (for Lead X) as:

$$P_{\text{res},X} = P_{\text{vcg},X} - (\alpha_X P_{\text{dvcg},X} - \beta_X) \tag{C.5}$$

where $P_{\text{vcg},X}$ and $P_{\text{dvcg},X}$ are the P waves of the recorded and derived VCG, respectively, $P_{\text{res},X}$ is the minimized residual, and α_X and β_X coefficients of amplitude scaling and offset that minimizes the residual. The same calculations were made for Leads Y and Z.

To find numerical values of the coefficients α and β, the MATLAB function fminsearch was used to minimize the function

$$f(\alpha_X, \beta_X) = \sum_{i=1}^{n} (P_{\text{res},X}(i))^2$$

to find the coefficients that minimize the Lead X residual. n is the length of the P wave. The coefficients of Leads Y and Z were found in the same way.

C.4.3 Magnitude of residual

The magnitude of the residual between P waves was calculated from the minimized residual in Equation (C.5), in order to avoid this being a measure of differences in amplitude scaling and offset rather than signal appearance,

The magnitude of the residual was expressed as the 2-norm of the residual divided by the 2-norm of the P wave of the recorded VCG. For Lead X, the calculation was

$$P_{\text{mag},X} = \frac{\sqrt{\sum_{i=1}^{n} |P_{\text{res},X}(i)|^2}}{\sqrt{\sum_{i=1}^{n} |P_{\text{vcg},X}(i)|^2}} \tag{C.6}$$

and analog for Leads Y and Z.

Appendix D

P wave modeling

To analyze the complexity of the system creating the P wave, i.e., the atria, the modeling approach illustrated in Figure D.1 was used. The atria were treated as

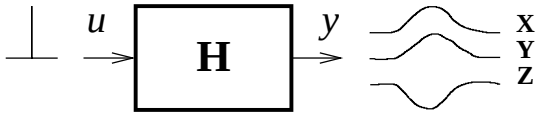

Figure D.1: The system, H, being analyzed by system identification. It is assumed that the input, u, is an impulse, and that the output, y, is the P wave represented by the orthogonal leads X, Y, and Z.

a 'box' with one input and one output. The input to the atria was thought of as a complex mix between electrical and chemical stimuli not possible to measure or control adequately (at least non-invasively). Instead, the input was modeled as an impulse and the output of the system, the P wave, would therefore be the impulse response. Since the input could not be manipulated, system identification could only be performed on the system impulse response, i.e., the recorded P waves.

Using Frank-lead recordings, P waves are represented by the vectors

$$\begin{aligned} X &= \{X(1), X(2), \ldots, X(k)\} \\ Y &= \{Y(1), Y(2), \ldots, Y(k)\} \\ Z &= \{Z(1), Z(2), \ldots, Z(k)\} \end{aligned}$$

where the length of the vectors, k, was different for each individual P wave.

D.1 System identification

A mathematical model on state-space-form would be:

$$\left\{ \begin{array}{rcl} x_{k+1} &=& A_n x_k + B_n u_k \\ y_k &=& C_n x_k + D_n u_k \end{array} \right. \tag{D.1}$$

where u and y are input and output of the model of order n. x denotes the state vector and k the time, in this case sample number. The corresponding transfer function would be:

$$H(s) = C(sI - A)^{-1}B + D = \frac{N(s)}{D(s)} \tag{D.2}$$

where $N(s)$ and $D(s)$ are numerator and denominator polynomials. Each output signal will have the same denominator, $D(s)$, but a different numerator polynomial: $N_X(s)$, $N_Y(s)$, $N_Z(s)$.

For each recording, the state-space model identification algorithm introduced by Ho and Kalman [85], and further developed by Kung [86], was used to find an estimate of the matrices A, B, C, and D.

Two Hankel matrices were constructed as

$$H_{r,s}^{(k)} = \begin{pmatrix} H_{k+1} & H_{k+2} & \cdots & H_{k+s} \\ H_{k+2} & H_{k+3} & & \vdots \\ \vdots & & \ddots & \\ H_{k+r} & \cdots & & H_{k+r+s-1} \end{pmatrix} \tag{D.3}$$

where the index k may be 0 or 1. The user-defined parameters r and s were chosen such that they had equal values and $r + s$ was the length of the individual P wave being modeled.

The elements of the Hankel matrices of Equation (D.3) were

$$H_1 = \begin{bmatrix} X(1) \\ Y(1) \\ Z(1) \end{bmatrix}, \quad H_2 = \begin{bmatrix} X(2) \\ Y(2) \\ Z(2) \end{bmatrix}, \quad \ldots \quad , \quad H_{r+s} = \begin{bmatrix} X(r+s) \\ Y(r+s) \\ Z(r+s) \end{bmatrix}$$

i.e., the Hankel matrices were built up by the consecutive sample values of the P wave.

The appropriate model order was chosen by singular value decomposition of the Hankel matrix $H_{r,s}^{(0)}$:

$$H_{r,s}^{(0)} = U\Sigma V^T \tag{D.4}$$

where the diagonal matrix Σ has the elements, or singular values, $\{\sigma_1, \sigma_2, \ldots, \sigma_s\}$. Plotting the singular values would ideally show a number of rapidly decreasing values $\{\sigma_1, \ldots, \sigma_n\}$ followed by a 'cut-off' and slowly decreasing values $\{\sigma_{n+1}, \ldots, \sigma_s\}$. The model order would then be chosen as the value n based on the assumption that the first n singular values correspond to the signal and the last to noise which was not desired to be included in the model.

The estimates of the state-space matrices A_n, B_n, C_n, and D_n were then

calculated using the Ho-Kalman/Kung [85, 86] algorithm:

$$\begin{array}{rcl} A_n & = & \Sigma_n^{-\frac{1}{2}} U_n^T H_{r,s}^{(1)} V_n \Sigma_n^{-\frac{1}{2}} \\ B_n & = & \Sigma_n^{\frac{1}{2}} V_n^T E_u \\ C_n & = & E_y^T U_n \Sigma_n^{\frac{1}{2}} \\ D_n & = & H_0 \\ E_u^T & = & \begin{bmatrix} I_{m\times m} & 0_{m\times(s-1)m} \end{bmatrix} \\ E_y^T & = & \begin{bmatrix} I_{p\times p} & 0_{p\times(r-1)p} \end{bmatrix} \\ \Sigma_n & = & \text{diag}\{\sigma_1, \sigma_2, \ldots, \sigma_n\} \\ U_n & = & \text{matrix of the first } n \text{ columns of } U \\ V_n & = & \text{matrix of the first } n \text{ columns of } V \end{array} \tag{D.5}$$

The matrix D_n was always zero since the onset of the P wave was defined to have an amplitude of 0 V in all leads.

D.2 Evaluation of system identification

To measure the accuracy of the system identification, the residual between the original P wave and the modeled was calculated as

$$S_{\text{res}} = S_{\text{P}} - \hat{S}_{\text{P}}$$

where S_{res} is the residual, S_{P} the original P wave and $\hat{S}_{\text{P}}$ the modeled P wave, calculated using the MATLAB function `ss2tf`. In these calculations all leads were merged into one, for example S_{P} would be:

$$S_{\text{P}} = \{X(1), \ldots, X(k), Y(1), \ldots, Y(k), Z(1), \ldots, Z(k)\} \tag{D.6}$$

where k is the length of the P wave.

The magnitude of the residual was calculated by dividing the 2-norm of the residual with the 2-norm of the original P wave using

$$\text{Residual magnitude} = \frac{\sqrt{\sum_{i=1}^{n} |S_{\text{res}}(i)|^2}}{\sqrt{\sum_{i=1}^{n} |S_{\text{P}}(i)|^2}} \tag{D.7}$$

where n in this case is $3k$, according to Equation (D.6).

Appendix E

Fisher linear discriminant

E.1 Fisher linear discriminant

The Fisher linear discriminant [87] is a method to classify a parameter set, $\hat{\theta}$, into one of two groups, A, or B.

By using a 'training set', consisting of two groups of parameter samples, θ_A, and θ_B, the discriminant is calculated.

The sample means and covariances are calculated as

$$\begin{aligned} m_i &= E\{\theta_i\} \\ R_i &= E\left\{(\theta_i - m_i)(\theta_i - m_i)^T\right\} \end{aligned}$$

where $i = A$ or B.

By using the sample means and the average covariance

$$R = \frac{1}{2}(R_A + R_B) \tag{E.1}$$

it is possible to calculate a hyperplane λ such that the projections of the different parameter sets, $\lambda^T\theta$, are expressed as single numbers which may then be compared and classified.

One possible choice of λ would be the Fisher linear discriminant

$$\lambda = R^{-1}(m_A - m_B) \tag{E.2}$$

The parameter sample to be examined, $\hat{\theta}$, would then be classified by calculating $\lambda^T\hat{\theta}$ and tested against a threshold, ϑ, using

$$\hat{\theta} \in \begin{cases} A, & \lambda^T\hat{\theta} > \vartheta \\ B, & \lambda^T\hat{\theta} \leq \vartheta \end{cases} \tag{E.3}$$

(assuming that the values of group A are larger than those of group B).

E.1.1 Classification threshold

In Paper II, the threshold chosen to separate the two groups was [108]:

$$\vartheta = \frac{\left(\sqrt{(\lambda^T R_A \lambda)}\lambda^T m_A + \sqrt{(\lambda^T R_B \lambda)}\lambda^T m_B\right)}{\sqrt{(\lambda^T R_A \lambda)} + \sqrt{(\lambda^T R_B \lambda)}} \tag{E.4}$$

E.1.2 Remarks

Normal distribution Since mean and covariance of data are used, it is assumed that the parameter sets are samples taken from normal distributions.

Uncertainty of covariances The covariances R_A and R_B of Equation (E.1) are estimates of the true values, based on the available material. With small materials, the confidence intervals of the estimates may be large. A confidence estimate for the threshold chosen from Equation (E.4) relative to the empirical distribution obtained will thus depend on the sample size. This may affect the reproducibility of the calculated discriminant of Equation (E.2).

Ill-conditioned covariance matrix When inverting the average covariance matrix R of Equations (E.1) and (E.2), it may be found that it is ill-conditioned due to redundancy of the parameters. In Paper II, the inverse was calculated using the MATLAB function pinv to overcome this.

E.2 Evaluation of the Fisher linear discriminant

To evaluate the performance of the Fisher linear discriminant, the 'training set' may be used (as is the case in Paper II) as a first test. All samples in θ_A, and θ_B may be subject to the test in Equation (E.3). Ideally, they should all be correctly classified.

Next, an 'evaluation set' of parameters with known classification that were not included in θ_A or θ_B may be used to evaluate the performance on unknown data.

Appendix F

Correlation function analysis of atrial electrograms

F.1 Linear substitution of ventricular artifacts

Figure F.1 shows an example of a signal from an electrode on a cardiac catheter. It is obvious that the recordings from the catheter did not only contain signals from the atria but also ventricular artifacts. Since the artifacts were of larger amplitude than the atrial signals, the result of a correlation function calculation would not be accurate unless the artifacts were reduced. Using Lead V_1 of the ECG, the onsets and ends of the artifacts, the QRS-complexes, were identified. To remove the artifacts from an electrode signal, they were replaced by a linear interpolation between the sample values at the artifacts' onsets and ends. Figure F.1 shows an example of the performance of the method.

F.2 Correlation function

To evaluate the similarity between two electrograms, x and y, a statistical approach where the correlation coefficient was calculated as a function of an introduced time delay was used. The correlation coefficient was defined as:

$$\rho(\tau) = \frac{C_{xy}(\tau)}{\sqrt{|C_{xx}(\tau)|}\sqrt{|C_{yy}(\tau)|}} \tag{F.1}$$

where

$$\tau = -n, \ldots, -1, 0, 1, \ldots, n$$

is the time delay. In Paper IV, where signals were sampled at a frequency of 1 kHz, the unit of τ was milliseconds. The maximum time delay, n, was chosen as 20, resulting in a minimum conduction velocity of 30 cm/s needed if the signals of two electrograms should be defined as belonging to the same, 'similar' wavefront, assuming a maximum distance of 6 mm between two adjacent electrodes of the catheter.

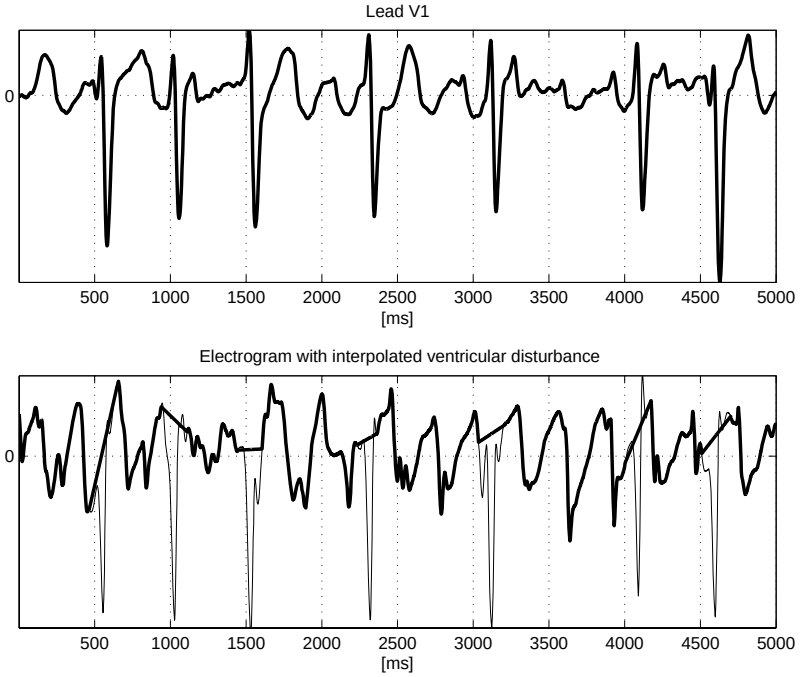

Figure F.1: The effect of removal of ventricular artifacts by linear interpolation. Top: Lead V_1 of the ECG used to identify the onsets and ends of the QRS complexes. Bottom: The thick line shows an electrode signal after linear substitution of the signal between each onset and end of the QRS complexes. The thin line shows the original signal where the ventricular artifacts are clearly of larger amplitude than the signal from the atrium.

Depending on the sign of τ, the sample covariances were defined as

$$C_{xy}(\tau) = \begin{cases} \dfrac{1}{N-\tau} \displaystyle\sum_{i=1}^{N-\tau} (x_i - \bar{x}_{1,N-\tau})(y_{i+\tau} - \bar{y}_{1+\tau,N})^T, & \tau \geq 0 \\ \dfrac{1}{N-|\tau|} \displaystyle\sum_{i=1}^{N-|\tau|} (x_{i+|\tau|} - \bar{x}_{1+|\tau|,N})(y_i - \bar{y}_{1,N-|\tau|})^T, & \tau < 0 \end{cases} \tag{F.2}$$

where N is the number of samples of the signals.

The sample means were defined as

$$\begin{aligned} \bar{x}_{1,N-\tau} &= \frac{1}{N-\tau} \sum_{i=1}^{N-\tau} x_i \\ \bar{x}_{1+\tau,N} &= \frac{1}{N-\tau} \sum_{i=1+\tau}^{N} x_i \end{aligned}$$

in the case $\tau \geq 0$, with τ substituted for $|\tau|$ in the case $\tau < 0$.

An example of the output of the correlation function of Equation (F.1) calculated on signals from two electrodes is shown in Figure F.2. In each recording of

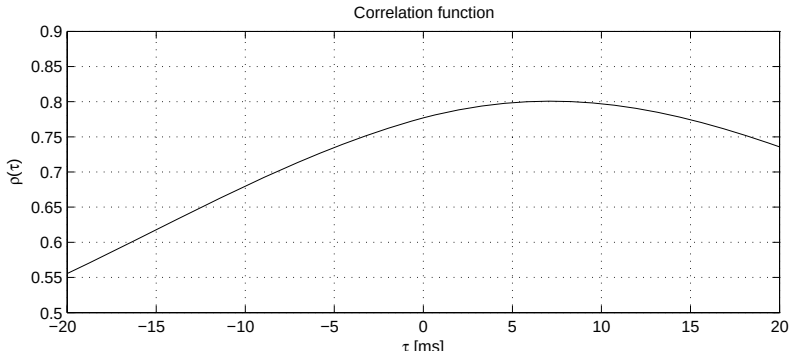

Figure F.2: Example result of the correlation function of Equation (F.1). In this case, the maximum correlation $\rho = 0.80$ was found at $\tau = 7$. A positive value of τ indicates that the signal y is delayed compared to x.

signals from ten electrodes, the correlation function was calculated for each adjacent pair of electrodes. The maximum values of ρ and their corresponding τ were used to create an analysis as shown in Figure F.3.

F.3 Interpretation of conduction direction

The value of the time delay, τ, was used to interpret the direction of the activation. The definitions in Equation (F.2) show that if maximum correlation is found for a positive value of τ, the signal y is delayed compared to signal x. In Paper IV, when calculating the correlation function between the signals from two electrodes, the signal from the electrode with lower number (i.e., closer to the tip) was always used as x. Thus, a positive time delay could be interpreted as conduction moving from the tip of the catheter.

To facilitate interpretation of activation direction, the cumulative sum of all values of τ was calculated. A consistent left-to-right activation would only have positive values of τ and the cumulative sum would show as a line with positive, increasing values. Consequently, a right-to-left activation would show as a line with negative, decreasing values. Figure F.3 shows an example of the former case.

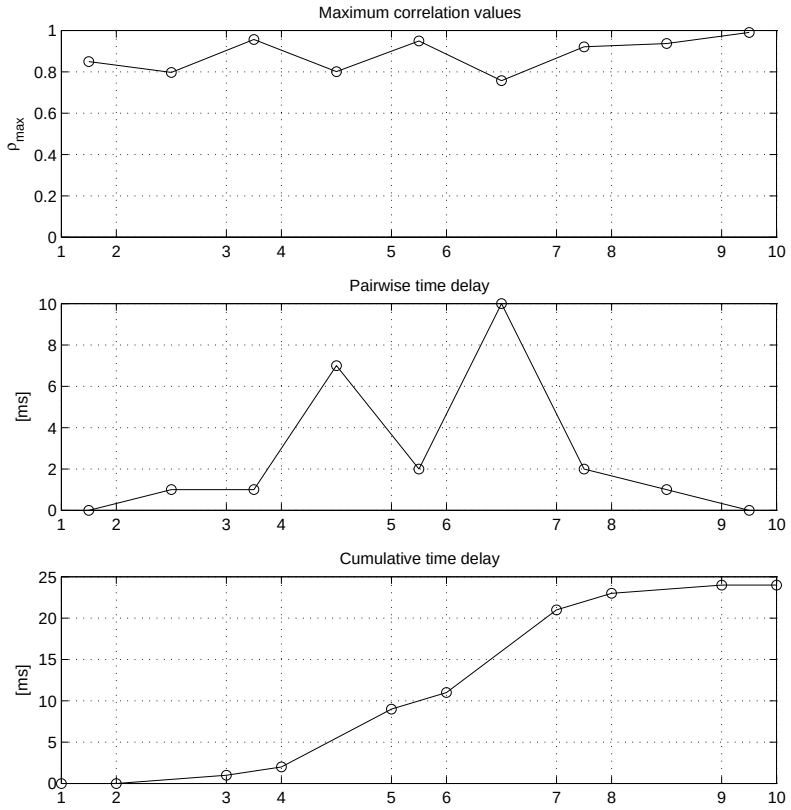

Figure F.3: Example of analysis of an atrial fibrillation recording. The numbering and spacing of the x-axes' gridlines illustrate electrode positioning on the catheter. Top: observations of maximum correlation, ρ, for each adjacent pair of electrodes. Middle: corresponding value of time delay, τ. Bottom: cumulative values of the time delay, used to interpret direction of conduction. In this case, a left-to-right conduction is observed.

Appendix G

Original papers

Paper I

M.P. Ingemansson, J. Carlson, and S.B. Olsson.

Modification of intrinsic AV-nodal properties by magnesium in combination with glucose, insulin, and potassium (GIK) during chronic atrial fibrillation.

Reprinted from *Journal of Electrocardiology*, 31(4):281–292, © October 1998, with permission from Elsevier.

Paper II

J. Carlson, R. Johansson, and S.B. Olsson.

Classification of electrocardiographic P-wave morphology.

© 2001 IEEE. Reprinted, with permission, from *IEEE Transactions on Biomedical Engineering*, 48(4):401–405, April 2001.

Paper III

J. Carlson, R. Havmöller, A. Herreros, P. Platonov, R. Johansson, and B. Olsson.

Can orthogonal lead indicators of propensity to atrial fibrillation be accurately assessed from the 12-lead ECG?

Reprinted from *Europace*, 7(Supplement 2): 39–48, © September 2005, with permission from Elsevier.

Paper IV

J. Carlson, S. Santos, P.G. Platonov, O. Kongstad Rasmussen, R. Johansson, and S.B. Olsson.

Left atrial conduction along the coronary sinus during ectopic atrial tachycardia and atrial fibrillation: A study using correlation function analysis.

© 2003 Blackwell Publishing. Reprinted, with permission, from *Journal of Cardiovascular Electrophysiology*, 14(10 Supplement):s148–s153, October 2003.